This Project has received funding from European Comission by means of Horizon 2020, The EU Framework Programme for Research and Innovation, under Grant Agreement no. 700174

WWW.RESCCUE.EU

#resccueEU

RESCCUE

RESILIENCE TO COPE WITH CLIMATE CHANGE IN URBAN AREAS.

Deliverable D1.3

Report on extreme events prediction

R. Monjo[1], C. Paradinas[1], E. Gaitán[1], D. Redolat[1], C. Prado[1], J. Pórtoles[1], L. Torres[1], B. Russo[2], M. Velasco[2], L. Pouget[3], S. Vela[3], L. M. David[4], M. Morais[5], J. Ribalaygua[1]

[1]Climate Research Foundation (FIC); [2]AQUATEC; [3]CETAQUA;
[4]National Laboratory for Civil Engineering (LNEC); [5]Câmara Municipal de Lisboa (CML)

17 December 2019

DELIVERABLE NUMBER:	D1.3
DELIVERABLE NAME:	Report on extreme events prediction
WP:	WP1
DELIVERY DUE DATE:	30/04/2018
ACTUAL DATE OF SUBMISSION:	17/12/2019
DISSEMINATION LEVEL:	Public
LEAD BENEFICIARY:	FIC
RESPONSIBLE SCIENTIST/ADMINISTRATOR:	Robert Monjo (FIC)
CONTRIBUTOR(S):	R. Monjo, J. Pórtoles, E. Gaitán, D. Redolat, C. Paradinas, C. Prado, L. Torres, B. Russo, M. Velasco, L. Pouget, S. Vela, J. Ribalaygua
INTERNAL REVIEWER:	Jaime Ribalaygua (FIC)
EXTERNAL REVIEWER:	Paul Fleming (Water Program Management, Microsoft)

Table of contents

Tables Summary

Figures Summary

Report Summary

Abstract

This deliverable describes the results on the generation of extreme climate scenarios for Barcelona, Lisbon and Bristol. For this purpose, several statistical downscaling methods have been combined to simulate and project extreme events at local scale according to the main identified drivers, specifically temperature, rainfall, snowfall, wind, wave height and sea level. The simulation of extreme events was validated according to the performance of the used downscaling models. Generally, systematic errors were small for most of the models and therefore they could be corrected, especially for the climate timescale. However, some nuances can stand out for the closer time horizons: Seasonal and decadal simulations are adequate for extreme precipitation if the teleconnection-based approach is used, while temperature is best simulated using drift-corrected dynamical outputs. Main outputs are available in https://www.ficlima.org/intercambio/indexed/RESCCUE/.

Main results

In general terms, climate change direction leads to a more extreme heat in the three RESCCUE cities, with a tendency towards more extreme rainfall behaviour (Figure 1). On the one hand, extreme temperature could rise up to +5.0±2.5°C and heat wave days will experience an increase about +1000%. On the other hand, daily and subdaily extreme rainfall (with at least 2y-return period) will increase in Barcelona and Bristol about +30%. For Lisbon, this change is expected only for 1-hour (or shorter) events. Moreover, extreme snowfall could also increase for 100y-return events in Barcelona, up to 40% during the next two decades. For the lesser extreme events (return periods from 2 to 10 years), snowfall would suffer a great decrease in Bristol and Barcelona due to the temperature rising.

Although significant changes in pluviometric drought are not expected (i.e. standardized precipitation index will not decrease), the water shortages (hydrological drought) will increment due to a greater evapotraspiration.

Regarding the windstorms, extreme gusts could increase in Barcelona up to 10±3% in the next two decades for all return periods, while storm surge is expected to rise in the three cities for 2y-return events by 2100. However, non-significant changes are projected for the extreme wave heights in the RESCCUE cities.

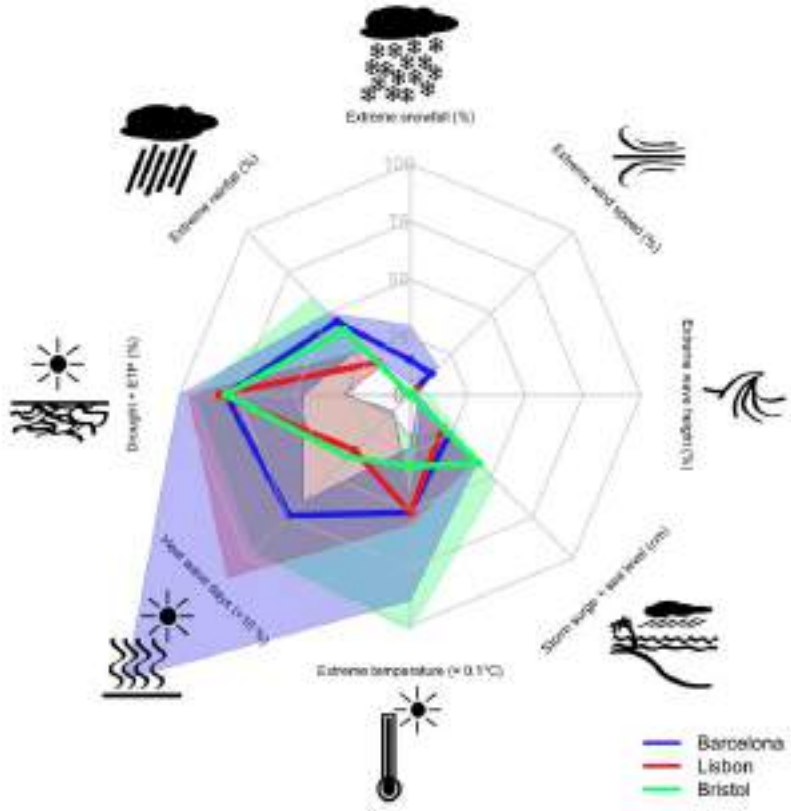

Figure 1. Extremes Compass Rose for Barcelona, Lisbon and Bristol: Extremes Compass Rose for Lisbon: Maximum point change in climate extreme events along the century taking into account return periods between 2 and 100 years. The centre represents no changes and the edge corresponds to an increase of 100% for every variable, except for heat wave days (border is +1000%), for storm surge (border is +100 cm) and extreme temperature (border is +10°C). Thick lines represent the median scenario and the shaded area is the uncertainty region (5-95%).

1. Introduction

1.1. Deliverable objectives

The goal of the third deliverable (D1.3) of the RESCCUE WP1 is to provide all climate extreme scenarios required to integrate the Climate Module of the HAZUR® tool. This integration constitutes the **Early and Climate Warning System** (ECWS) planned in the Description of the Action (DoA). Particularly, the deliverable contents correspond to the Task 1.4, "Projection/prediction of climate/weather extreme events", scheduled between months 12 and 24, reporting in month 26 and leaded by the Climate Research Foundation (FIC).

Within the four tasks that make up the WP1, the Task 1.4 is the last one:

Task 1.1: Climate change drivers
Task 1.2: Data collection & quality control
Task 1.3: Generation of climate simulation for the pilot cases
Task 1.4: Projection/prediction of extreme events

According to the WP1 Implementation plan and the RESCCUE Grant Agreement, extreme events simulation is expected to be generated under near-term and long-term climate horizons, according to the downscaled results of the previous deliverable D1.2. In order to complete the near-term climate prediction, a seasonal forecast of extreme events was also planned in the DoA. Weather forecasting is not included in the RESCCUE project because it is generally out of the climate monitoring.

This last WP1 deliverable summarises the main results of verification, validation and projection/prediction of the extreme events estimated for the climate variables identified and collected in the D1.1 for the three RESCCUE cities. The main variables analysed are maximum temperature, wind gust, rainfall, snowfall and oceanic variables as the wave height and the total sea level.

1.2. Previous concepts

1.2.1. Extreme event definition

The analysis of extremes in meteorology and climatology presents some problems that should be considered in every study. The first one is the definition of extreme event. The definition necessarily assumes a low occurrence probability, and in most of studies, this is combined with potential high-impacts on the studied area (WMO 2001).

For the RESCCUE project, it is important to consider the potential impacts because, in some cases, a low-recurrent event may cause an unappreciated impact. This is the case, for instance, of the snowfall in Lisbon, where the rare snowfall events do not cause any problems in the city (see D1.1).

In any case, the most important element of the definition, the low occurrence, is related to the tails (extremes) of a given probability distribution (usually from the analysed climate variable). For a given distribution, the problem is to determine where each tail starts. Some authors use a threshold that splits a tail from the general distribution, but an arbitrary threshold could occur too many times or never. Therefore it is important to identify specific thresholds that cause problems in each city.

Other authors use classical quantiles as 0.90, 0.95 or 0.99 to determine the extremes from a distribution. Generally, these values correspond to relatively frequent events (every year) and then they usually do not cause potential impacts.

In order to better represent the low occurrence, return periods are used in the RESCCUE project. Logically, each return period (T) is related to a quantile ($1 - 1/T$) very close to 1, which guarantees that is a real extreme. As complement, specific thresholds were identified for each city and were summarised in a common criteria (Sec. 2.2).

The low recurrence of the extreme events has an additional problem: There are a limited number of observed extreme events and then statistical measures are less robust. To reduce the uncertainty, it is advisable to use an ensemble strategy and theoretical distributions that can be fitted to the entire empirical distribution (Monjo *et al.* 2016).

1.2.2. Seasonal-to-decadal limitations

Anthropogenic contribution to the climate change signal is expected to be greater for the long term than for the medium and near term. In fact, the near-term (decadal) climate prediction is highly influenced by the natural variability of the climate. This natural contribution is mainly due to the quasi-oscillations of the climate system components, which are coupled (e.g. ocean-atmosphere or ocean-cryosphere). The main atmospheric patterns in Europe are North Atlantic Oscillation (NAO), the Arctic Oscillation (AO) and the East Atlantic Oscillation (EAO). Regarding the oceanic contributions, the most known variability modes are the Atlantic Multi-decadal Oscillation (AMO) and the Pacific Decadal Oscillation (PDO).

Dynamical models try to simulate these variability modes of the climate, but present many difficulties to reproduce the real intensity and frequency of their phases. For example, CMIP5 decadal models only simulate adequately a few of these natural oscillations, as the AMO (Kim *et al.* 2012, Gaetani and Mohino 2013). Moreover, the assimilation of the initial conditions (e.g. anomaly of the oceans) is limited to the scarcity of observed data, especially from the deep currents of the oceans. All these limitations cause a low skill of the dynamical climate models applied to the decadal and seasonal scales and then they need to be complemented with statistical methods.

1.3. Structure of the report

Following the objectives, the report is divided into two main sections, Methodology and Results & Discussion. In turn, these sections are structured in several subsections corresponding to the report objectives:

- **Used methodology (Sec. 2)**
  - Description of all used methods
  - Description of the uncertainty analysis
- **Results and discussion**
  - Validation of the methods to be applied to climate models **(Sec. 3)**
  - Extreme events prediction for each city and time scale **(Sec. 4)**

All the results about extreme events (summarised in **Appendix I**) are detailed for each studied area, variable and horizon including the long and medium-term (climate), the near-term (decadal) and the seasonal timescale.

2. Methodology

2.1. General view

This report focuses on the generation of extreme events scenarios for increasingly closer time horizons, from the end of the century to the next month passing through the next decade (Figure 2). Within the climate change context, the monitoring of monthly anomalies is important to detect possible extreme deviations due to the climate change or natural variability.

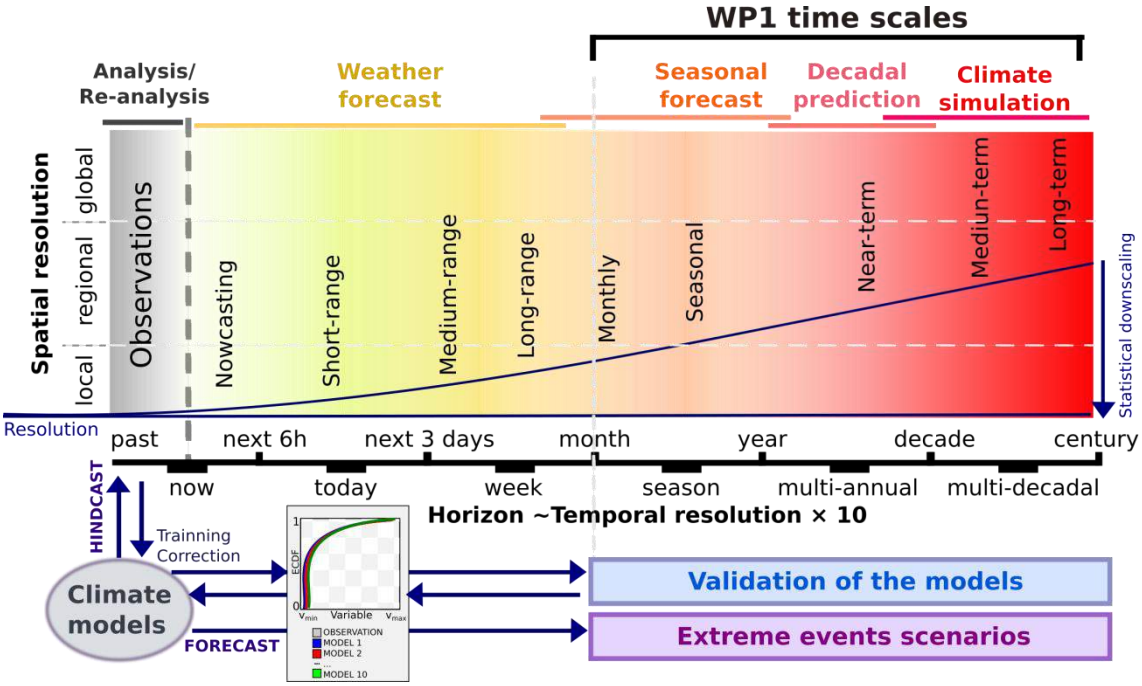

Figure 2. General scheme of the time scales analysed in this report.

The performing of the climate models is tested in the past through a back prediction (*hindcast*) of the extreme events for the three time scales. Synthetic extreme events were estimated by using theoretical probability distributions fitted to the Empirical Cumulative Distribution (ECDF) of each time-series. The ECDFs are obtained from the observations and simulations of the climate models used in each time scale. Systematic errors up to ±3°C in temperature and ±30% in rest of variables were accepted to be corrected in the final simulation. Once the models have been validated, those that pass the tests were corrected and used to analyse the absolute and relative changes in the main climate variables. Finally, Keyhole Markup Language (KML) polygons are obtained to summarize the areas affected by values above specific hazard thresholds (Figure 3).

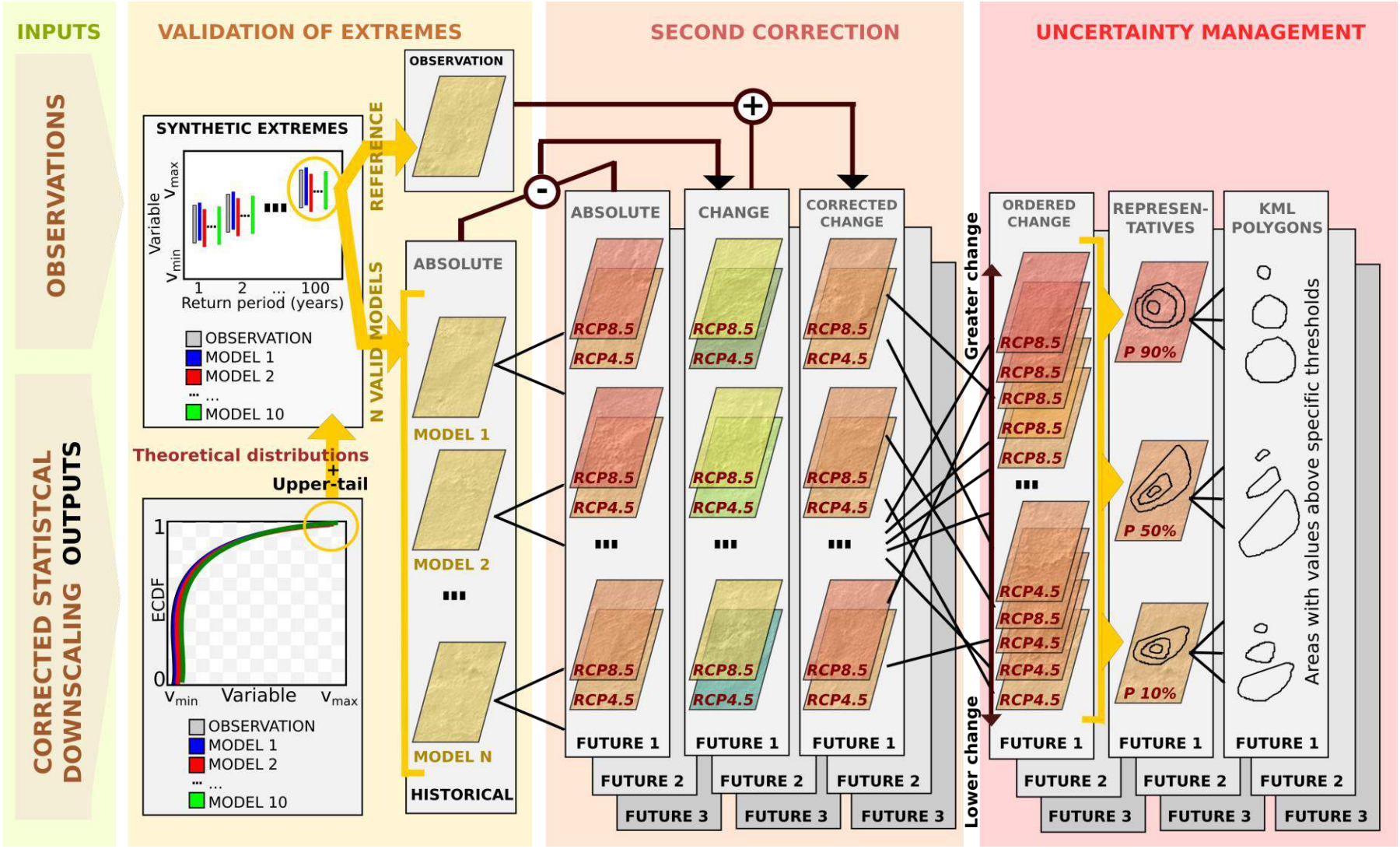

Figure 3. Detailed scheme of the method used to obtain extreme events scenarios for a climate variable in a city, according to three specific thresholds.

2.2. Common criteria

2.2.1. Synthetic extreme events

Common criteria have been established regarding extreme meteorological events for the three cities considered in the RESCCUE project. After considering the different characteristics of each city's climate and the already known trends obtained for future climate projections of each variable (temperature, rainfall, snowfall, wind, wave height and storm surge), we have designed **synthetic extreme (SE)** events to represent the most interesting events. Each SE is defined according to a particular *return period* and was represented by several isolines (contour lines) drown according to *specific thresholds*.

- **Point return periods:** Eight SEs were defined according to 1, 2, 5, 10, 20, 50, 100 and 500 years of *point return period*. Different (theoretical) probability distributions were used to find the best fit to the variability of each station: 2, 3 and 4-parametric versions of Gamma, Weibull, Classical Gumbel, Reverse Gumbel and Modified Log-logistic distributions (Monjo *et al.* 2014, 2016).
- **Specific thresholds:** For each SE, the expected extreme value is estimated for each station and then a spatial distribution can be obtained using Thin Plate Spline (TPS) methods. This spatial distribution is summarised by a few isolines, which are specific for each variable. According to the hazard thresholds (potential impacts to particular urban services) identified by the RESCCUE partners, the isolines match with three levels, excepting some cases in Barcelona and Lisbon (Table 1).

Table 1. Specific thresholds for isolines that summarise the spatial distribution of the extreme events.

Variable		Low			Medium			High		
		Barcelona	Bristol	Lisboa	Barcelona	Bristol	Lisboa	Barcelona	Bristol	Lisboa
Temperature (°C)		34	30	34	38	35	38	40	40	40
Rainfall	1h (mm)	20	10	10	40	20	20	60	40	40
	12h (mm	60	60	30	100	100	40	140	140	60
Snowfall[1] (cm/12h)		6	6	-	10	10	-	14	14	-
Wind (km/h)		70	70	70	90	90	90	130	130	130
Wave height (m)		3	3	4	5	5	5	7	7	7
Sea level + storm surge (m)		0.5	0.5	0.5	1.0	1.0	1.0	2.0	2.0	2.0

[1]Snowfall intensity scaling is considered using a n-index equal to 0.3. Variable not identified as hazard for Lisbon

Barcelona and Lisbon usually presents warmer summers than Bristol and consequently it is used upper thresholds (34°C and 38°C) for the low and medium levels. Note that high temperature of 40°C is not recorded in Bristol but is expected to be observed in this century. Regarding the rainfall, the thresholds of 10mm and 20mm in 1 hour are low for Barcelona and, therefore, they considered higher values for the city. Snowfall is not applicable for Lisbon because this variable is not identified as hazard for the city.

Note that thresholds for extreme winds and coastal hazards (wave height and storm surge) are generally common to the three cities because they are very linked to vulnerability values for critical infrastructure elements and human health. However, for temperature and precipitation, significant differences were found among the cities due to the particular climate features. In these sense, common thresholds (especially in upper values) are completed by specific thresholds differentiated for each city (especially for lower values). The low thresholds correspond to the current climate, and the high values are more related to danger thresholds (to resist damage from climatic hazards).

2.2.2. Baselines and horizons

The study of changes in future extreme values was performed considering several periods in both historical and future years. A baseline was required to compare the simulated and observed past periods, while three future horizons were defined from the near-term (prediction) to the long-term (projection) climate simulations.

The historical experiment (1950-2005) has been considered for validating the downscaled model outputs according to the extended observations (combined with ERA-Interim, 1979-2017) in the common period, usually 1979-2005.

Regarding the projection of the climate variables, mainly RCP 4.5 and RCP 8.5 are considered. Within those RCPs, three thirty-year climate periods were selected to analyse the progression of the changes along the century: 2011-2040, 2041-2070 and 2071-2100, with respect to the 1986-2015 baseline (Table 2). For the near-term climate predictions, the period 2016-2035 was considered with respect to the baseline period 1986-2015. Finally, the seasonal forecast was performed for a 6-month horizon from June 2018. The 30-year period of 1986-2015 was considered as the most recent period for the reference climate (baseline), but the lack of seasonal forecasts limits the validation period to 2016-2018.

Table 2. Time periods considered in the study: baselines (past) and projected periods (future).

Use	Period				
	Validation	Baseline	Near-term	Medium-term	Long-term
Climate projections	1976-2005	1986-2015	2011-2040	2041-2070	2071-2100
Decadal predictions	1986-2015		2016-2035		
Seasonal predictions	2015-2018		2018		

It should be noted that the term “prediction” is used for the near-term climate simulations in contrast with the “projection” of the long-term future climate. This difference is due to the fact that the long-term simulations depend on the selected RCP scenario, which is not directly associated with a probability concept but with a political decision that is not related to numerical prediction models.

2.2.3. Spatial distribution

The spatial distribution of a SE is obtained from a TPS interpolation method that depends on the climate variable. For height-dependent variables as temperature, snowfall and wind, it is considered a 3-dimensonal approach (TPS-3D), while the no height-dependent variables as precipitation are interpolated by a simple 2-dimensional approach (TPS-2D). For both methods, a cross-validation is applied to measure the uncertainty level.

Some variables as total sea level (including storm surge) and wave height are considered constant planes and they do not require any interpolation (these variables are considered as spatially constant because observations of only one buoy were available for each city port).

Spatial interpolation of the rest of variables are summarised using the isolines corresponding to the specific thresholds considered in the Sec. 2.2.2. Particularly, a polygon shape is constructed for each isoline in a Keyhole Markup Language (KML) format, which is used as input in the HAZUR® tool. Total number of KML polygons is given by the combination of 5 specifications:

a) **Variables (4)**: Daily maximum temperature (°C), daily maximum wind gust (km/h), 12h snowfall amount (mm) and 12h rainfall amount (mm)
b) **Thresholds (3)**: Generally three levels for each variable and common for the three cities (see Table 1). In addition, there are official and personalized thresholds that depend on the user/city.
c) **Occurrence (8, 3):** The probability of occurrence is taken from the following return periods: 1, 2, 5, 10, 20, 50, 100 and 500 years. As representative sample, it is advisable to use at least three of them: 2, 10 and 100 years.
d) **Scenarios (3, 1):** From the ensemble of predictions/projections (e.g. combining multi-model and RCP scenarios), only three change levels are considered: the low (10%), medium (50%) and high (90%). It is advisable to use at least the high change level (90%).
e) **Periods (6)**: In addition to the reference period (observations), future periods are considered for the three temporal scales (climate, decadal and seasonal):
    - 1986-2015: Current climate
    - 2016-2036: Near-term climate prediction (decadal)
    - 2011-2040: Near-term climate projection
    - 2041-2070: Medium-term climate projection
    - 2071-2100: Long-term climate projection
    - Seasonal forecast (2018)

2.2.4. Extreme indicators

Measure of changes in extremes

In general terms, changes in extreme values were estimated according to the variation of each simulated variable under the considered return periods. For instance, given a synthetic extreme gust event of 100 years of recurrence, the area affected by a wind

gust above a hazard threshold of 130 km/h for a future period could be different than the reference period (baseline).

To analyse these changes in a general way, three projected changes at 10%, 50% and 90% level were considered for each climate variable and return period respect to the baselines.

Specific indices

Additional extremes indices were considered for temperature and precipitation according to several authors (Table 3). Two different definitions of heat/cold wave are mainly based on the Expert Team on Climate Change Detection and Indices (ETCCDI), from the World Climate Research Program (WRP) of the World Meteorological Organization (WMO 2001, 2017). The first definition is the Long Heat/Cold Wave (LHW/LCW), according to the events with at least five days with temperature above/below 5°C respect to the normal period (STARDEX 2004). This is commonly used in Lisbon and Bristol. However, some authors define *heat wave* when as the period in which temperatures are above a particular percentile during three or more days (Pezza *et al.* 2012). This is an interesting definition to be used in the RESCCUE project because it is commonly applied in Barcelona (SMC 2015, AEMET 2016).

Table 3. Criteria for additional extreme indices based on potential impacts

Index	Description	Source	Criterion	Variable	Threshold	Reference period
LHW / LCW	Long heat/cold wave	WMO (2001, 2017)	sdc 5	TX / TN	±5°C	Jul-Aug / Jan-Feb
HW / CW	Heat/cold wave	SMC (2015) and AEMET (2016)	sdc 3	TX / TN	98 / 2%	Jun-Aug / Dec-Feb
TN90 / TN10	Warm/cold night	Zhang et al. (2011)	nd	TN	90 / 10%	whole
TX90 / TX10	Warm/cold days	Zhang et al. (2011)	nd	TX	90 / 10%	whole
TR	Tropical nights	Zhang et al. (2011)	nd	TN	> 20°C	whole
FD	Frost nights	Zhang et al. (2011)	nd	TN	< 0°C	whole
CDD	dry spell duration	Zhang et al. (2011)	x	P	< 1 mm	whole
CWD	wet spell duration	Zhang et al. (2011)	x	P	≥ 1 mm	whole
SPI12, SPI24 SPEI12, SPEI24	SPI & SPEI of 12 & 24 months	McKee et al. (1993) Hargreaves (1994) Thornthwaite (1948)	pSPI	P, TA	≥ 0.1mm	whole
DPB5	Days with light rain	AMB et al. (2017)	nd	P	≥0.1&<5mm	whole
DPA50, DPA100	Days with heavy rain	AMB et al. (2017)	nd	P	>50mm >100mm	whole
CI	Concentration Index	Martin-Vide (2004)	a	P	≥ 0.1mm	whole
n, I_0	*n*-index	Monjo (2016)	a	P	≥ 90%	whole
Warmest period	Warmest period	FIC	x	TA	95%	whole
Summer	Warm spell	FIC	x*, s	TA	75%	whole
Winter	Cold spell	FIC	x*, s	TA	25%	whole
Coldest period	Coldest period	FIC	x	TA	5%	whole

Legend:

TX: maximum temperature
TN: minimum temperature
TA: average temperature
P: precipitation
W: wind

H: humidity
sdc: sum of days with at least … consecutive days
nd: number of days per year
x: maximum duration per year
*: opposite spells up to 7 days are exceptions allowed
a: average per year
s: starting date, day of the year
pSPI: probability of SPI or SPEI < -1, -2, -3

The most used extreme indices are defined by Zhang et al. (2011), but other interesting and commonly used indices are the Standardized Precipitation Index (SPI, McKee et al. 1993) and the Concentratrion Index (CI) of Martin-Vide (2004). The reference intensity (I_0) and the *n*-index (Monjo 2016) are useful to measure the rainfall concentration at sub-daily scale.

In addition to the SPI, drought can be also analysed by using the Standardized Precipitation Evapotranspiration Index (SPEI). Therefore, it is required to distinguish between two different types of drought: The abnormally low precipitation leads to a *pluviometric drought*, but the shortage of surface water depends on additional factors as the evapotranspiration (included in the SPEI). This last case is usually referred as *hydrological drought* (Vicente-Serrano *et al.* 2012).

Finally, seasonal analysis is performed by using some definitions as the starting and duration of the summer/winter and the duration of the warmest/coldest period.

2.3. Application to each time scale

2.3.1. Long and medium-term climate extremes

To obtain reference SEs, observations were previously filled and extended in order to obtain a complete series from 1986 to 2015 using the bias-corrected downscaled ERA-Interim, which was presented in the D1.2. Thanks to the large common period (at least 30 years), these extended observations are the best choice to compare with past climate simulations and to combine using the projected climate change signal (Monjo *et al.*, 2016).

For the past climate simulations it is important to dispose the equivalent current SEs according to the downscaled climate models presented in D1.2. Recall, the downscaled outputs corresponded to 10 climate models collected from the Coupled Model Intercomparison Project 5 (CMIP5), on which the IPCC Fifth Assessment Report (AR5) is based.

In order to update the extent of the *historical experiments* (1951-2005) used in these downscaled climate simulations, it was considered the RCP4.5 scenario extending the period ten years more (2006-2015). Note that, throughout the first projected decade, there are non-significant differences between the main RCPs, and therefore the selection does not affect the result (Sec. 4 of D1.2).

On the other hand, extreme events simulated under climate change conditions can present important systematic error despite of the general correction applied to the entire probability distribution (Sec. 2.2.2 of D1.2). In order to reduce their effects in the future projections, this study considered an additional procedure of bias correction for the extreme values according to the common criteria periods (Sec. 2.2).

The approach is performed in two steps: First o all, it is obtained the projected change in the SEs for each future period (2011-2040, 2041-2070 and 2100) with respect to the baseline (1986-2015). Secondly, it is obtained reference SEs based on extended observations for the same period and then the projected change is applied. The climate change projected in extremes has been obtained in absolute and relative units depending on the considered variable.

With all this, the projected climate change is obtained taking the extended observations as a reference and, therefore, the mean bias is zero. Moreover, in terms of relative changes, errors in standard deviation also approach zero. From now on, KML polygons are obtained according to the common criteria.

2.3.2. Near-term climate extremes

In addition to the previous problems, the extreme events simulation for the near-term climate forecast presents temporal discontinuity: Each experiment/run used in the hindcast procedure is projected up to 10 years horizon. Therefore, the past period used as reference (1986-2015) requires to be covered by a set of overlapping projections.

As the downscaled decadal simulations were drift-corrected (Sec. 2.2.3 of D1.2), there is a temporal coherence within each overlap. In order to synthesise a continuous time series, the most recent fragment is selected for each overlap. Note that it is

preferable the selection of one of them instead of the average because it is required to preserve the probability distribution at daily scale (which is essential to the extreme calculus). For the future period (2016-2035), the decadal outputs of the CMIP5 models provide projections up to 30 years of horizon; and thus, no selection was required.

Each SE is estimated for the past and future periods and the relative change is obtained. This predicted change is then applied to the reference SE, obtained from the reference period (1986-2015) using extended observations. As in the climate scale, this way allows to reduce the bias of the prediction.

2.3.3. Seasonal extremes

Seasonal forecast techniques

In order to improve the seasonal forecast skill, two complementary approaches were considered: A mixed statistical-dynamical technique and a purely statistical teleconnection-based method.

The statistical-dynamical technique is based on the operational forecast outputs collected from the Climate Forecast System (CFSv4) of the US National Centers for Environmental Prediction (NCEP). Particularly, an ensemble of 25 perturbed initial conditions is considered from the last 7 runs for each experiment output. The CFSv4 outputs were downscaled for all time horizons by using transfer functions between predictand (temperature, precipitation and wind) and predictor variables (500hPa geopotential height, 850hPa temperature, surface wind and precipitation probability).

The teleconnection-based seasonal technique consists on the partial predictability of the natural variability modes, which can be fitted to quasi-oscillation functions as in the approach used for the decadal scale (see Sec. 2.2.4 of the D1.2). This method has been adapted to seasonal forecast using training windows with shorter length.

In general terms, the ensemble strategy is used to manage the uncertainty level and, with this, standardized mean anomalies are calculated for at least two sets of 30 days of prediction. As the seasonal forecast shows very low skill in Europe, extreme events need to be obtained by using additional techniques (Pepler *et al.* 2015). For the RESCCUE project, WP1 has opted for a statistical extreme inference approach.

Extreme inference approach: analogous anomalies

Given a predicted anomaly for a month, it is possible to estimate the expected extreme (maximum/minimum) daily values according to the *n* most similar anomalous months in the past. The relation between a mean value and the probability distribution depends on the climate variable and the station considered. This statistical link is expected to remain during at least the next year and, therefore, it does not present a "stationary problem" in contrast with some statistical downscaling methods applied for the climate change scale (Ribalagua *et al*. 2013).

The similarity between pairs of months can be measured according to large-scale predictor fields or by using one-dimensional physical features. In numerical weather forecast, the predictand is also commonly used as predictor or input to apply transfer functions or non-linear techniques (Chardon *et al.* 2018). For this study, the monthly anomaly is used as predictor for the similarity measure. Particularly, let x_i the mean

anomaly of a problem month-*i*, the *n* most similar anomalies $x_{j<i}$ from the past are given by the set:

$$\{X_i^k\}_{k=1}^n := \left\{ x_j : \quad j \in \underset{j<i}{^{n}order} |x_i - x_j| \right\}$$

Then, the daily distribution $\pi(x_i)$ of the problem month can be obtained from the daily distribution of the selected analogous months, i.e. $\pi(x_i) \approx \pi\left(\{X_i^k\}_{k=1}^n\right)$.

In a second stage, the probability distribution is linearly interpolated, quantile-to-quantile, from the *n* analogous month to the problem month. That is, although some analogues are far from the problem value x_i, the corresponding quantile qQ_k, is obtained taking into account this distance and thus the closest analogues weigh more:

$$qQ_i = lm(qQ_k \sim X_i^k)_{k=1}^n \circ x_i$$

where qQ_k is the quantile-Q of the month-*k*, while *lm* represents the linear model fitted using its arguments (qQ_k versus $X^k{}_i$) and ∘ is the *application symbol*, i.e., the function on the left is applied to the right argument. This study considers *n* = 10 analogous months to fit each quantile. For instance, $q00_k$, $q10_k$, $q50_k$, $q90_k$ and $q100_k$ represent the probability distribution of daily values within the month-*k*.

Finally, the expected seasonal extremes are estimated. Within a problem month-i, the expected maximum or minimum value ($q00_k$ or $q100_k$) can be obtained according to the probability distribution defined by the set of all maximum (or minimum) daily values taken from all analogous months (i.e., $q00_k$ or $q100_k$, for *k* = 1,...,*n*) (Figure 4). For non-Gaussian variables, a quantile mapping is applied to translate each daily anomaly to the corresponding absolute extreme value.

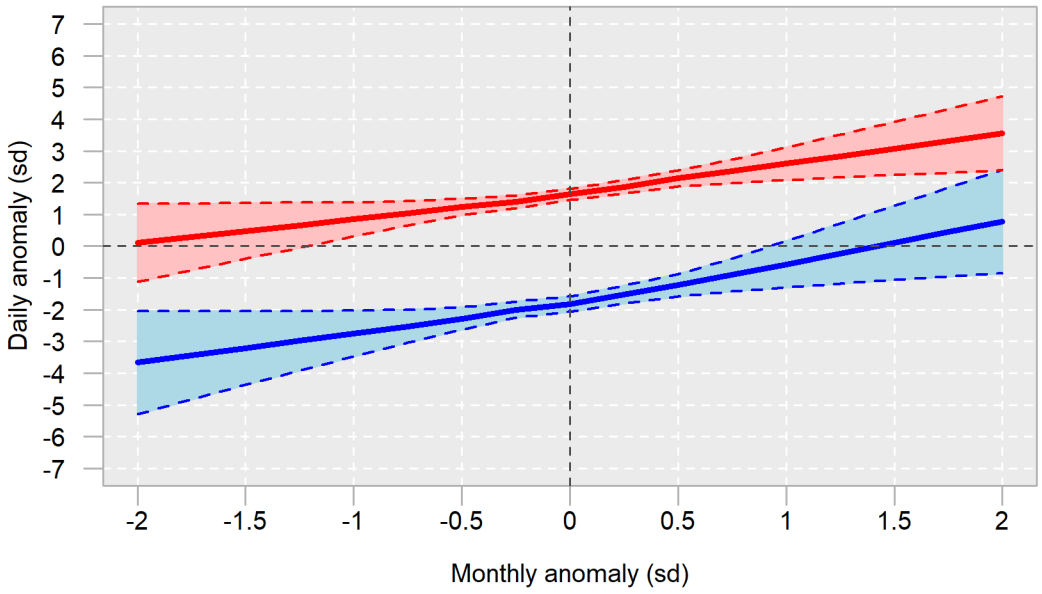

Figure 4. Example of inference of maximum (red) and minimum (blue) daily values found in a month for the maximum temperature variable, according to the monthly anomaly. All the anomalies (daily and monthly) are standardized using the daily standard deviation (sd) of each considered month. The shaded area represents the 10-90% interval error.

The spatial distribution of the seasonal extremes is considered to obtain the KML polygons according to the specific thresholds defined in the Sec. 2.2.1.

2.4. Uncertainty analysis

2.4.1. Validation of the methodology applied

All used methods were validated to be applied in the extreme events simulations by using the downscaled climate models. As a reference, observations extended with the corrected downscaled ERA-Interim (1979-2015) were used, in a similar way to the validation process explained in the D1.2.

The main statistic for a model validation is the *bias* of the analysed output. In this case, it was analysed the bias of extreme events given by the selected return periods. As in the validation of the mean climate values (D1.2), the *bias* is important because a model output should adequately reproduce the dispersion of the spatial distribution of the extreme values. That is, bias presenting a high dispersion for a set of observatories could suppose a distortion of this regional variability.

The Mean Absolute Error (MAE) has no sense in the climate scale because models do not try to reproduce the real day-to-day or month-to-month weather evolution; rather they try to simulate the climate variability at a daily scale. In contrast, seasonal forecast systems aim to predict the climate anomalies usually at a monthly scale, as a real time evolution. For that case, the Standardised mean Absolute Error (SAE) is estimated according to the ratio between the MAE of the seasonal forecast and the MAE of a reference forecast based on historical climatology averages. Particularly, a hindcast cross-validation was considered to measure the performance in the reference period according to the SAE.

The acceptance level for each downscaled climate output is given by the number of cases (comparisons of simulated and observed time-series) that pass the Kolmogorov-Smirnov test with a significance level of 0.05. The level of 70% of cases is considered acceptable because, when only a few nearby time-series (<30%) is bad simulated by all the climate models, it is likely due to residual problems derived from undetected inhomogeneities or non-representative climate features (e.g. bad locations). In other words, if most of nearby stations (>70%) are well simulated, it indicates that the regional climate is well represented/simulated.

2.4.2. Projection uncertainty

Continuing with the cascade of uncertainties analysed in the D1.2, extreme events simulation is affected by: (1) The method-model performance [validation process], (2) the RCP scenarios considered, and (3) the climate natural variability.

As in the study of the mean climate values (D1.2), the last two uncertainty sources are commonly represented using the ensemble strategy. That is, once bias-correction is applied to all validated models, combination (ensemble) of the outputs provides an estimation of the uncertainty caused by the (past and future) climate variability. An ensemble is performed for each RCP scenario in order to evaluate the effect of the possible future economies. Projections are performed for derived variables (mainly extreme indices) using a continuous temporal evolution, while the changes in return periods were mapped to represent the spatial distribution in each future period.

The ensemble of projections is represented by using uncertainty areas. Particularly, it is considered as the 10th–90th percentile values and the median value for each year-horizon, calculated from all stations and models validated for each climate variable (Figure 5).

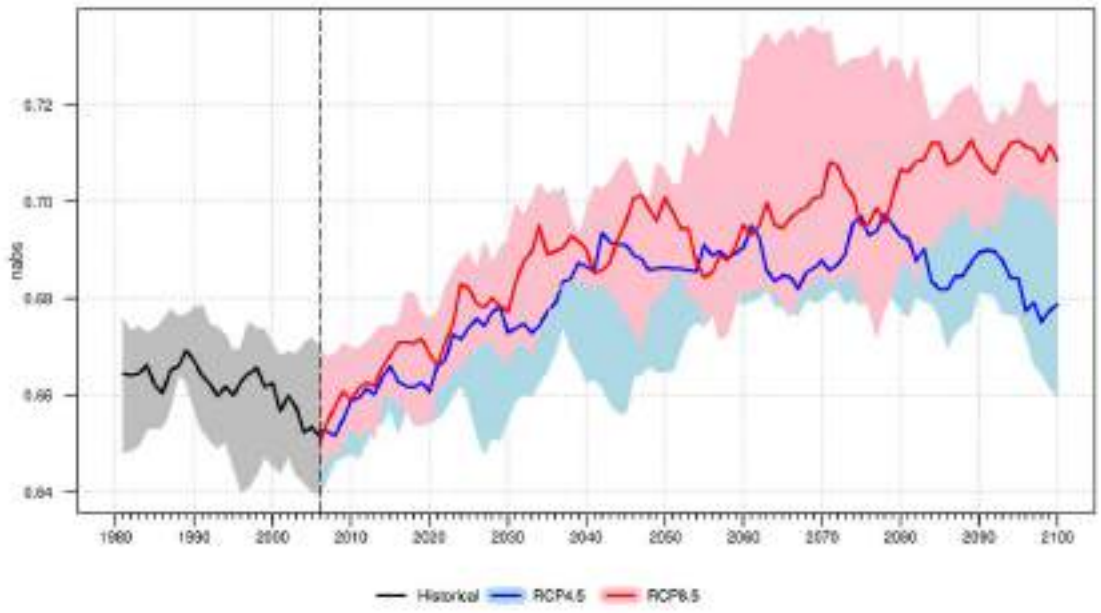

Figure 5. Example of ensemble strategy for derived variables. Panel shows climate projections of changes in the *n*-index for a random city. The ensemble median (solid lines) and the 10th–90th percentile values (shaded areas) are displayed. The vertical dashed line marks the end of the Historical data (2005).

A final ensemble was performed combining the main RCP scenarios to sort the climate change from the smallest to the greatest change. This product allowed obtaining representative samples of the uncertainty interval for each climate projection.

2.4.3. Robustness of the teleconnection-based method

In order to reduce possible effects of the climate change on the teleconnection-based method, it was applied a two-step robust technique:

(1) The method was trained with moving windows, whose optimum length is obtained by cross-validated hindcast (Sec. 2.2.4 of the D1.2). A wavelet analysis was also performed as a gauge test on the temporal variability/robustness of the oscillation periods for each teleconnection index in order to identify the most stable periods comparing with the optimum ones.

(2) Final fitting parameters are obtained from the last disposition (movement) of the optimum windows and, therefore, progressive climate changes do not affect the application of the parameters.

Therefore, the verification of the robustness was performed comparing the optimum lengths with the most stable oscillation periods of each teleconnection.

3. Results of validation

3.1. Climate scale

3.1.1. About this

Section 3.1 presents the validation results of the simulations applied to extreme events at a multi-decadal timescale (climate scale). The validation process consisted on the comparison of representative synthetic extreme events simulated by the climate models and the estimated using extended observations.

Results of validation are structured in three subsections according to the studied cities (Barcelona, Lisbon and Bristol) and their surrounding areas. In turn, each subsection enumerates the verification of all climate variables simulated using the climate models. Finally, Sec. 3.1.5 summarises the main results of the verification process for all the variables and cities.

3.1.2. Barcelona

3.1.2.1. Temperature

Extreme temperature is correctly simulated by all the downscaled models for Barcelona, except in two cases: NorESM1 for high return periods and MIROC-ESM-CHEM for low return periods (Figure 6).

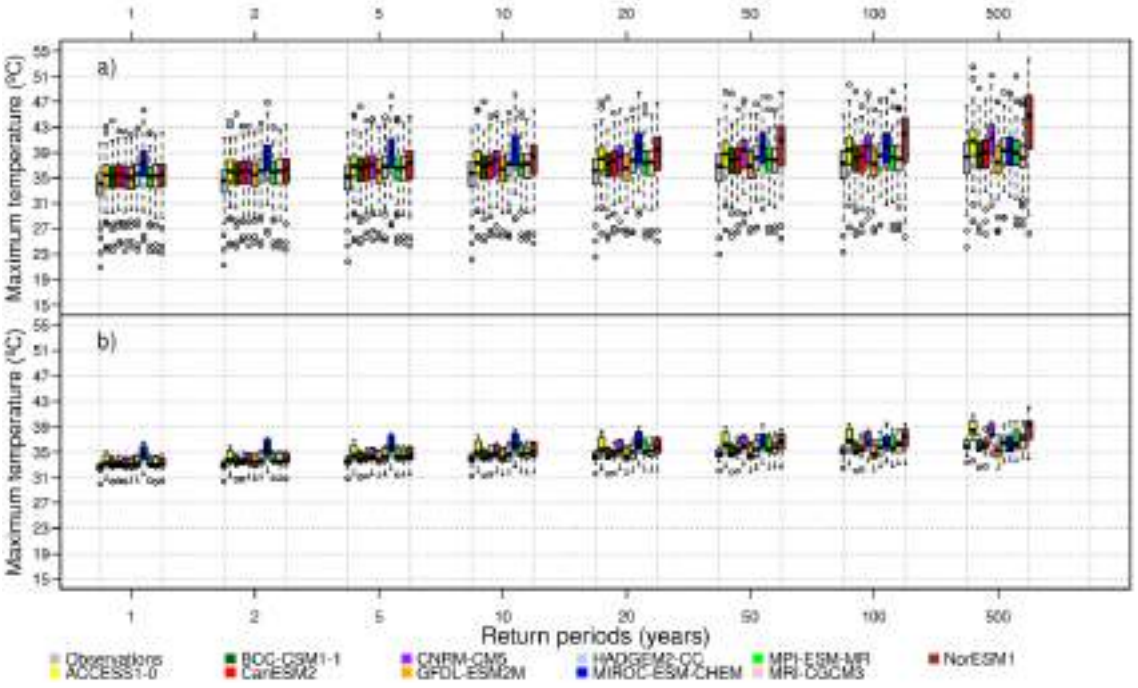

Figure 6. Validation of the climate simulation for extreme maximum temperature in Barcelona area: a) Ter-Llobregat system, b) Barcelona city. Box: 25th and 75th percentiles; whiskers: 5th and 95th percentiles; points: outliers.

The heat wave features, i.e. duration, mean intensity and maximum intensity, were adequately reproduced by the downscaling method (Figure 7). The validation process for Barcelona only presented remarkable biases in a few models. For instance, GFDL-ESM2M outputs overestimate mean and maximum intensities up to +2.5°C, while MRI-ESM-CHEM and ACCES1-0 overestimate the heat duration about +2 days (+50%). These biases are within the common error interval of the climate simulations and, therefore, they were corrected.

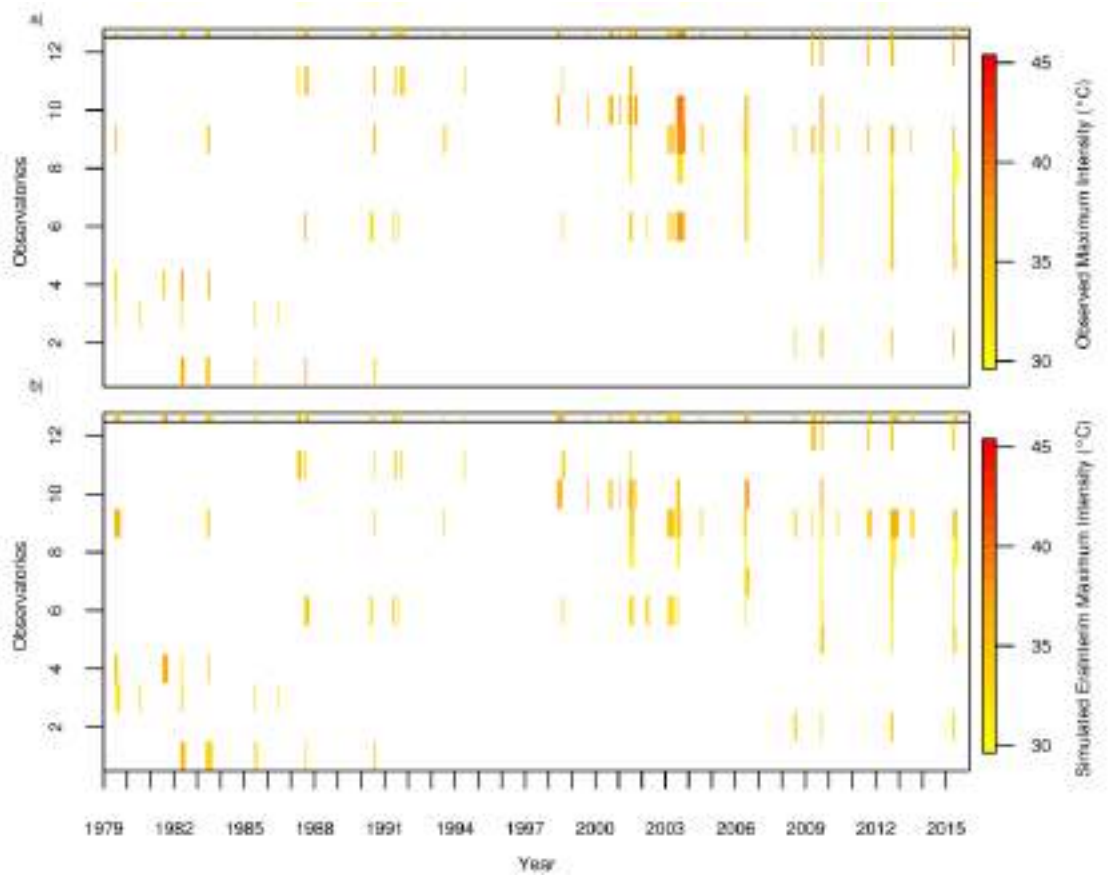

Figure 7. Climate simulation for maximum intensity of heat waves in Barcelona area: a) real observations, b) simulations obtained from downscaled ERA-Interim.

3.1.2.2. Rainfall

Subdaily rainfall is well simulated for Barcelona on the time resolution of 5-min (Figure 8). Probability distribution of both precipitation and n-index values of wet spells passed the Kolmogorov-Smirnov test for most of the cases, comparing historical experiments and observed time series. However, six downscaled climate models presented difficulties to simulate n-index for some observatories (Figure 8b). Despite of this problem, bias of the n-index distribution is zero and, therefore, it does not affect the results (thanks to that the method of empirical transfer functions is unbiased).

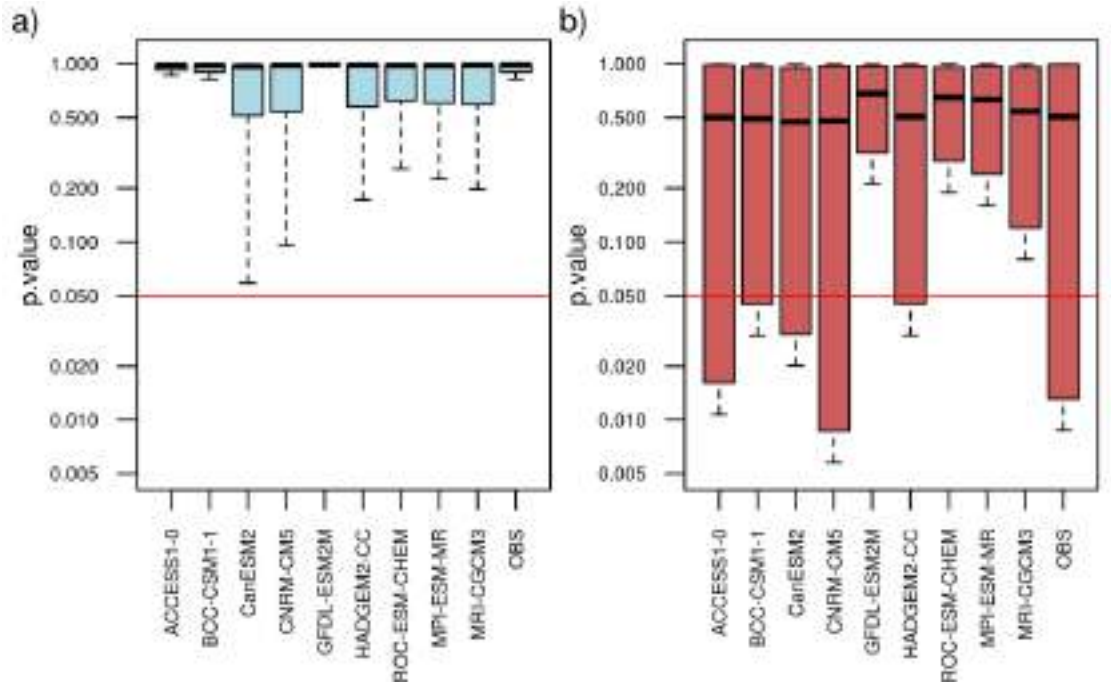

Figure 8. Kolmorov-Smirnov test p-value obtained by comparing probability distribution of subdaily precipitation observed in Barcelona and downscaled outputs from historical experiment: a) 5-minute values of precipitation, b) n-index values for the corresponding wet spells. Box: 25th and 75th percentiles; whiskers: 5th and 95th percentiles.

Maximum precipitation accumulated in 12 hours is well simulated by most of the models compared with the reference values (extended observations). Only GFDL-ESM2M outputs presented problems reproducing extreme rainfall in the Ter-Llobregat system (Figure 89). For Barcelona city, most of downscaled models slightly overestimate extreme precipitation.

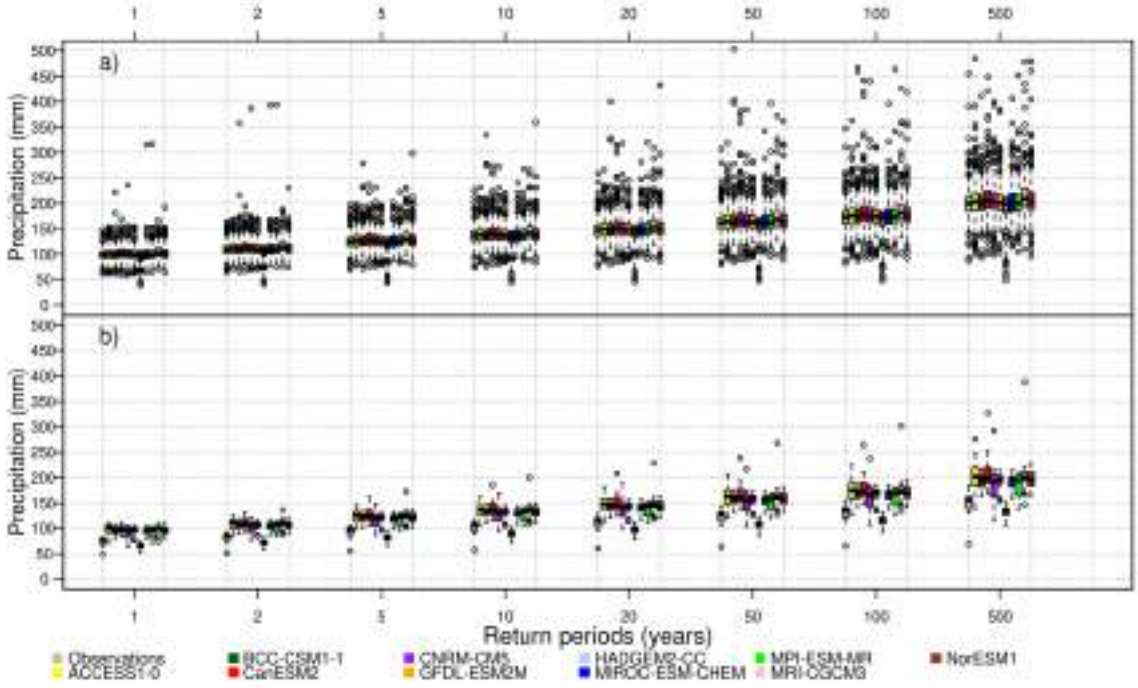

Figure 9. The same as Figure 5 but for extreme rainfall.

Regarding the validation of the drought, the historical trend is well simulated by all downscaled models. In fact, the SPEI was significantly decreasing about –0.5 dec^{-1} in the reference period (Figure 10).

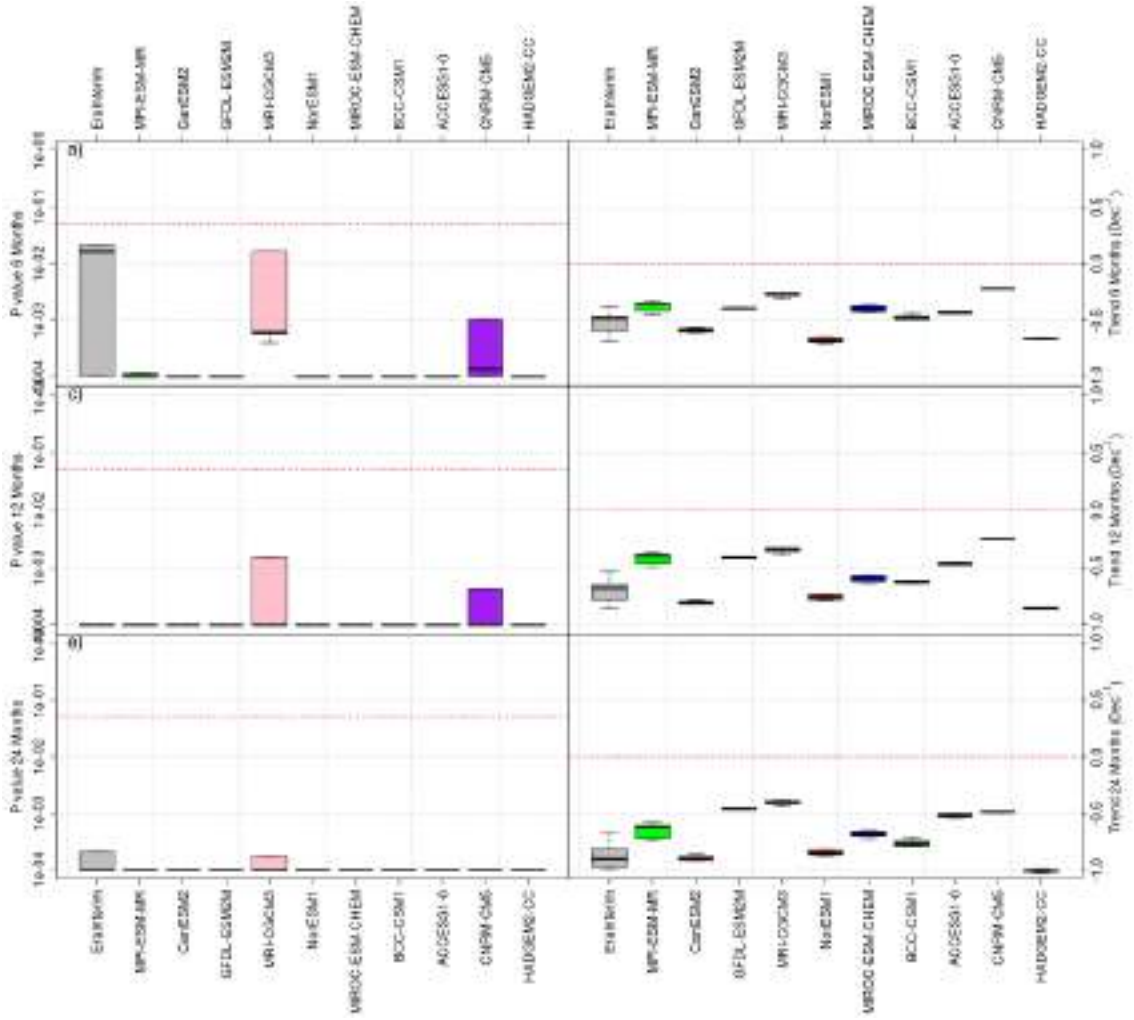

Figure 10. Validation of the climate simulation for SPEI in Barcelona area according to the significance of the historical trend (left) and the value of the decadal trend (right) for: a) 6-months moving windows, b) 12-months moving windows, c) 24-months moving windows. Box: 25th and 75th percentiles; whiskers: 5th and 95th percentiles.

3.1.2.3. Wind gust

Extreme wind in Barcelona is generally well simulated for low return periods, but is overestimated for high return periods (greater than 100 years). That is because length of the time series is usually less than 50 years and, therefore, theoretical distributions fitted can show difficulties to be fitted to the long-term natural variability (in this case with relatively negative cycle). However, it is a general systematic error that can be corrected without losing climatic signal in the probability distributions simulated by climate models.

Within in detail, HADGEM-CC and MIROC-ESM-CHEM outputs showed problems in the simulation of wind for Barcelona city (Figure 11). Particularly, they underestimate wind gust for low return periods, and overestimate for the highest return period (500 years).

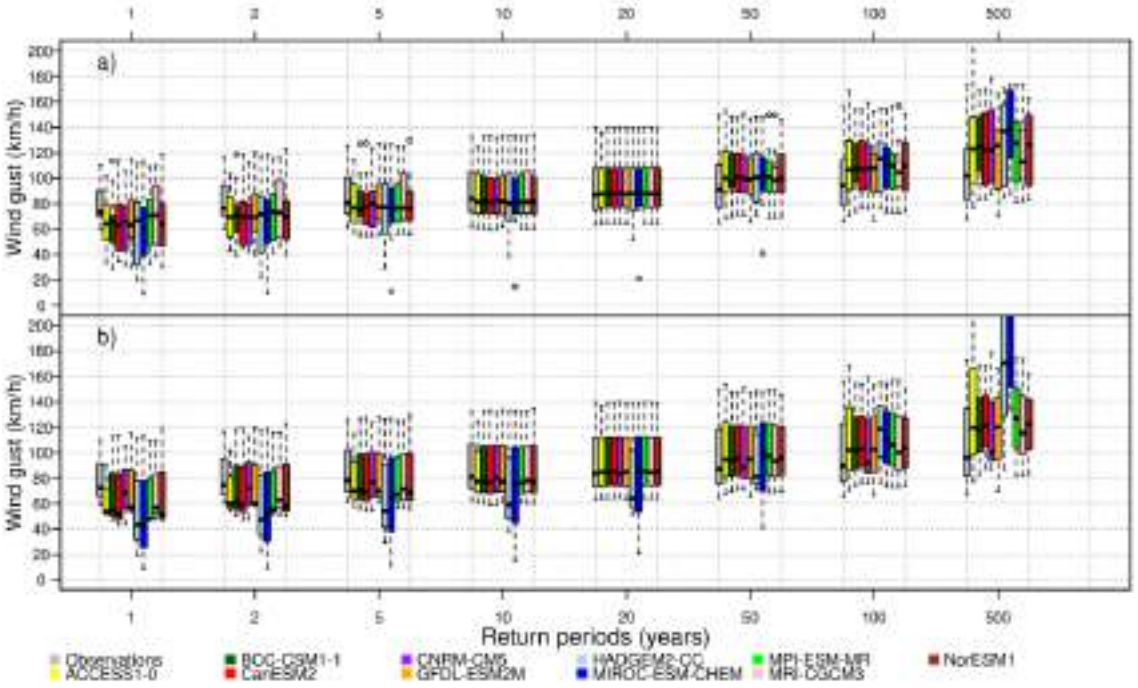

Figure 11. The same as Figure 5 but for extreme wind gust.

3.1.2.4. Oceanic variables

Regarding the oceanic variables simulated for Barcelona, the performance of all the downscaled models is adequate for the storm surge in all return periods (Figure 12). However, extreme height wave is generally underestimated for the highest return periods.

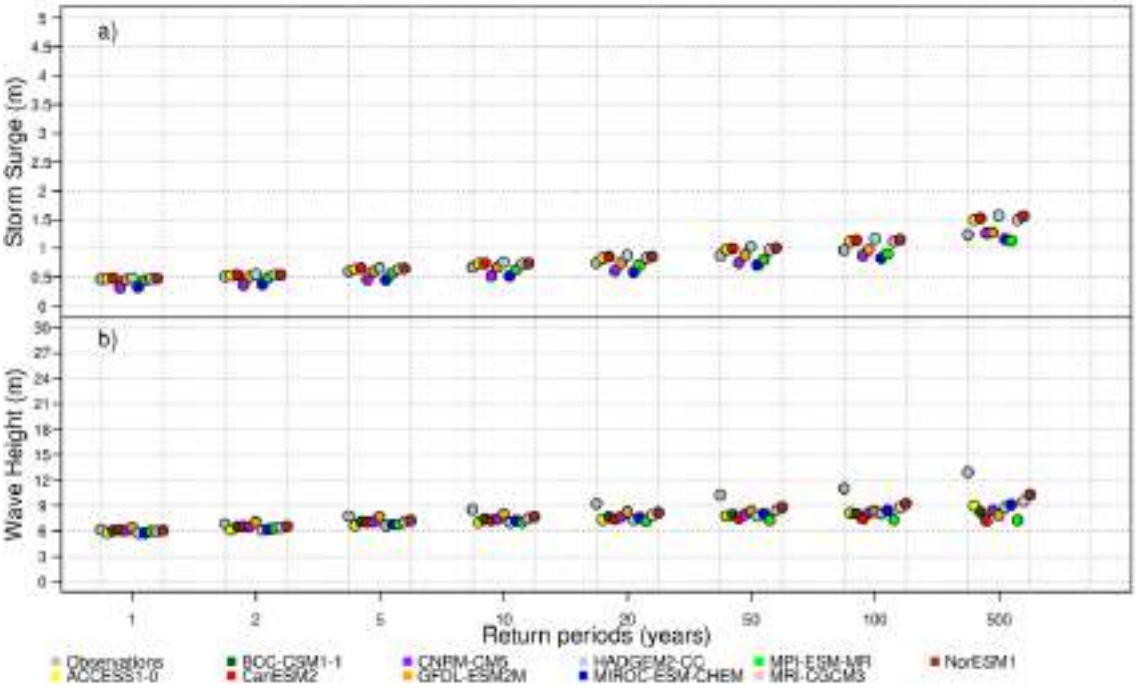

Figure 12. Validation of the climate simulation for extreme oceanic values in the Barcelona buoy according to: a) Storm surge and b) Wave height.

3.1.3. Lisbon

3.1.3.1. Temperature

Extreme maximum temperature is correctly simulated by half of the downscaled models, for both low and high return periods (Figure 13). The rest of the model outputs presented a systematic error about 3 or 4°C.

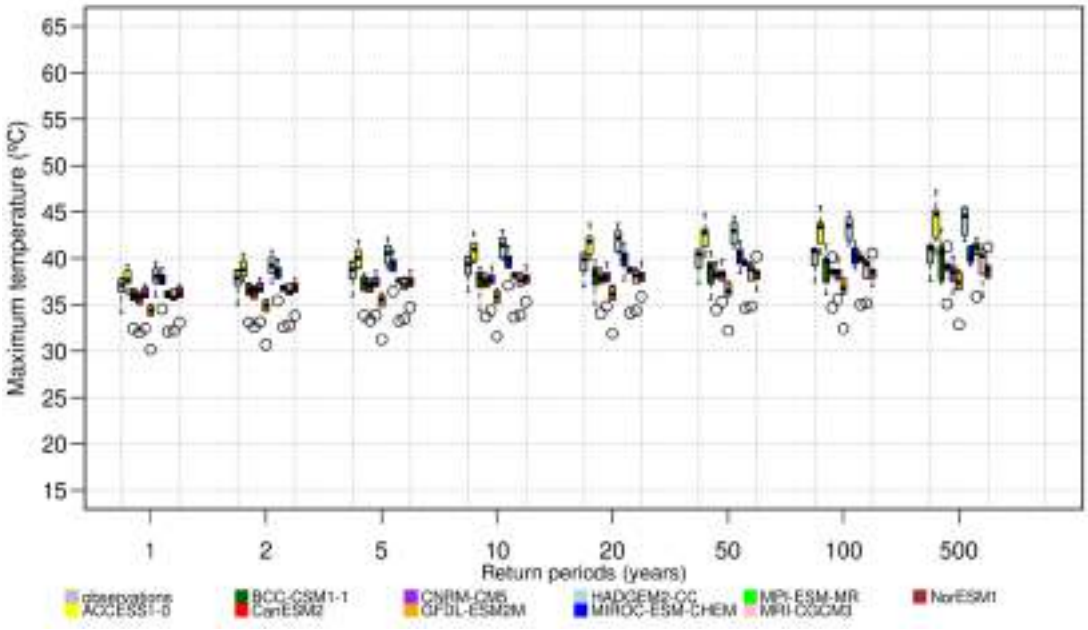

Figure 13. Validation of the climate simulation for extreme maximum temperature in Lisbon. Box: 25th and 75th percentiles; whiskers: 5th and 95th percentiles; points: outliers.

As in Barcelona, the duration, mean intensity and maximum intensity of heat wave in Lisbon are adequately reproduced by the downscaling method using ERA-Interim reanalysis (Figure 14). However, the validation process shows an important underestimation (about –2.5°C) in the mean and maximum intensities for all downscaled model outputs except for MIROC-ESM-CHEM, ACCESS1-0 and HADGEM2-CC. The duration of the heat waves is better simulated for the outputs, except by the downscaled NorESM1 that presented a bias up to +2 days (+50%). These errors range within the common error interval found in the climate simulations and, therefore, they were corrected.

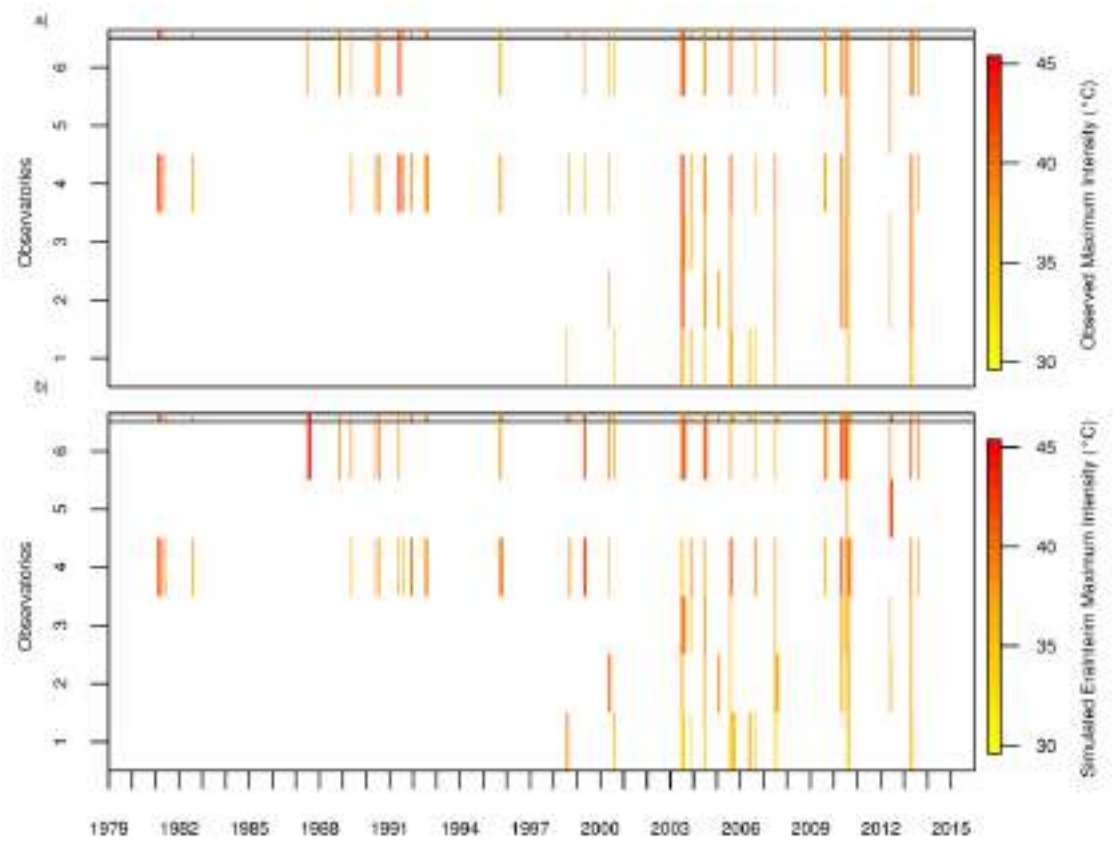

Figure 14. Climate simulation for maximum intensity of heat waves in Lisbon area: a) real observations, b) simulations obtained from downscaled ERA-Interim.

3.1.3.2. Rainfall

Subdaily rainfall is also well simulated for Lisbon, but in this case the maximum available time resolution was 1-hour (Figure 15). Probability distribution of precipitation values of wet spells passed the Kolmogorov-Smirnov test for most of the cases, comparing historical experiments and observed time series. Regarding the n-in2dex feature, sub-daily time-series of one observatory was not adequately simulated by nine downscaled climate models (Figure 15b). However, in a similar way to Barcelona, bias of the n-index distribution is also zero for Lisbon and therefore it does not affect the results.

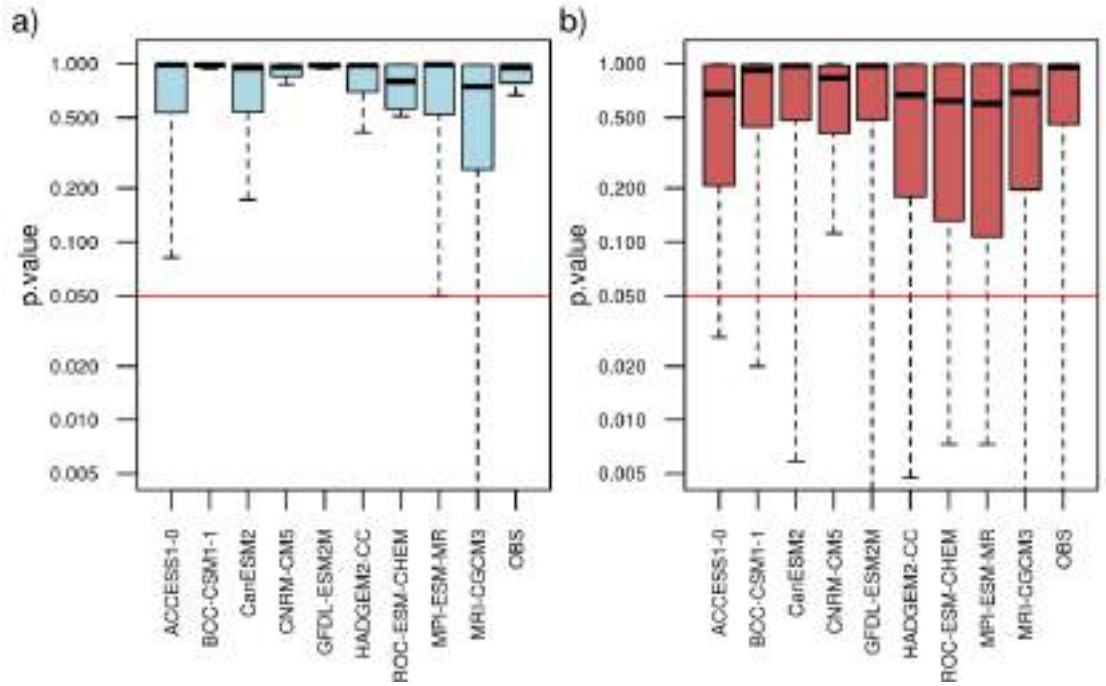

Figure 15. Kolmorov-Smirnov test p-value comparing probability distribution of subdaily precipitation observed in Lisbon and downscaled outputs from historical experiment: a) 1-hour values of precipitation, b) n-index values for the corresponding wet spells. Box: 25th and 75th percentiles; whiskers: 5th and 95th percentiles.

Maximum precipitation accumulated in 12 hours is correctly estimated by every model. However, some stations present underestimation down to 50% (Figure 16).

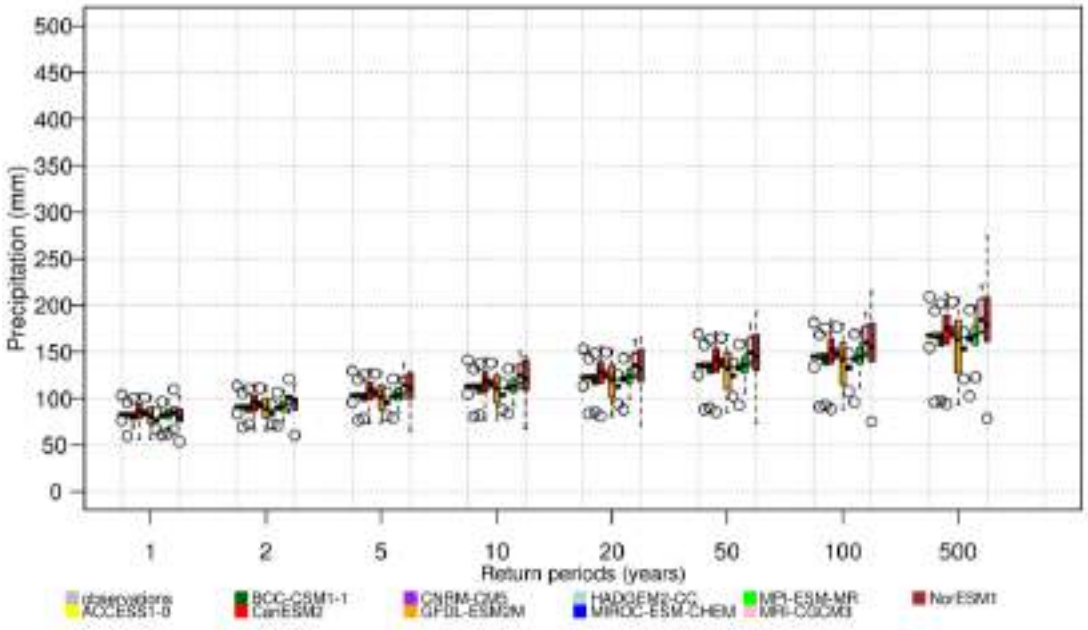

Figure 16. The same as Figure 10 but for extreme rainfall.

For the drought simulation, the validation process concluded that three downscaled models did not pass the tests for Lisbon: GFDL-ESM2M, ACCES1-0 and CNRM-CM5. In particular, these models obtained statistically significant differences in the simulated historical trend respect to the observed one (Figure 17).

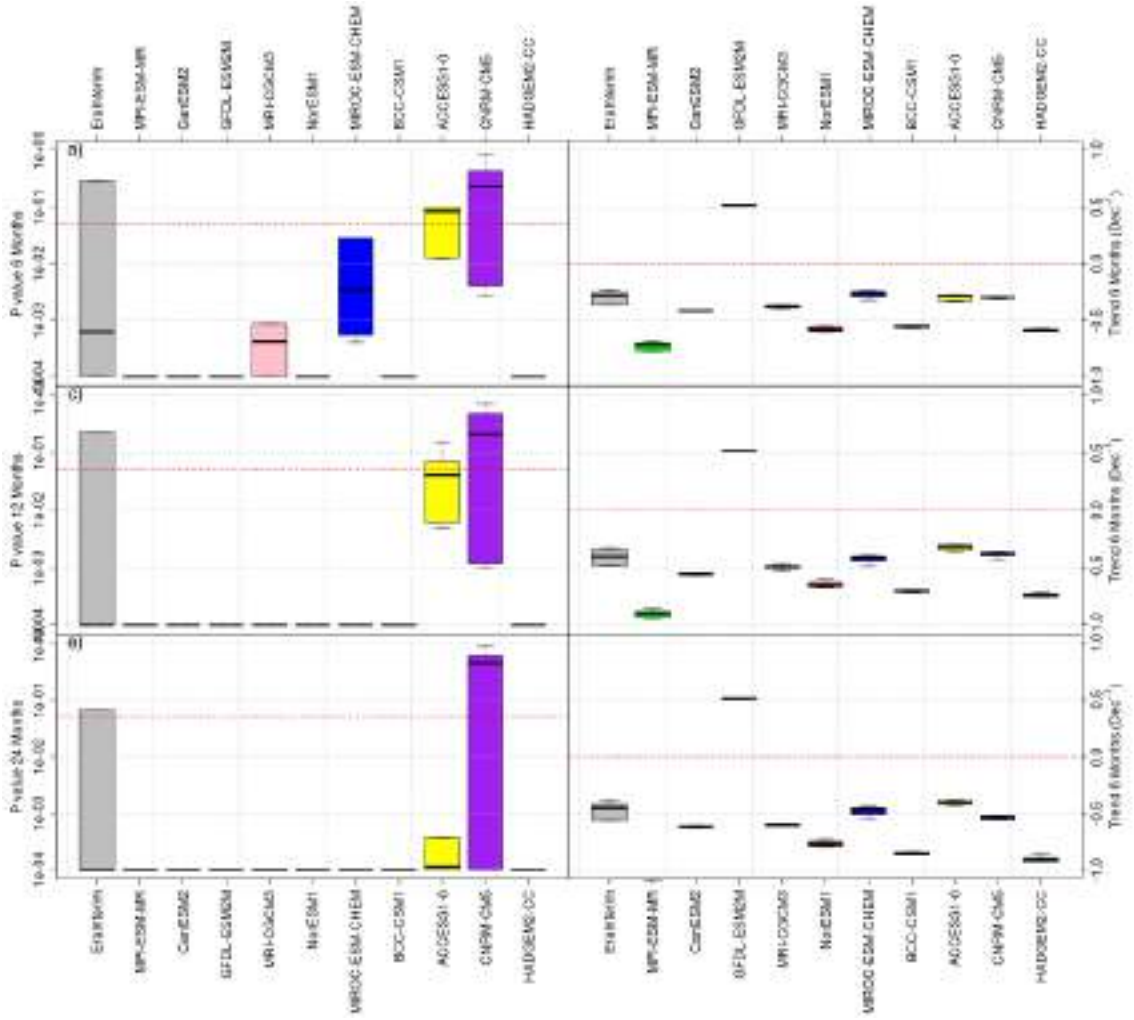

Figure 17. Validation of the climate simulation for SPEI in Lisbon area according to the significance of the historical trend (left) and the value of the decadal trend (right) for: a) 6-months moving windows, b) 12-months moving windows, c) 24-months moving windows.

3.1.3.3. Wind gust

Extreme wind gust is correctly estimated by every model for most of the stations. However, half of the models tend to underestimate wind gusts in some stations in the case of return periods greater than 100 years (Figure 18).

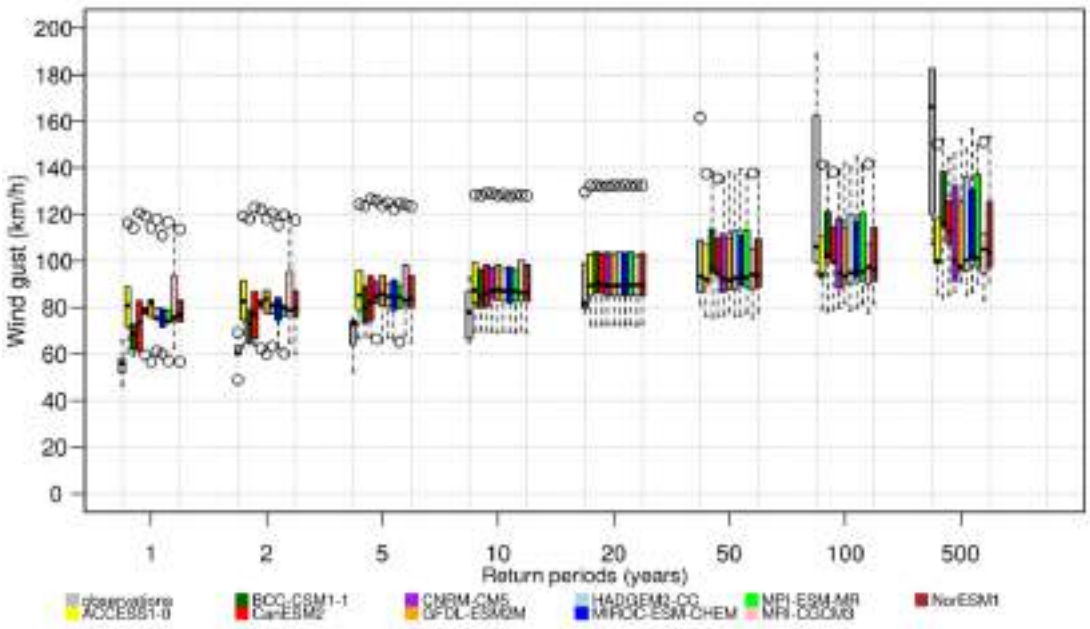

Figure 18. The same as Figure 10 but for extreme wind gust.

3.1.3.4. Oceanic variables

Storm surge is correctly estimated by most of the models for every return period (Figure 19). Only the MIROC-ESM-CHEM output underestimates the values for the longest return periods.

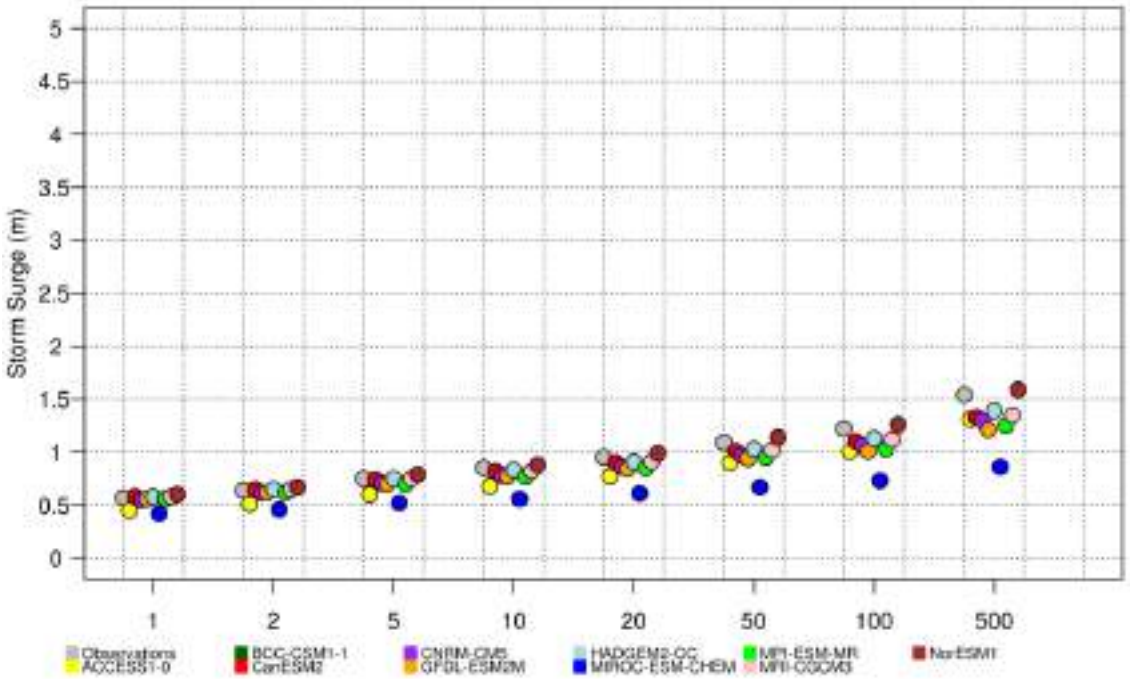

Figure 19. Validation of the climate simulation for extreme storm surge in the Cascais buoy.

3.1.4. Bristol

3.1.4.1. Temperature

Half of the models are not able to estimate accurately maximum temperature in Bristol for any of the return periods considered. Except GFDL-ESM2M, models tend to overestimate maximum temperature, being greater this deviation for larger return periods (Figure 20).

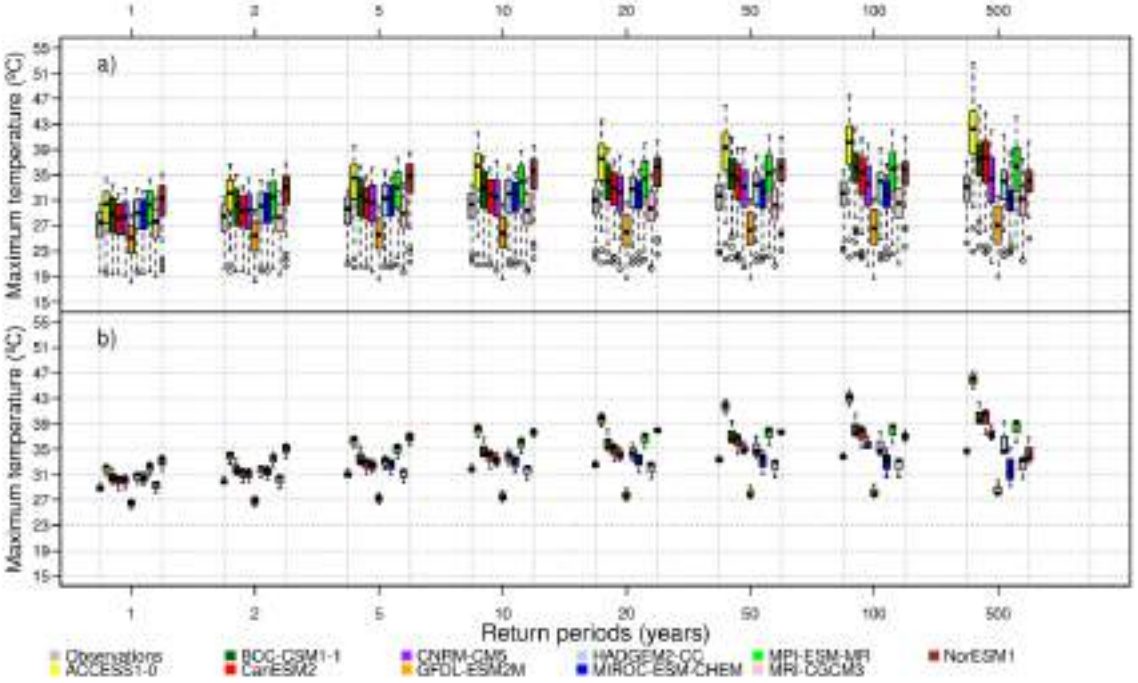

Figure 20. Validation of the climate simulation for extreme maximum temperature in Bristol area: a) Southwest England - South Wales and b) Bristol city. Box: 25th and 75th percentiles; whiskers: 5th and 95th percentiles; points: outliers.

The heat wave features (duration, mean intensity and maximum intensity) in Bristol are generally well simulated by the downscaling method using ERA-Interim reanalysis. However, the most intense events (2013-2014) are modelled with important differences (Figure 21). In fact, the validation process showed remarkable problems in half of the model outputs (Figure 22): GFDL-ESM2M underestimates the wave duration in almost 100% of the cases and therefore this simulation was rejected. ACCESS1-0 overestimates the duration about +50% and thus it was corrected. Finally, MPI-ESM-MR, NorESM1, BCC-CSM1 and ACCESS1-0 overestimate the maximum intensity in +2°C. In this last case, a correction was possible.

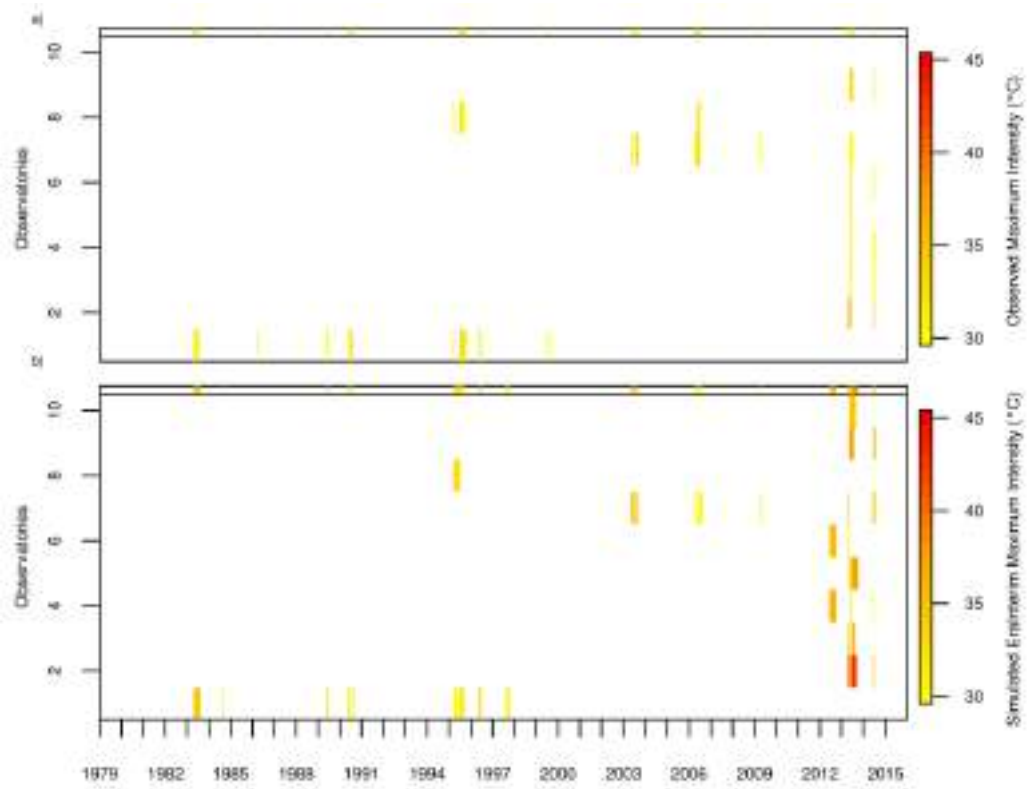

Figure 21. Climate simulation for maximum intensity of heat waves in Bristol area: a) real observations, b) simulations obtained from downscaled ERA-Interim.

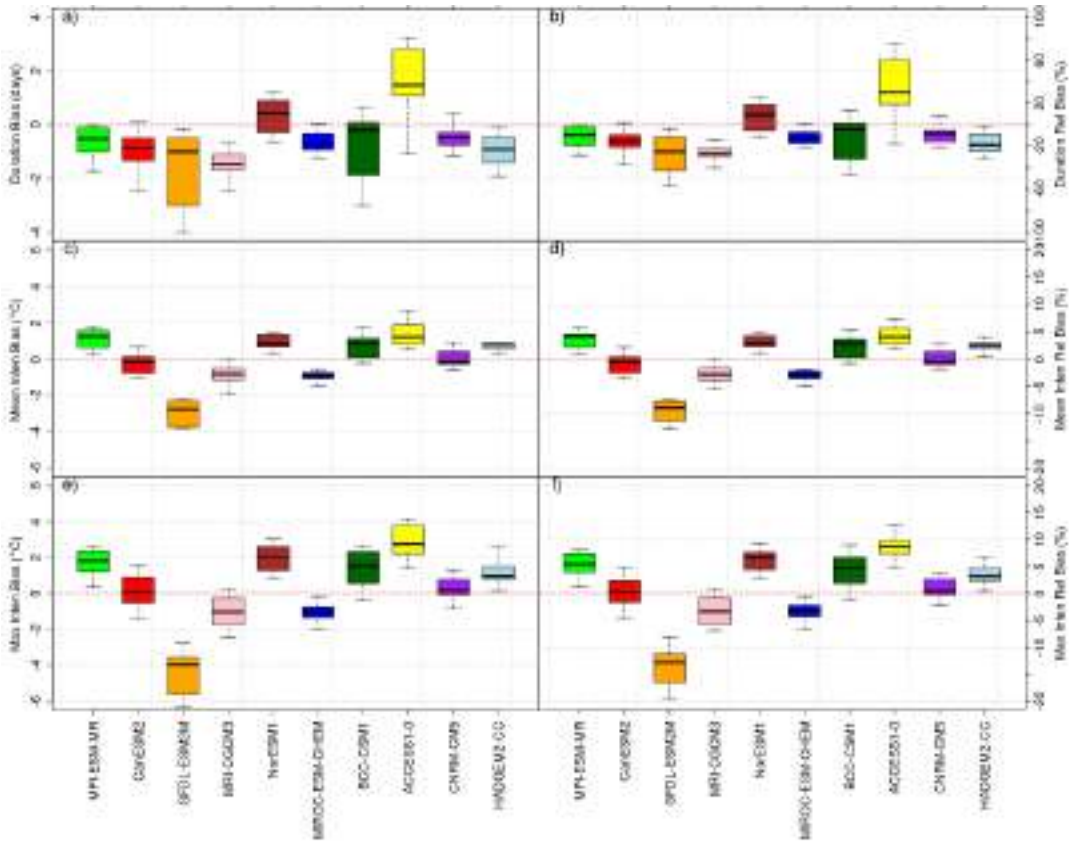

Figure 22. Validation of the simulation of heat wave features in Bristol area: a) duration, b) mean intensity, c) maximum intensity. Box: 25th and 75th percentiles; whiskers: 5th and 95th percentiles.

3.1.4.2. Rainfall

For Bristol, subdaily rainfall is generally well simulated by the historical experiment of the downscaled climate models (Figure 23). Probability distribution of n-index values of wet spells passed the Kolmogorov-Smirnov test for most of the cases, comparing historical experiments and observed time series. The performance of the *n*-index simulation is poorer in four cases (BCC-CSM1-1, CanESM2, GFDL-ESM2M and MRI-CGSM3) for more than 25% of the time-series (Figure 23b). However, in a similar way to Barcelona and Lisbon, bias of the n-index distribution is also zero for Bristol and therefore it does not affect the results.

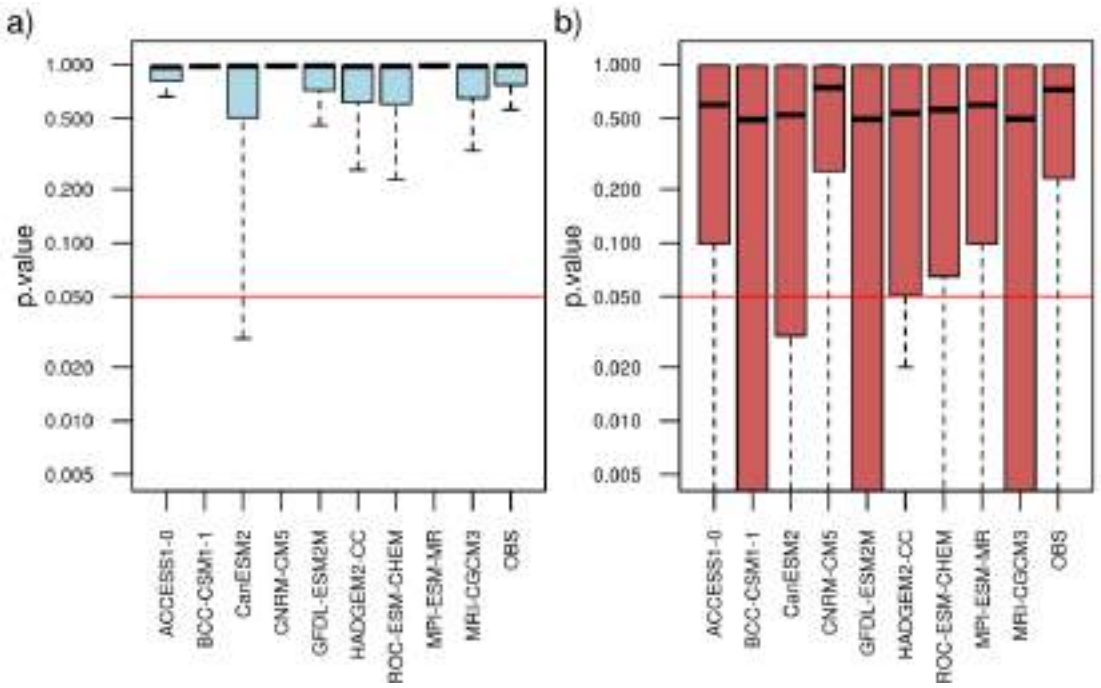

Figure 23. Kolmorov-Smirnov test p-value comparing probability distribution of subdaily precipitation observed in Bristol and downscaled outputs from historical experiment: a) 1-hour values of precipitation, b) n-index values for the corresponding wet spells. Box: 25th and 75th percentiles; whiskers: 5th and 95th percentiles.

For both short and long return periods, most of the models estimate correctly maximum precipitation in 12h (Figure 24). Only the downscaled BCC-CSM1 output underestimates extreme rainfall in Bristol and thus it is not valid for more than 50% of the analysed stations.

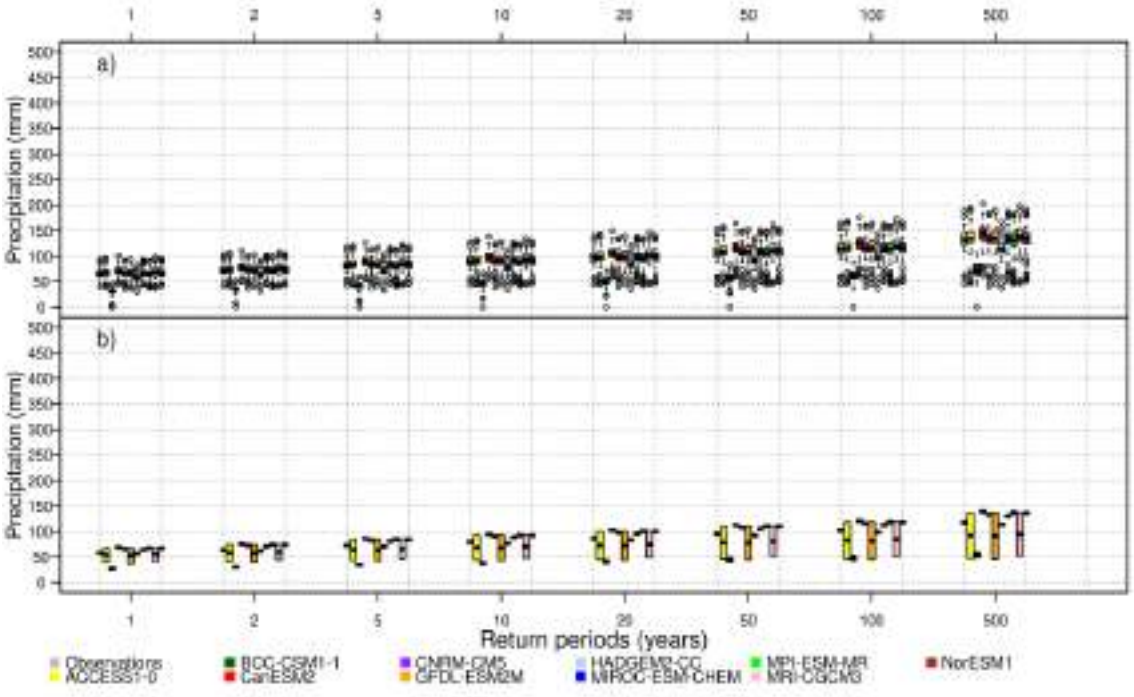

Figure 24. The same as Figure 12 but for extreme rainfall.

On the other hand, validation of the drought simulation for Bristol showed that five downscaled model did not pass the tests: GFDL-ESM2M, MIROC-ESM-CHEM, BCC-CSM1, CNRM-CM5 and HADGEM2-CC. These model outputs simulated a historical trend significantly different respect to the observed one (Figure 25).

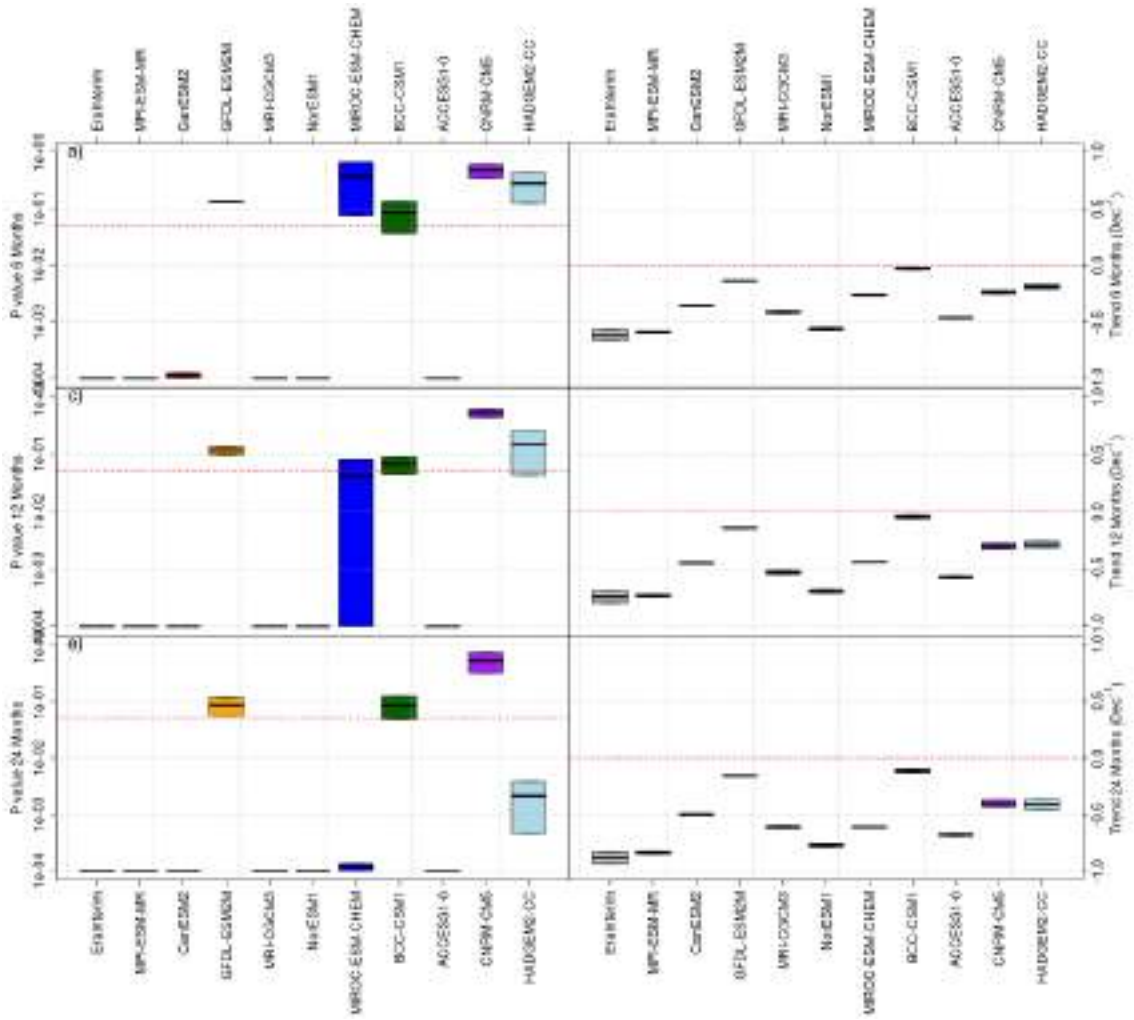

Figure 25. Validation of the climate simulation for SPEI in Bristol area according to the significance of the historical trend (left) and the value of the decadal trend (right) for: a) 6-months moving windows, b) 12-months moving windows, c) 24-months moving windows. Box: 25th and 75th percentiles; whiskers: 5th and 95th percentiles.

3.1.4.3. Wind gust

Extreme wind gust validation is very successful in Bristol as every model estimates the maximum value with a high level of accuracy for every return period in more than 70% of the stations. The good performance of the climate simulations is remarkable even for the greatest return periods of 100 and 500 years (Figure 26).

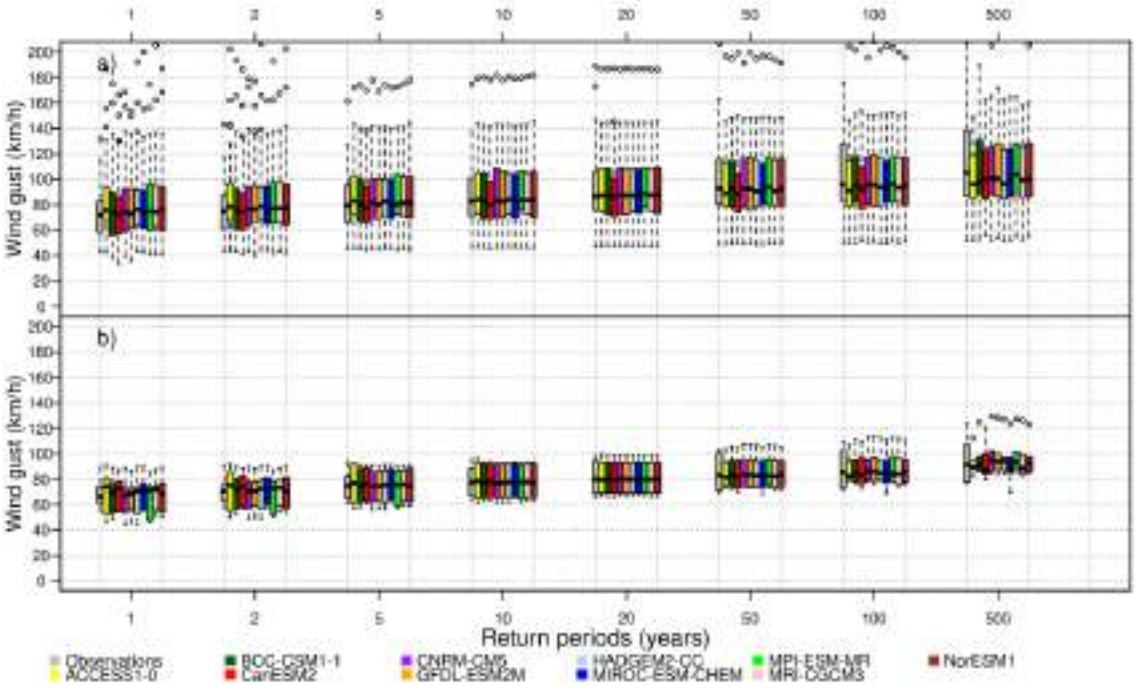

Figure 26. The same as Figure 12 but for extreme wind gust.

3.1.4.4. Oceanic variables

Storm surge and wave height estimation is reasonably good for return periods smaller than 50 years. However, for longer return periods of 100 and 500 years, every model output overestimates oceanic extremes, especially for wave height (Figure 27).

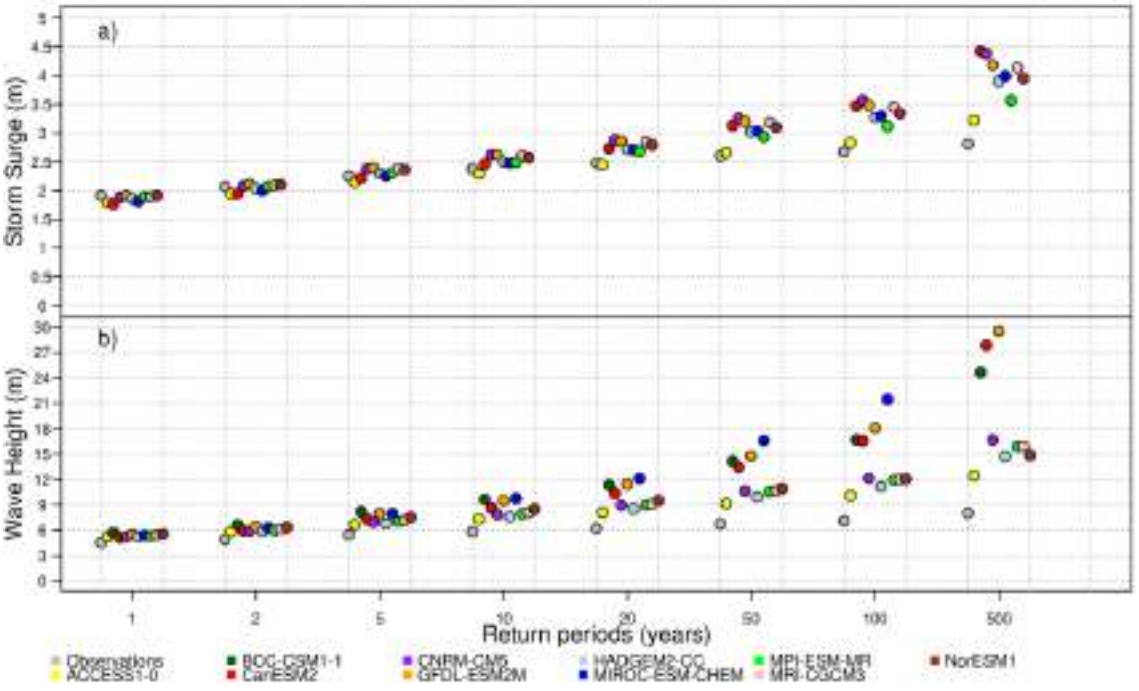

Figure 27. Validation of the climate simulation for extreme oceanic values in the Bristol buoy according to: a) Storm surge and b) Wave height.

3.1.5. Summary of the validation for the climate scale

For high return periods before correction, simulation of extreme temperature was only acceptable in a few climate models applied to Lisbon and Bristol, while most of the downscaled models passed the tests for Barcelona (Table 3). Wind gust extremes presented problems to be simulated properly in the Barcelona area, and the rest of variables perform correctly under most of climate models.

Table 3. Summary of the validation process for long-term climate simulations downscaled for the three cities.

Return period	CMIP5 climatic models	Max. Temp.			Rainfall			Snowfall			Wind gust			Storm surge			Wave height		
		Barcelona	Bristol	Lisbon	Barcelona	Bristol	Lisbon	Barcelona	Bristol	Lisbon	Barcelona	Bristol	Lisbon	Barcelona	Bristol	Lisbon	Barcelona	Bristol	Lisbon
2 years	ACCESS1-0																		
	BCC-CSM1-1																		
	CanESM2																		
	CNRM-CM5																		
	GFDL-ESM2M																		
	HADGEM2-CC																		
	MIROC-ESM-CHEM																		
	MPI-ESM-MR																		
	MRI-CGCM3																		
	NorESM1																		
10 years	ACCESS1-0																		
	BCC-CSM1-1																		
	CanESM2																		
	CNRM-CM5																		
	GFDL-ESM2M																		
	HADGEM2-CC																		
	MIROC-ESM-CHEM																		
	MPI-ESM-MR																		
	MRI-CGCM3																		
	NorESM1																		
100 years	ACCESS1-0																		
	BCC-CSM1-1																		
	CanESM2																		
	CNRM-CM5																		
	GFDL-ESM2M																		
	HADGEM2-CC																		
	MIROC-ESM-CHEM																		
	MPI-ESM-MR																		
	MRI-CGCM3																		
	NorESM1																		

KS-test passed for more than 70% of the analysed stations.
KS-test passed between 50% and 70% of the analysed stations.
KS-test passed for less than 50% of the analysed stations.
Not available or variable not identified as hazard for the city.

3.2. Annual and decadal scales

3.2.1. About this

Section 3.2 presents the results of the validation process for the near-term climate (decadal) forecast based on two methods: drift-corrected CMIP5 models and teleconnections. As commented in the multi-decadal timescale, extreme events simulated from sub-decadal time-series were compared with the extreme values obtained from the extended observations.

Validation results are structured in three subsections according to the studied cities (Barcelona, Lisbon and Bristol) and their surrounding areas. The CMIP5 decadal outputs correspond to temperature, rainfall and wind, while the teleconnection-based simulations are available only for temperature and rainfall. Finally, Sec. 3.2.5 summarises the main results of the validation process for all cases.

3.2.2. Barcelona

3.2.2.1. Temperature

The validation of maximum temperature shows that the estimation behaves well for most of the models in every return period. Exceptionally, drift-corrected MPI-ESM-LR and MRI-CGCM3 outputs presented problems of overestimation in temperature for return periods greater than 10 years, so they should not be taken into account in these cases (Figure 28).

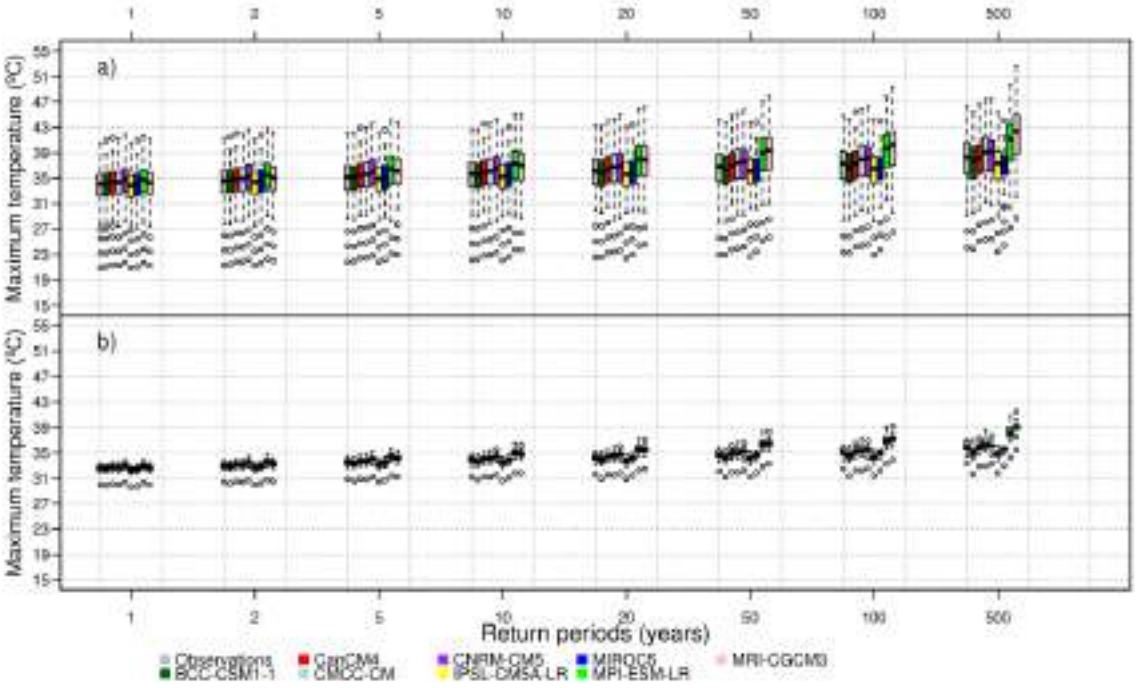

Figure 28. Validation of drift-corrected decadal simulation for extreme maximum temperature in Barcelona area: a) Ter-Llobregat system, b) Barcelona city.

3.2.2.2. Rainfall

Teleconnection-based decadal simulations perform adequately for extreme rainfall in Barcelona. Its estimation is quite accurate for every return period (Figure 29). However, drift-corrected decadal models presented poor results: only the model BCC-CSM1-1 passes the main climate test for Barcelona.

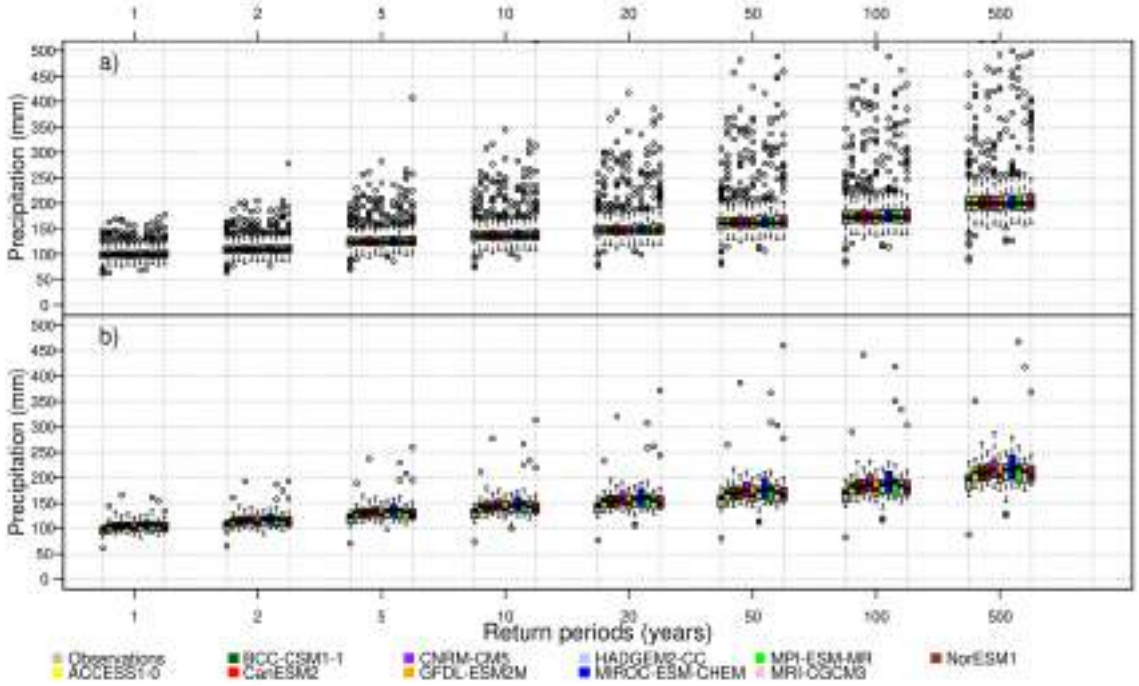

Figure 29. Validation of teleconnection-based decadal simulations for extreme daily rainfall in Barcelona area: a) Ter-Llobregat system, b) Barcelona city.

3.2.3. Lisbon

3.2.3.1. Temperature

Downscaled climate models tend to slightly underestimate extreme maximum temperature along most of return periods in their decadal simulation for Lisbon (Figure 30). Thus, only half of the models pass the validation test.

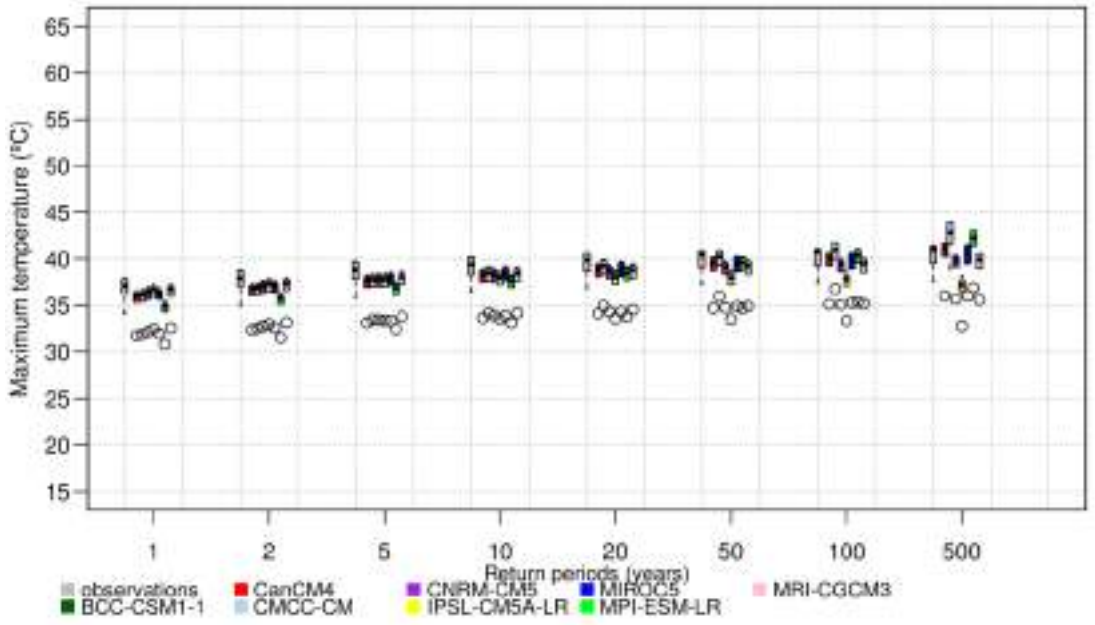

Figure 30. Validation of drift-corrected decadal simulations for extreme maximum temperature in Lisbon.

3.2.3.2. Rainfall

Only three downscaled models passed the verification test for extreme rainfall in Lisbon: BCC-CSM1-1, IPSL-CM5A-LR and MIROC5. Regarding teleconnection-based decadal estimations, all model outputs are reasonably good taking into consideration every return period (Figure 31).

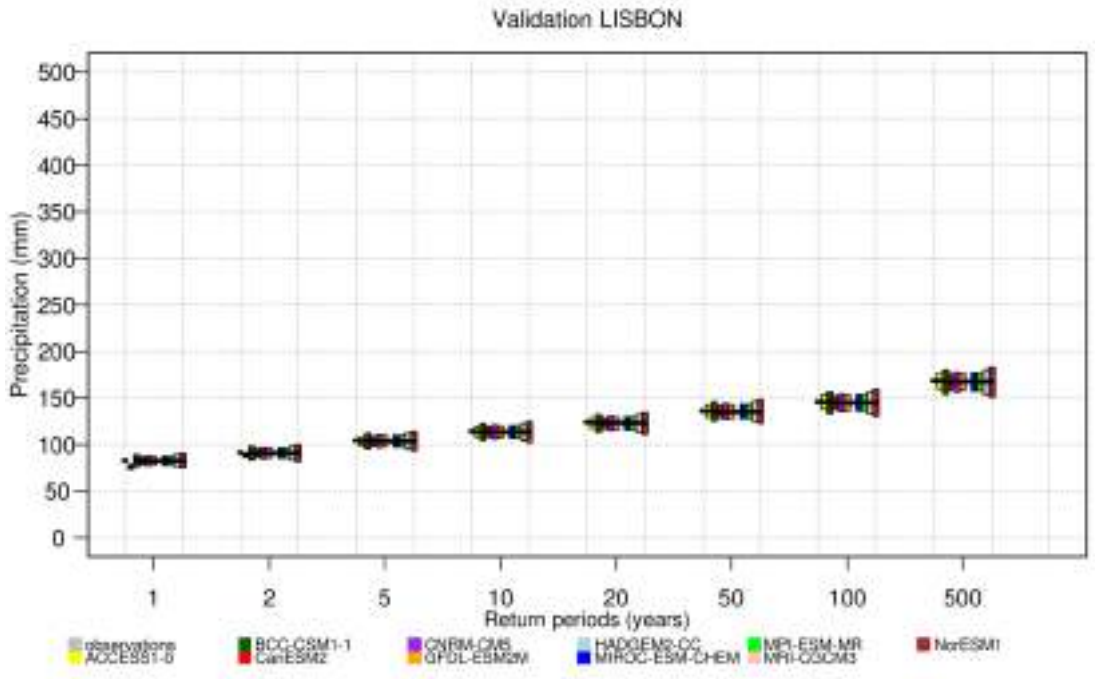

Figure 31. Validation of teleconnection-based decadal simulations for extreme daily rainfall in Lisbon.

3.2.4. Bristol

3.2.4.1. Temperature

Extreme temperature estimation is correct for every model except for IPSL-CM5A-LR for short return periods because it tends to underestimate temperature (Figure 32). As the return period gets longer, this model improves its behaviour and, on the other hand, MRI-CGCM3 output fails the validation test.

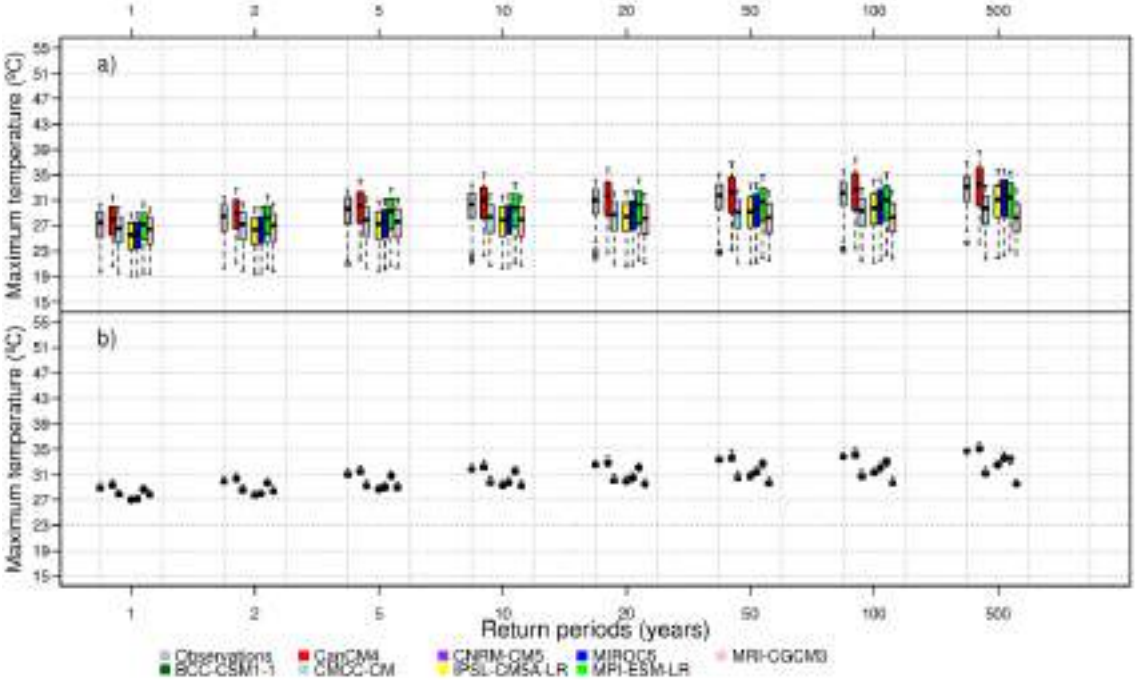

Figure 32. Validation of drift-corrected decadal simulations for extreme maximum temperature in Bristol area: a) Southwest England - South Wales and b) Bristol city.

3.2.4.2. Rainfall

Only two downscaled models passed the validation test for extreme daily rainfall in Bristol: CanCM4 and CNRM-CM5. The estimation of the rest of the models is not valid for any of the stations considered. Regarding teleconnection-based decadal estimation, all of the model outputs perform well and pass the validation test (Figure 33).

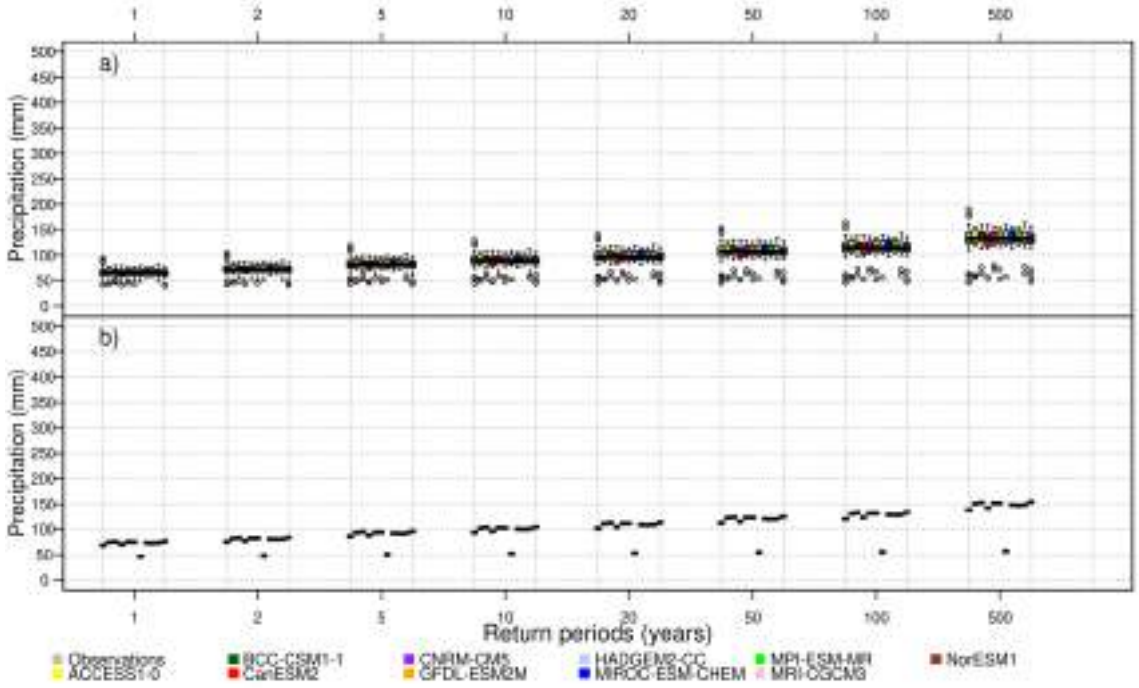

Figure 33. Validation of teleconnection-based decadal simulations for extreme daily rainfall in Bristol area: a) Southwest England - South Wales and b) Bristol city.

3.2.5. Summary of the annual and decadal validation

Temperature is well simulated by most of the drift-corrected decadal models considering low and high return periods (Table 5). Rainfall is better simulated by decadal teleconnections combined with climate models. Wind gust extremes are not correctly simulated for Lisbon, and snowfall presented problems in Barcelona for the highest return periods.

Table 4. Summary of the validation process for near-term (decadal) climate simulations according to two approaches: Combination of teleconnections with climate models (left) and drift-corrected decadal models (right).

Return period	Downscaled models combined with decadal teleconnexions	Maximum temperature			Rainfall		
		Barcelona	Bristol	Lisbon	Barcelona	Bristol	Lisbon
2 years	ACCESS1-0						
	BCC-CSM1-1						
	CanESM2						
	CNRM-CM5						
	GFDL-ESM2M						
	HADGEM2-CC						
	MIROC-ESM-CHEM						
	MPI-ESM-MR						
	MRI-CGCM3						
	NorESM1						
10 years	ACCESS1-0						
	BCC-CSM1-1						
	CanESM2						
	CNRM-CM5						
	GFDL-ESM2M						
	HADGEM2-CC						
	MIROC-ESM-CHEM						
	MPI-ESM-MR						
	MRI-CGCM3						
	NorESM1						
100 years	ACCESS1-0						
	BCC-CSM1-1						
	CanESM2						
	CNRM-CM5						
	GFDL-ESM2M						
	HADGEM2-CC						
	MIROC-ESM-CHEM						
	MPI-ESM-MR						
	MRI-CGCM3						
	NorESM1						

Return period	CMIP5 decadal models drift-corrected	Maximum temperature			Rainfall			Snowfall			Wind Gust		
		Barcelona	Bristol	Lisbon	Barcelona	Bristol	Lisbon	Barcelona	Bristol	Lisbon	Barcelona	Bristol	Lisbon
2 years	BCC-CSM1-1												
	CanCM4												
	CMCC-CM												
	CNRM-CM5												
	IPSL-CM5A-LR												
	MIROC5												
	MPI-ESM-LR												
	MRI-CGCM3												
10 years	BCC-CSM1-1												
	CanCM4												
	CMCC-CM												
	CNRM-CM5												
	IPSL-CM5A-LR												
	MIROC5												
	MPI-ESM-LR												
	MRI-CGCM3												
100 years	BCC-CSM1-1												
	CanCM4												
	CMCC-CM												
	CNRM-CM5												
	IPSL-CM5A-LR												
	MIROC5												
	MPI-ESM-LR												
	MRI-CGCM3												

KS-test passed for more than 70% of the analysed stations
KS-test passed between 50% and 70% of analysed stations
KS-test passed for less than 50% of the analysed stations
Model did not pass the main climate tests for the city
Variable not identified as hazard for the city

3.3. Seasonal timescale

3.3.1. About this

Section 3.3 presents the results of the validation carried out for the seasonal forecast at local scale based on two methods: the CFSv4 and teleconnections. As seen in the annual and decadal timescales, climate variables simulated by teleconnections are temperature and precipitation, while the downscaling outputs of the CFSv4 also include extremes for wind.

These results are structured in three subsections according to the studied cities and their surrounding areas. Finally, Sec. 3.3.5 summarises the main results of the validation process for all variables and cities.

3.3.2. Barcelona

3.3.2.1. Temperature

Cross-validation

The dynamical approach based on downscaled CFSv4 showed significant skill in temperature forecasting, but with a mean absolute error slightly lower than the reference climatology-based prediction (i.e. SAE < 1, Figure 34).

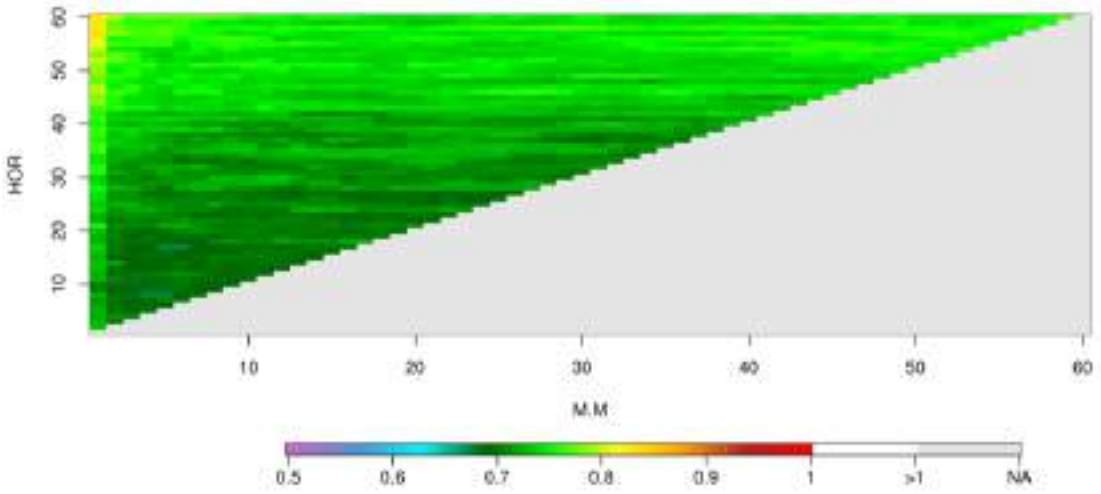

Figure 34. Validation of the dynamical approach of the seasonal forecast (downscaled CFSv4) for temperature in Barcelona, according to the Standardized Absolute Error (SAE). Y-axis represents the horizon (days) and the x-axis represents the moving average windows (days).

Regarding seasonal forecast based on teleconnections, the model performance is good for temperature at horizons greater than 6 months. In particular, a 2-month moving window is the most optimum for predicting a 6-month horizon, and a 6-month moving windows is the best to predict a 12-month horizon (Figure 35).

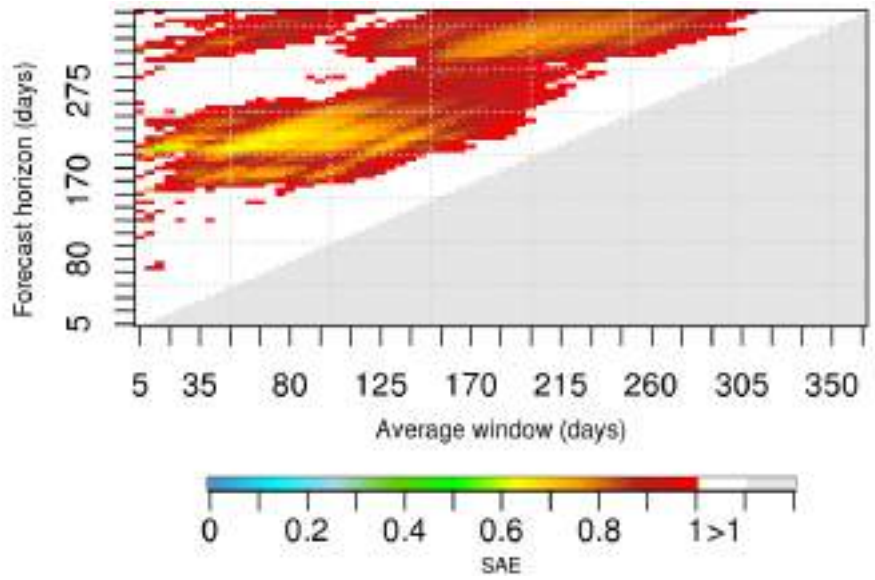

Figure 35. Validation of the teleconnection-based seasonal forecast for temperature in Barcelona, according to the Standardized Absolute Error (SAE).

Extremes inference

Extreme maximum temperature is correctly inferred for all months of the year in Barcelona (Figure 36). Not significant differences were found between both approaches used for the obtaining of extreme values from analogous monthly anomalies.

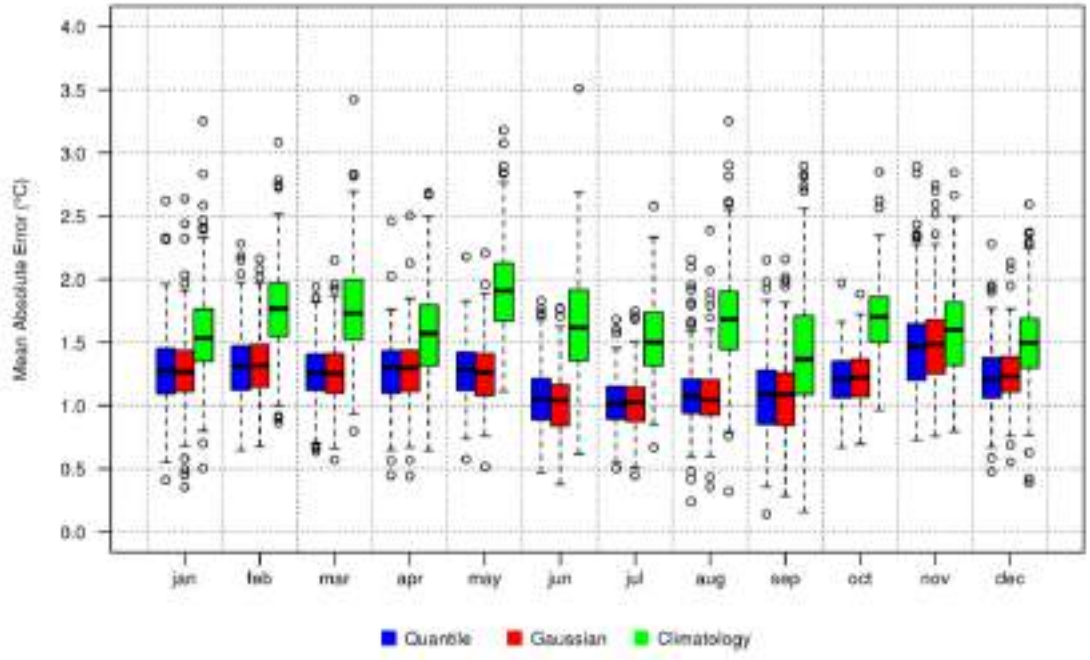

Figure 36. Validation of the extreme inference method for temperature in Barcelona according to the Mean Absolute Error of two approaches from analogous anomalies: Quantile Mapping (blue boxes) and Gaussian extrapolation (red boxes), comparing to the Climatology-based method (green boxes), which uses the average of the maximum daily value for each month of the year.

3.3.2.2. Precipitation

Cross-validation

Regarding seasonal forecast of precipitation in Barcelona, no skill is found from the hindcast based on downscaled CFSv4 outputs. For all time horizons greater than 1 months, the SAE obtained corresponds to values greater than 1.

However, the performance of the approach based on teleconnections is better. Seasonal forecast of precipitation is valid for Barcelona except at 7-9 months horizons (Figure 37).

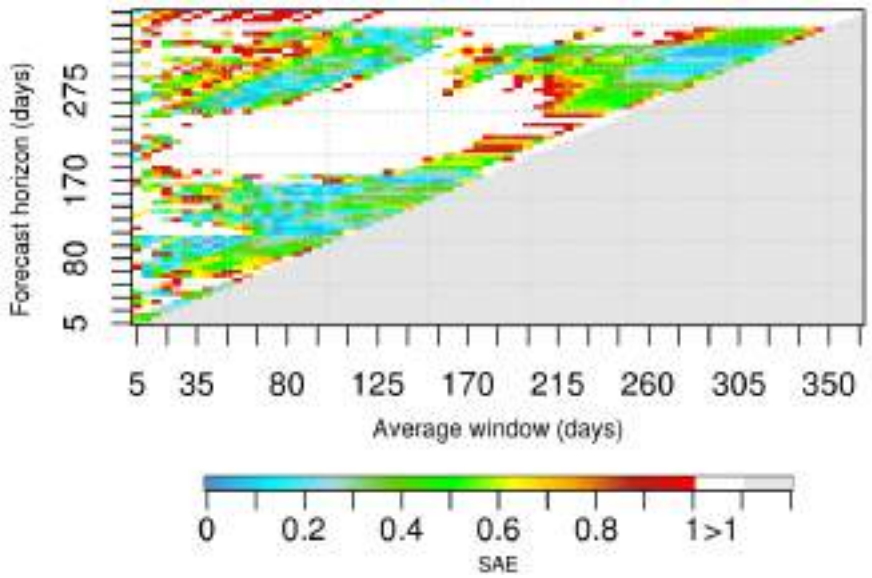

Figure 37. Validation of the teleconnection-based seasonal forecast for precipitation in Barcelona, according to the Standardized Absolute Error (SAE).

Extremes inference

Extreme daily precipitation is well simulated by using the inference method from analogous anomalies (Figure 38). All maximum values of daily rainfall are better predicted by the quantile mapping than by the climatology-based method.

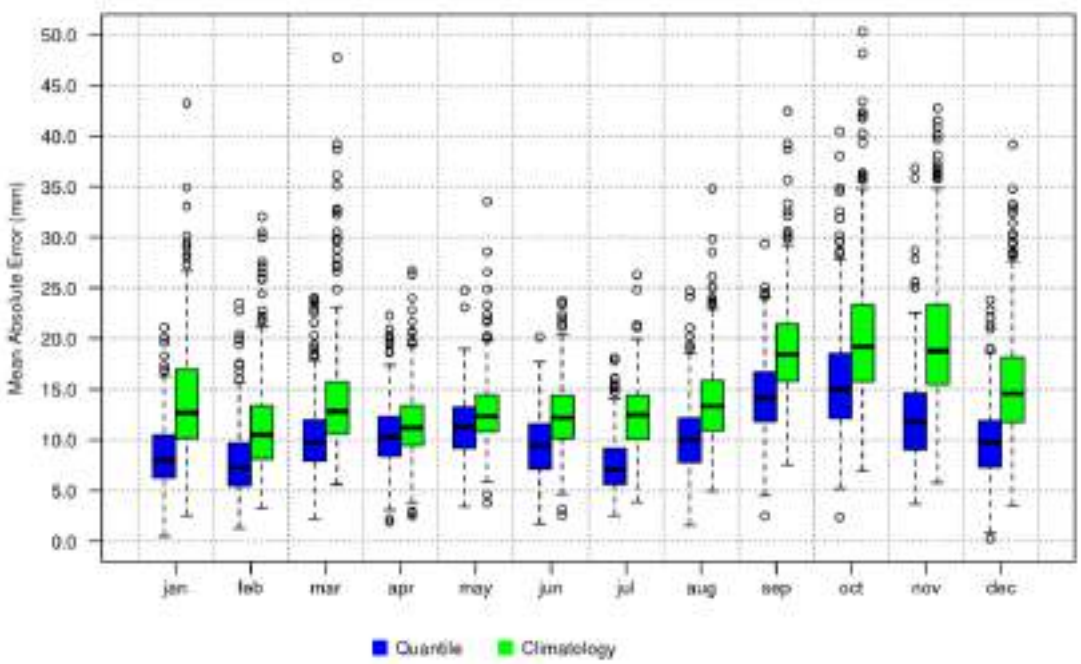

Figure 38. Validation of the extreme inference method for precipitation in Barcelona according to the Mean Absolute Error of the Quantile Mapping (blue boxes), comparing to the Climatology-based method (green boxes).

3.3.3. Lisbon

3.3.3.1. Temperature

Cross-validation

Significant skill for temperature is found in the seasonal hindcast applied to Lisbon area (Figure 39). The mean absolute error is lower than the obtained from a reference climatology-based prediction (i.e. SAE < 1).

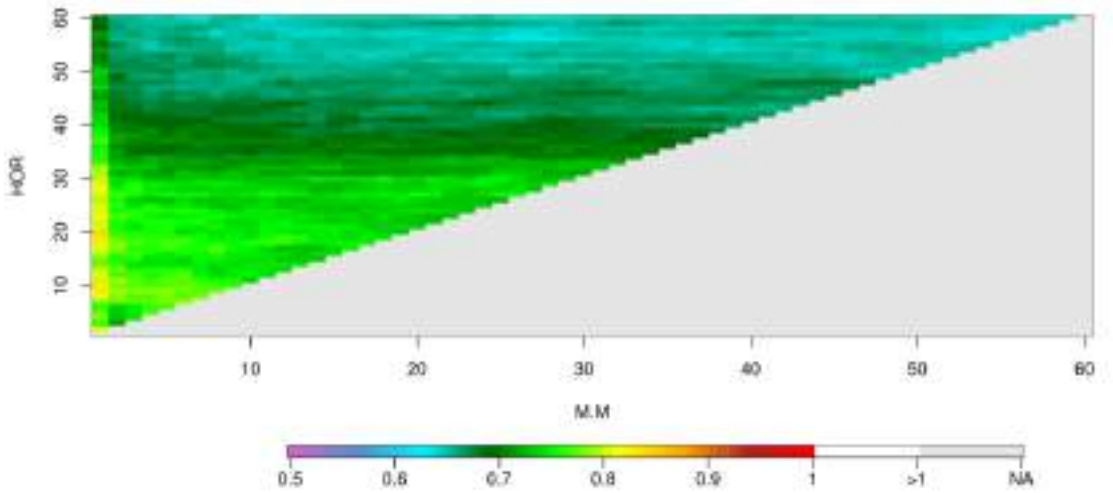

Figure 39. Validation of the dynamical approach of the seasonal forecast (downscaled CFSv4) for temperature in Barcelona, according to the Standardized Absolute Error (SAE). Y-axis represents the horizon (days) and the x-axis represents the moving average windows (days).

Extremes inference

Extreme daily values obtained from seasonal forecast are better simulated than the reference climatology-based prediction. No differences were found between the Quantile Mapping approach and the Gaussian interpolation method (Figure 40).

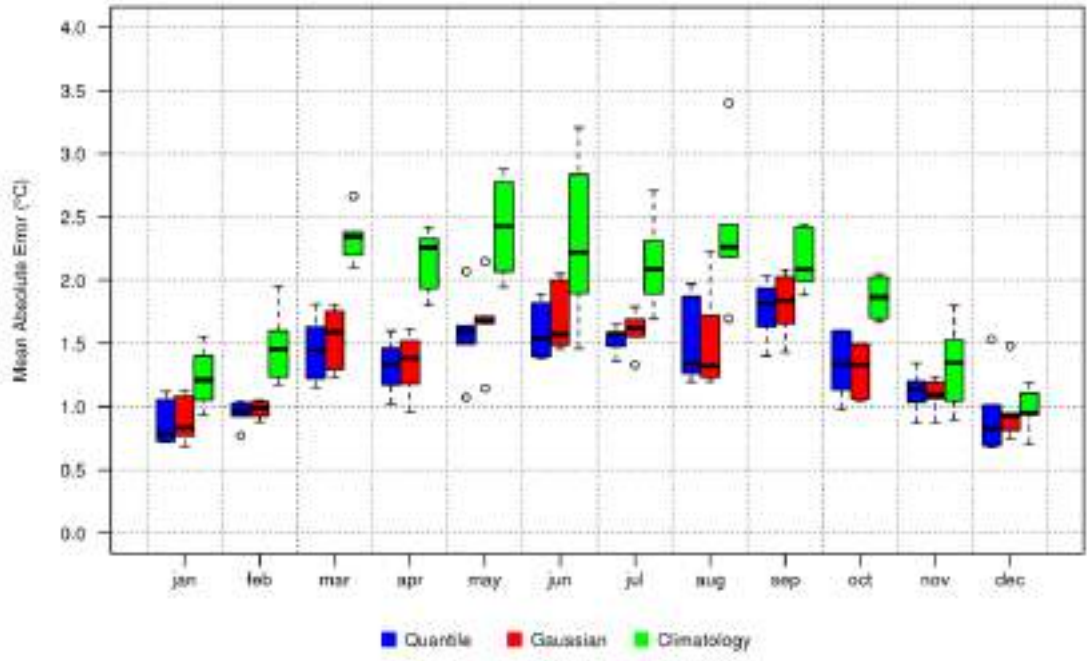

Figure 40. Validation of the extreme inference method for temperature in Lisbon according to the Mean Absolute Error of two approaches from analogous anomalies: Quantile Mapping (blue boxes) and Gaussian extrapolation (red boxes), compared to the Climatology-based method (green boxes), which uses the average of the maximum daily value for each month of the year.

3.3.3.2. Rainfall

Cross-validation

The dynamical approach based on downscaled CFSv4 showed a very low skill for precipitation forecasting, with a mean absolute error greater than a reference climatology-based prediction (i.e. SAE > 1).

However, seasonal forecast based on teleconnections showed an adequate performance for precipitation, especially at time horizons greater than 6 months (Figure 41). Moving windows between 30 and 90 days are suitable for 6-month horizons, while the optimum prediction for a 12-month horizon was obtained with moving windows of 9 to 12 months.

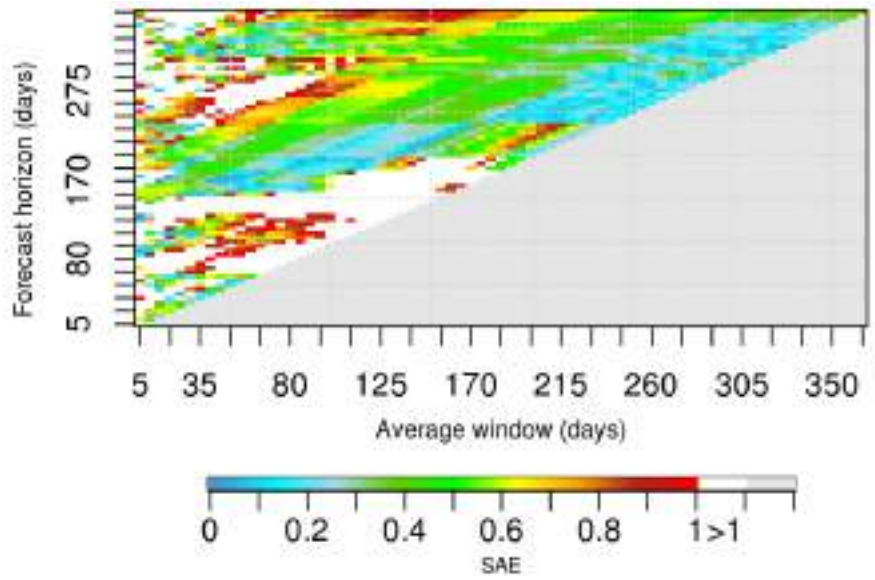

Figure 41. Validation of the teleconnection-based seasonal forecast for precipitation in Lisbon, according to the Standardized Absolute Error (SAE).

Extremes inference

Regarding the seasonal precipitation simulated for Lisbon, the method of extremes inference from analogous anomalies is better than the reference climatology-based prediction for all months, except for April and December (Figure 42). The maximum precipitation is more frequently observed in October or November, which are well simulated and thus a sufficient skill is obtained to predict extreme rainfall in Lisbon.

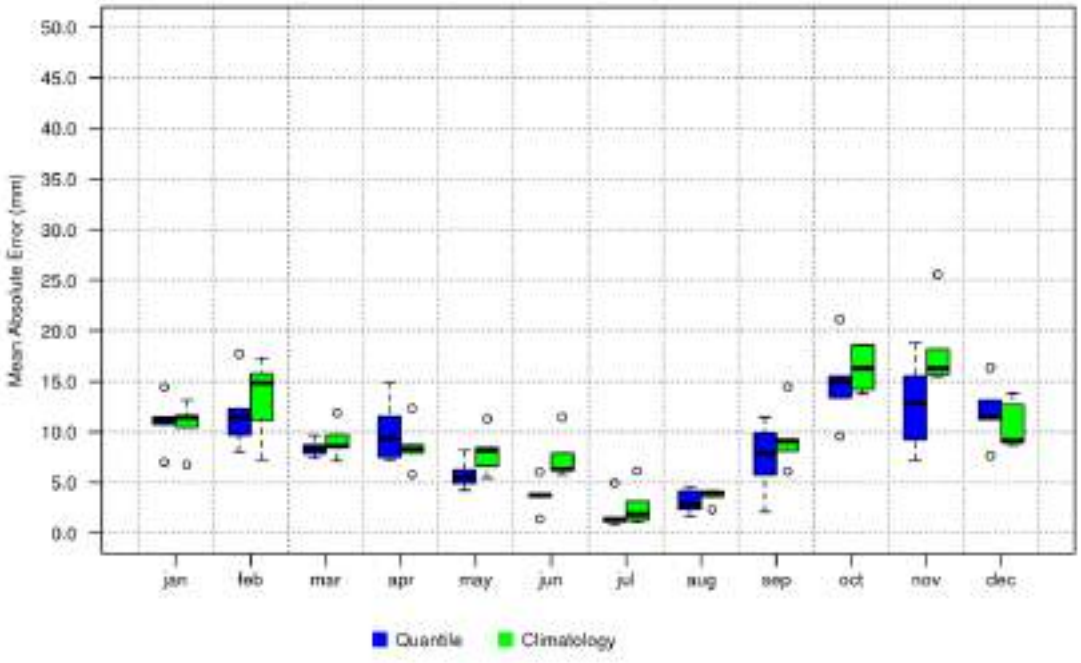

Figure 42. Validation of the extreme inference method for precipitation in Lisbon according to the Mean Absolute Error of the Quantile Mapping (blue boxes), compared to the Climatology-based method (green boxes).

3.3.4. Bristol

3.3.4.1. Temperature

Cross-validation

As in the previous cases, significant skill for temperature is found in the seasonal hindcast applied to Bristol area (Figure 43). The mean absolute error is lower than the obtained from a reference climatology-based prediction (i.e. SAE < 1).

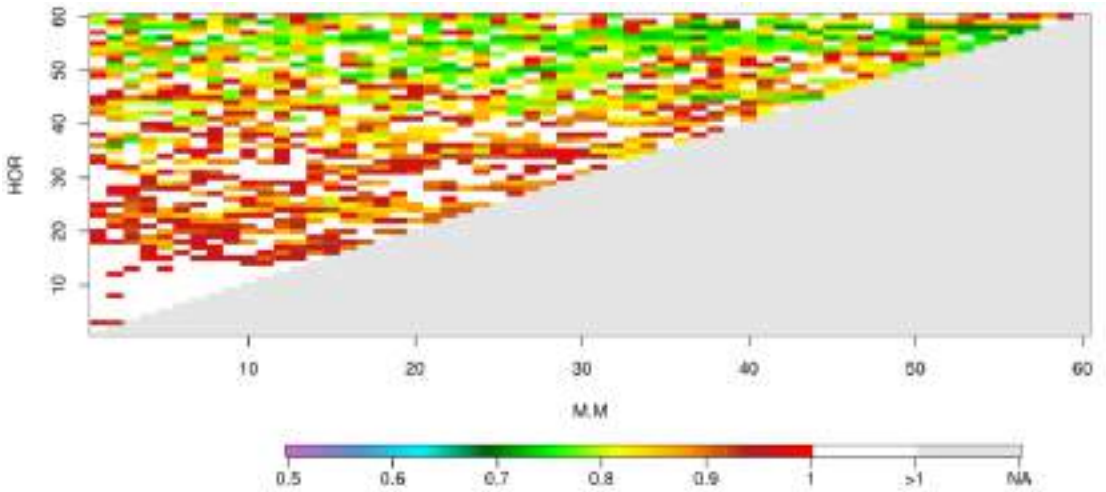

Figure 43. Validation of the dynamical approach of the seasonal forecast (downscaled CFSv4) for temperature in Bristol, according to the Standardized Absolute Error (SAE). Y-axis represents the horizon (days) and the x-axis represents the moving average windows (days).

Seasonal forecast based on teleconnections showed a noisy behaviour in Bristol. Due to the high nonlinear nature of the atmosphere, the used quasi-oscillation technique only finds a good fit for some combinations between horizons and average windows (Figure 44).

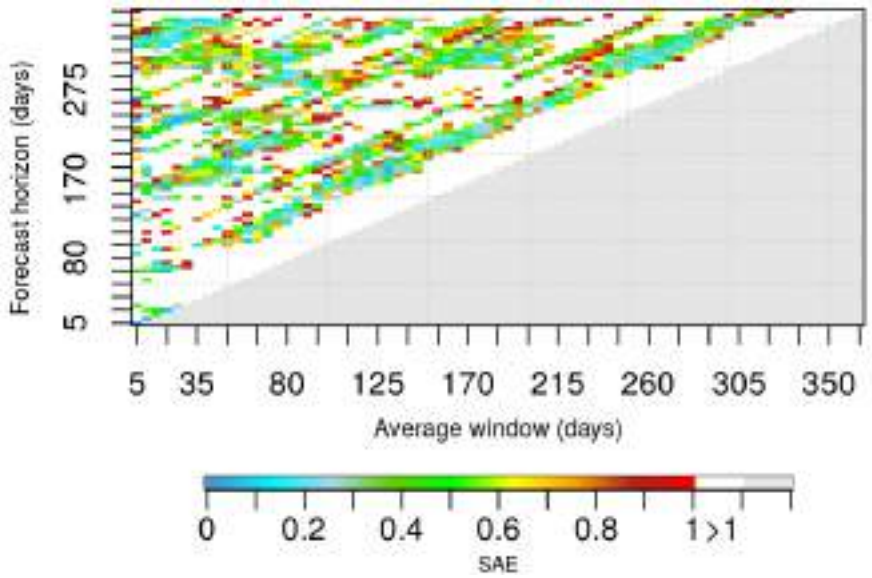

Figure 44. Validation of the teleconnection-based seasonal forecast for temperature in Bristol, according to the Standardized Absolute Error (SAE).

Extremes inference

Seasonal extreme temperature is adequately simulated by the Quantile Mapping of analogous anomalies for all months of the year (Figure 45). However, the Gaussian approach is generally acceptable except for the winter months.

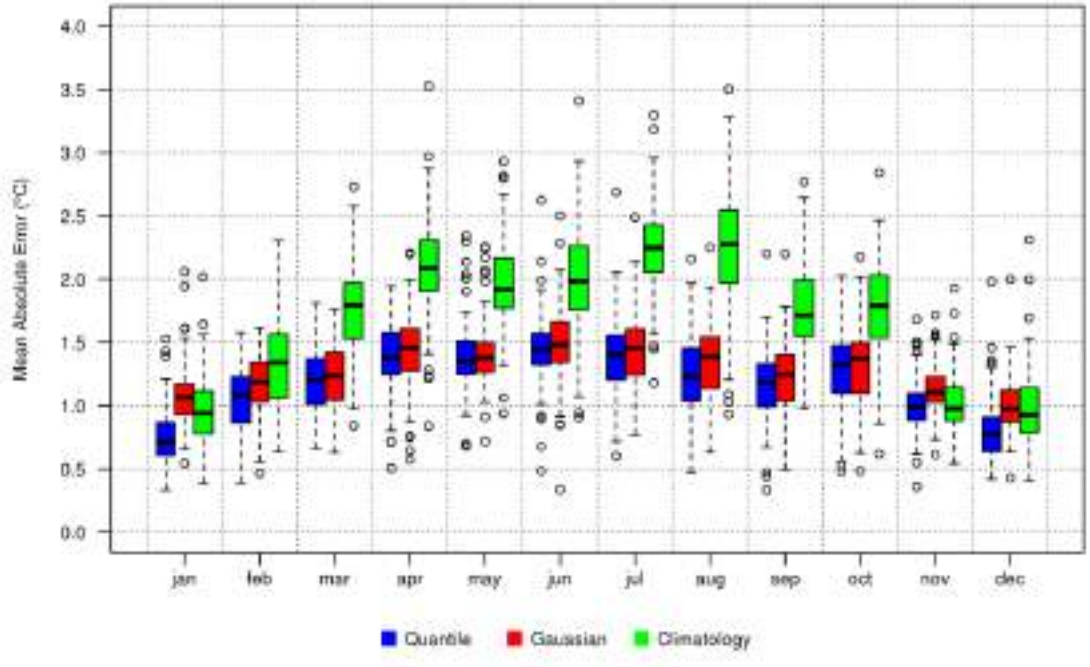

Figure 45. Validation of the extreme inference method for temperature in Bristol according to the Mean Absolute Error of two approaches from analogous anomalies: Quantile Mapping (blue boxes) and Gaussian extrapolation (red boxes), compared to the Climatology-based method (green boxes), which uses the average of the maximum daily value for each month of the year.

3.3.4.2. Precipitation

Cross-validation

As in the cases above, downscaled CFSv4 outputs showed a very low skill for precipitation forecasting, with a mean absolute error greater than the reference climatology-based prediction (i.e. SAE > 1).

Nevertheless, seasonal forecast based on teleconnections obtained a significant skill for precipitation especially at time horizons about 6 months (Figure 46). Specifically, moving windows between 20 and 100 days are suitable for 6-month horizons. No significant skill is found for 12-month horizon.

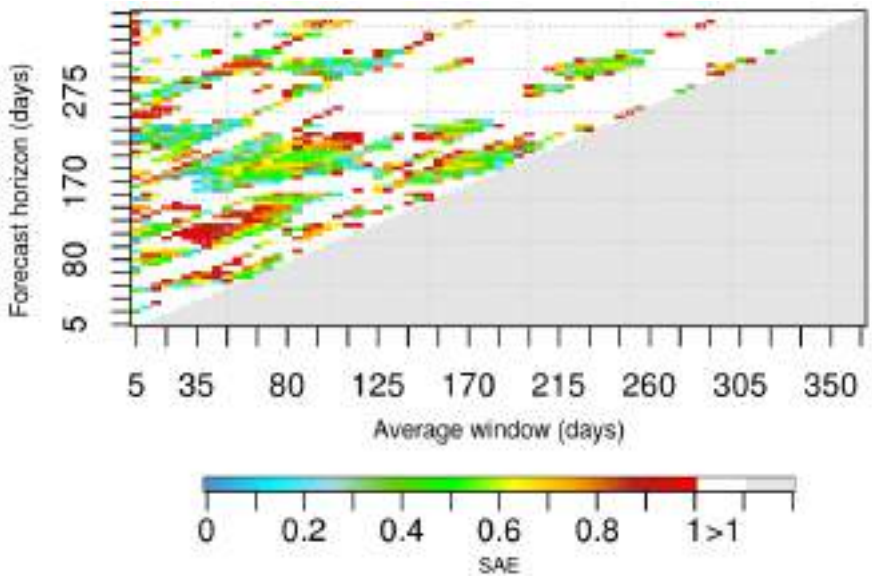

Figure 46. Validation of the teleconnection-based seasonal forecast for precipitation in Bristol, according to the Standardized Absolute Error (SAE).

Extremes inference

Seasonal extreme precipitation is adequately simulated for Bristol according to the MAE obtained for all the months of the year (Figure 47). Maximum rainfall usually recorded in the summer months is the best simulated for the Bristol area.

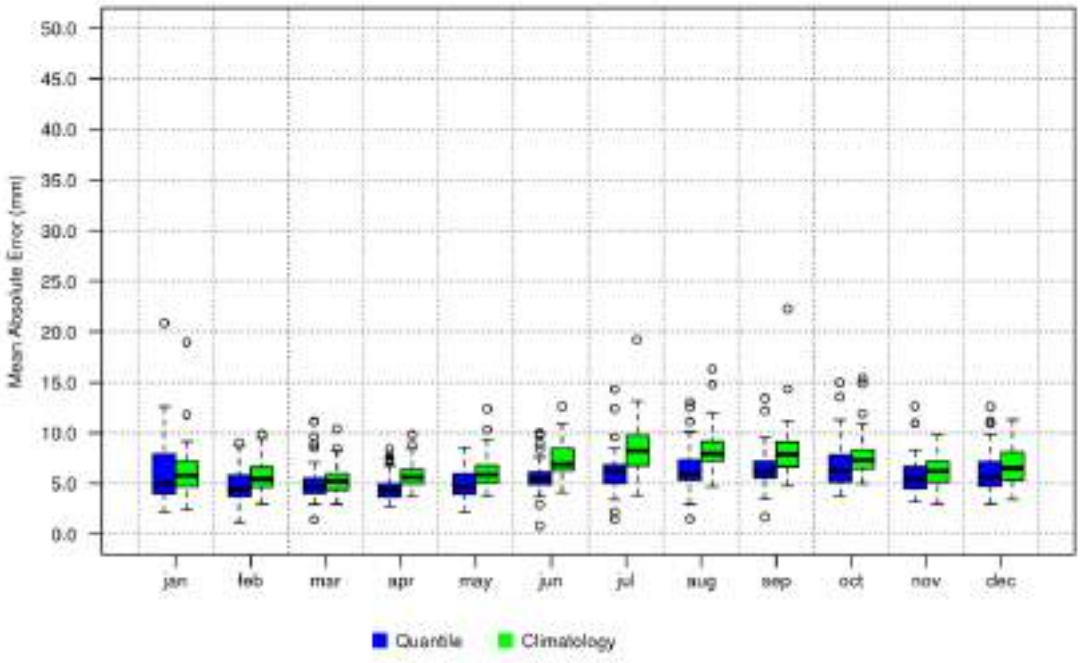

Figure 47. Validation of the extreme inference method for precipitation in Bristol according to the Mean Absolute Error of the Quantile Mapping (blue boxes), compared to the Climatology-based method (green boxes).

3.3.5. Summary for the seasonal verification

The general result for the seasonal hindcast is that the model performance when simulating extreme precipitation is more adequate in the teleconnection-based approach, while temperature is best simulated using drift-corrected dynamical outputs (Table 5).

Except for Bristol, precipitation is well predicted at the 12-month horizon according to the teleconnection-based method. Temperature presents more troubles at 1 and 3-month horizons.

Table 5. Summary of the validation process for the seasonal forecast.

Method	Time horizon	Maximum Temperature			Precipitation		
		Barcelona	Bristol	Lisbon	Barcelona	Bristol	Lisbon
Downscaled CFSv4	1 month						
	3 months						
	6 months						
	12 months						
Teleconnections	1 month						
	3 months						
	6 months						
	12 months						

KS-test passed for more than 70% of the analysed cases
KS-test passed between the 50% and 70% of the analysed cases
KS-test passed for less than 50% of the analysed cases
Horizon not available for the method

Regarding the stability of the teleconnection-based method within a context of climate change, the wavelet analysis showed that the optimum training windows correspond to the most stable oscillation periods of each teleconnection. This results is generally valid for both decadal and seasonal timescale (Redolat *et al.* 2019a, 2019b). More details on the verification of the general method can be found in **Section 3.2** of the Deliverable D2.

4. Extreme events prediction

4.1. Barcelona

4.1.1. Extremes in temperature

Near and long-term climate change

For Barcelona, extreme maximum temperature will tend to rise throughout the century. Taking into account events of 2 and 100-years return periods, extreme values would rise respectively about 4°C (from +2 to +8°C) and 5°C (from +2 to 9°C) by the end of the century (Figure 48).

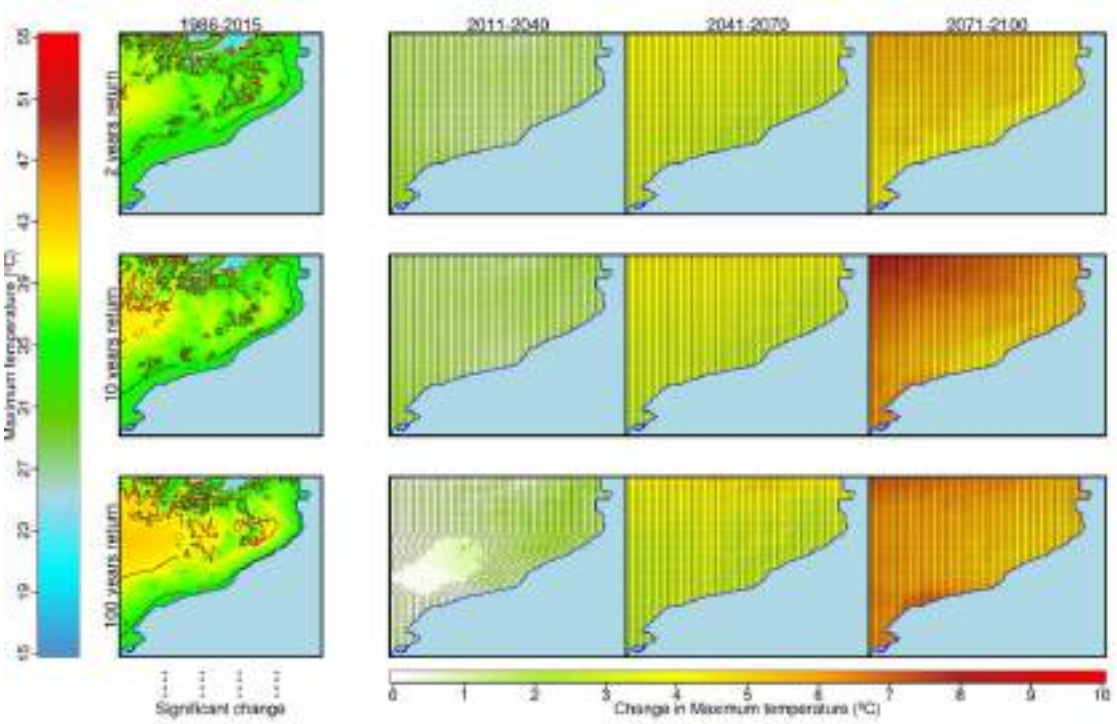

Figure 48. Multi-model median scenario of changes in extreme events of maximum temperature projected for the Ter-Llobregat system. Changes correspond to 2, 10 and 100-year return periods (rows) and three future time periods (2011-2040, 2041-2070 and 2071-2100, second to fourth column) with respect to the reference period 1986-2015 (first column).

For the next two decades (2016-2035), a warming between 1 and 2°C is expected with respect to the extreme events recorded in the baseline time period (1986-2015). The area within the isotherm of 40°C could increase for 10-year and 100-year return events according to the three methods used: downscaled climate models, drift-corrected decadal models and teleconnection-based decadal approach (Figure 49).

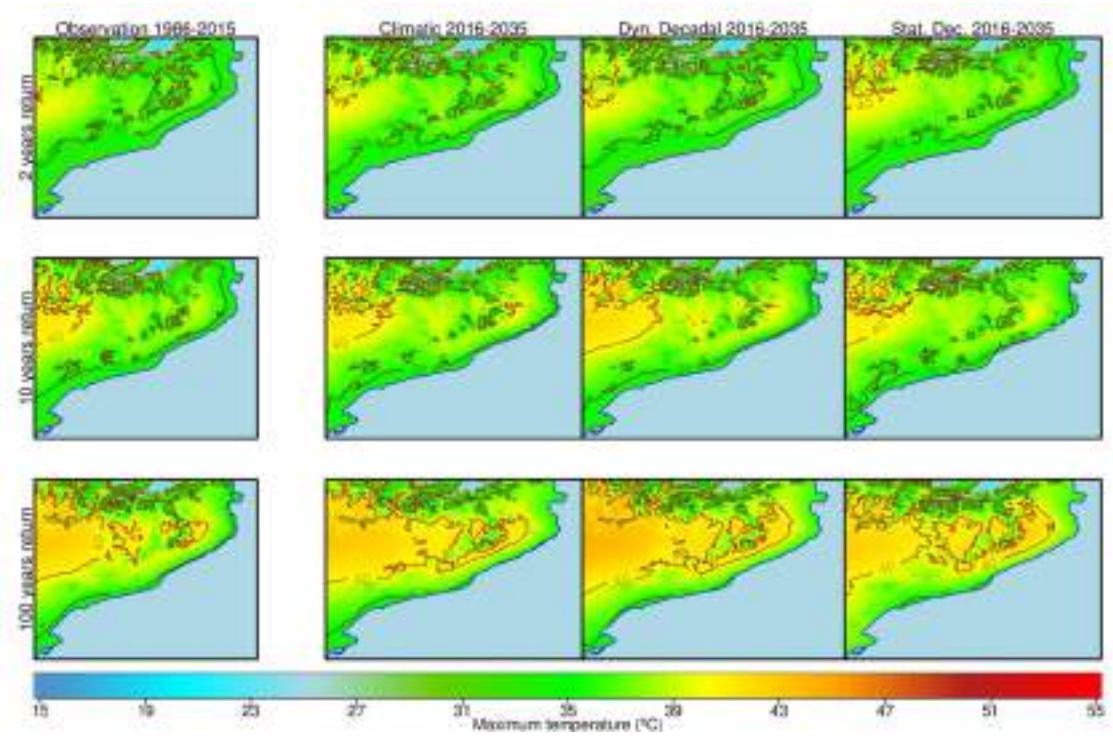

Figure 49. Comparison between three different projections of maximum temperature for the 2016-2035 period for the area of Barcelona. Changes correspond to 2, 10 and 100-year return periods (rows) and for three methods (statistical downscaling of climate CMIP5 models, drift-corrected decadal CMIP5 models and teleconnection-based approach, second to fourth column) with respect to the reference period 1986-2015 (first column).

A strong decrease tendency in the number of cold days, frost nights, winter duration and coldest-period duration is expected in Barcelona. The number of cold days could reduce from 40 to 10; frost nights would practically be reduced to zero, while winter duration would decrease from 100 to 40 days and the duration of the coldest period cold reduce from 23 days to 10 (Figure 50). Winter's starting day could delay about one and a half month, from the beginning of December to mid-January and the beginning of the coldest period could delay about a fortnight. Meanwhile, the beginning of the summer and the warmest period would tend to advance one month in both cases: from mid-June to mid-May and from mid-July to mid-June respectively. The summer duration could expand from 100 to 150 days and the warmest period from 30 to 90 days. The number of warm days and tropical nights could increase sharply from 40 to 100 and from 10 to 90 respectively.

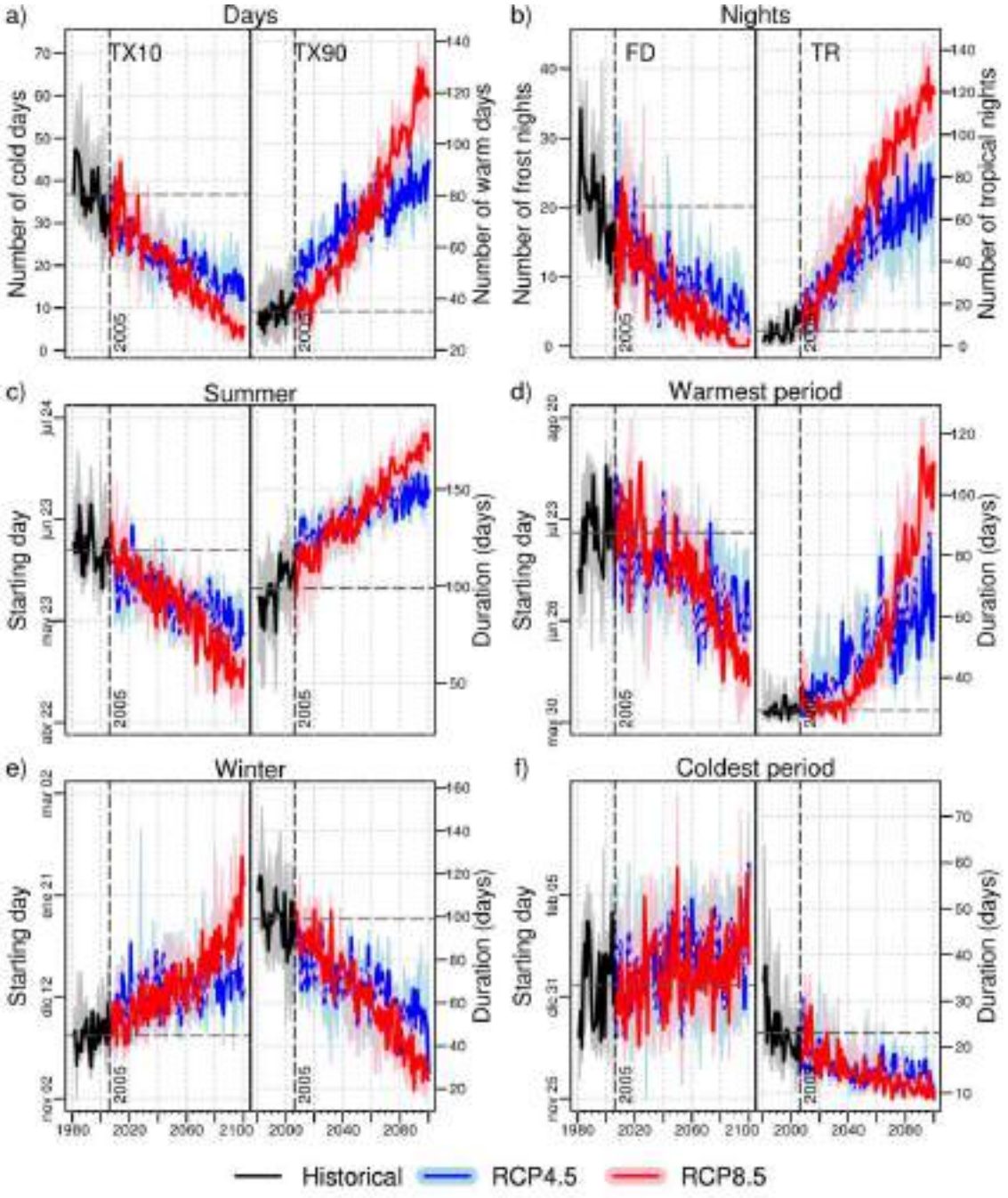

Figure 50. Climate projection of extreme indices (Table 3) based on temperature in Barcelona: a) Cold Days (TX10, left) and Warm Days (TX90, right), b) Frost Nights (FD, left) and Tropical Nights (TR, right), c) Summer starting day (left) and duration (right), d) Warmest period starting day (left) and duration (right), e) Winter starting day (left) and duration (right), f) Coldest period starting day (left) and duration (right).

Consequently, a dramatic increase in the number of heat waves is expected for Barcelona, going from the average of about 1 wave per year (particularly 0.9±0.2) to 4±1 waves per year by the end of the century. Moreover, the averaged duration of a heat wave could be doubled by 2100. With this, total heat wave days could increase from the initial value of 4.7±0.3 to 40±20 days per year. Finally, the average intensity and the maximum intensity of heat wave could increase respectively about +0.5°C and +1°C (Figure 51).

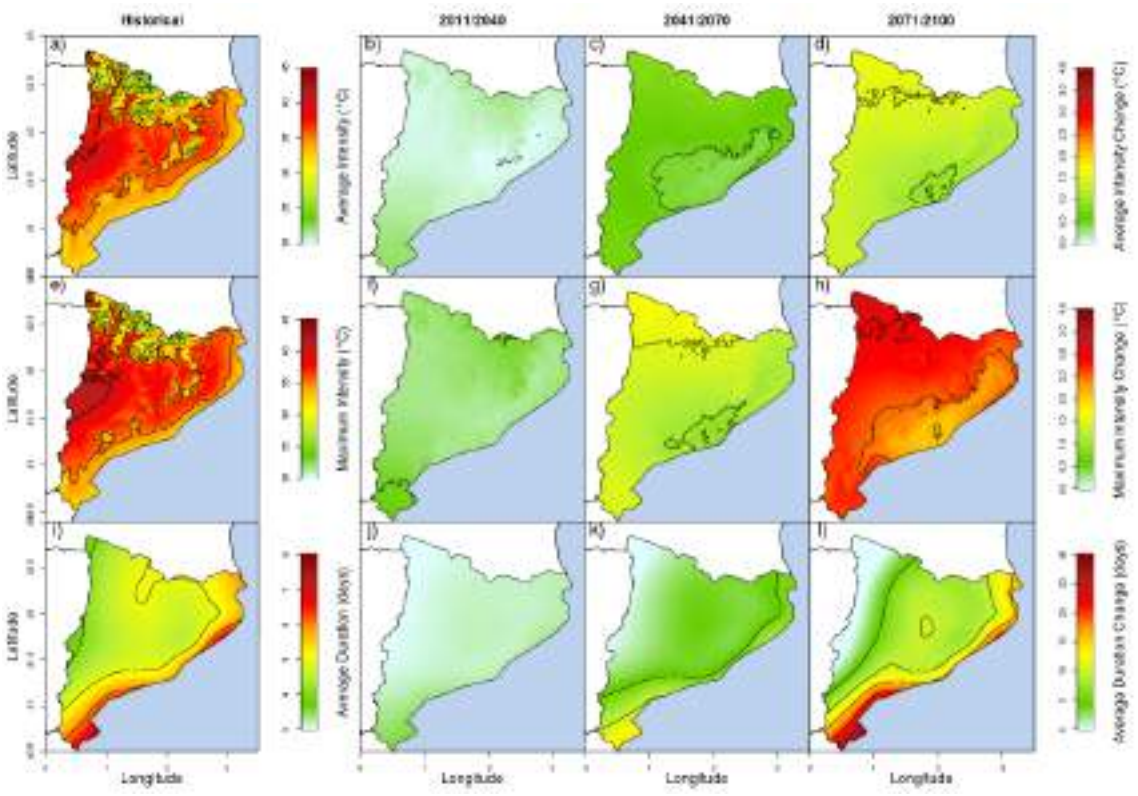

Figure 51. Past values (a, e, i) and projections of absolute change (b, c, d, f, g, h, j, k, l) of heat wave features in the area of Barcelona under the RCP8.5 according to the downscaled multi-model median: Average intensity (a, b, c, d), maximum intensity (e, f, g, h) and average duration (i, j, k, l).

Seasonal forecast

An anomaly about +2°C is expected for the extreme value of maximum temperature predicted for the next six months in Barcelona. The anomaly could rise up to +4 or +5°C inside Catalonia (Figure 52). The worst-case scenario implies a great area that covers western and central regions exceeding 40°C, and 35°C affecting all the coastal line.

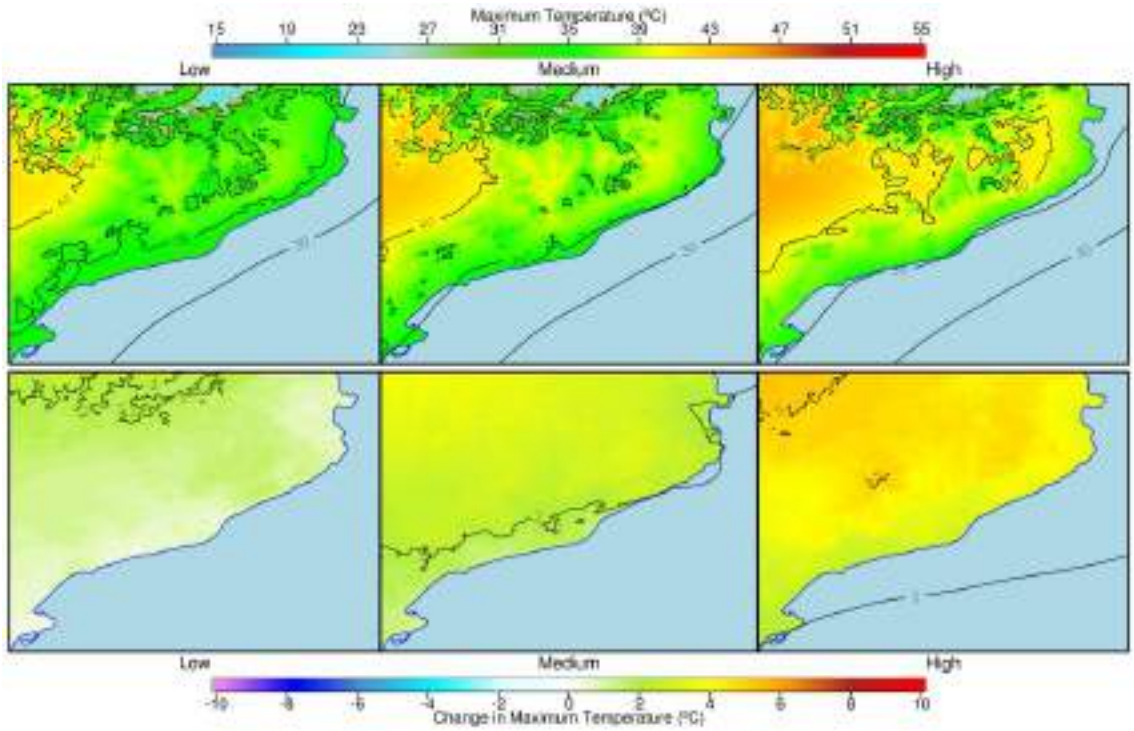

Figure 52. Probable scenarios for extreme maximum temperature expected in the Ter-Llobregat system for the next six months according to the seasonal forecast (bias-corrected dynamical model output from the CFSv4). From the left to the right: low (10%), medium (50%) and high (90%) percentiles of the predicted probability distribution for the expected maximum temperature (top) and the difference with respect to climatology (bottom).

4.1.2. Extremes in precipitation

Climate changes in long-duration events

Maximum precipitation in 12h would increase around a 6% in the first half of the century and more than 26% in the last three decades considering a return period of two years. Taking into account return periods of 10 and 100 years, extreme precipitation could potentially escalate in the second half of the century more than 40%, reaching 93mm and 124mm respectively (Figure 53).

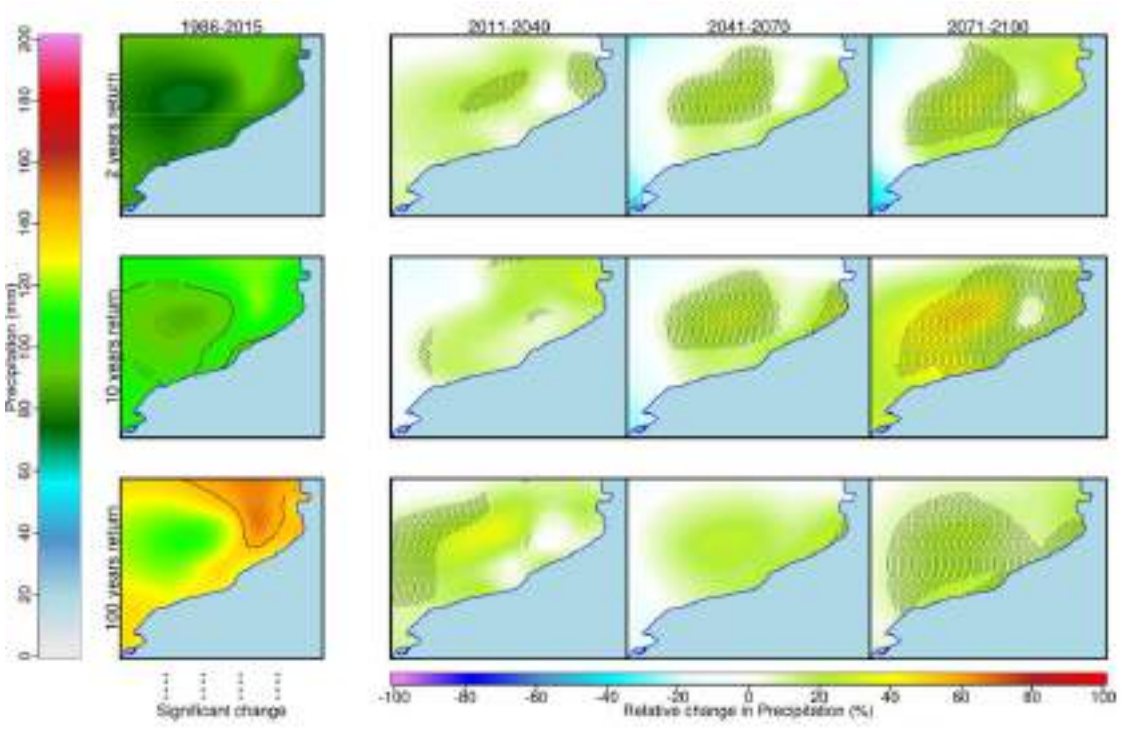

Figure 53. Multi-model median scenario of changes in extreme events of precipitation projected for the Ter-Llobregat system, according to 2, 10 and 100-year return periods (rows) and for three future time periods (2011-2040, 2041-2070 and 2071-2100, second to fourth column) with respect to the reference period 1986-2015 (first column).

Regarding the climate projections for drought in Barcelona, it is expected that SPEI decreases down to -1 by the end of the century, although SPI will remain approximately constant (Figure 54). That is, despite the high natural variability of the precipitation, the increase of the evapotranspiration (due to the warming) will cause a greater water stress and a consequent greater scarcity of water.

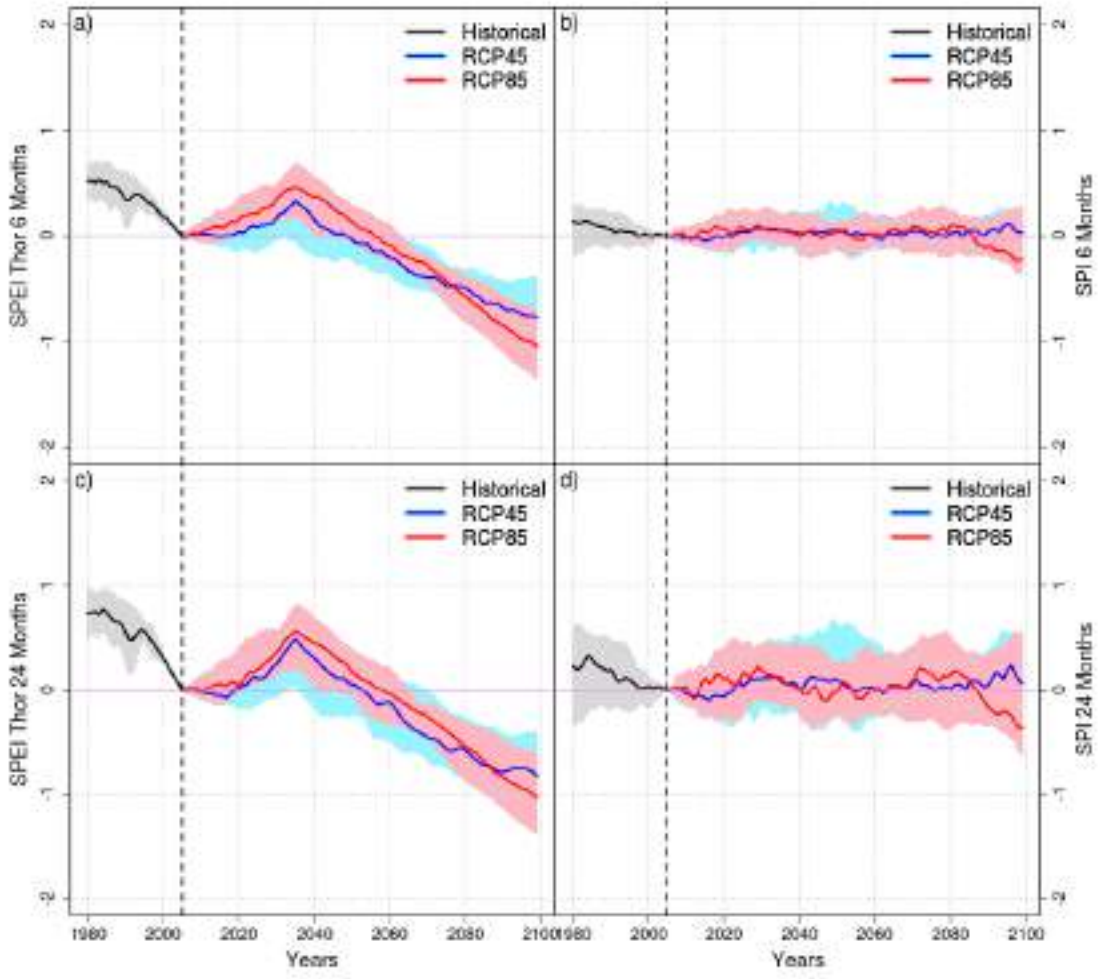

Figure 54. Ensemble of projections for SPEI (left) and SPI (right) for the Barcelona area according to 6 and 24-month moving windows.

Climate changes in short-duration events

Under both RCP scenarios, the number of subdaily events per year whose total precipitation exceed 20mm will decrease slightly, from 6 to 5. The mean duration of these events will oscillate throughout the century around the current mean (160 min). The reference intensity I_0 shows a continuous increasing trend, from 6.3mm/5min to 7.3mm/5min and the *n*-index also shows an increasing trend from 0.37 to 0.39.

Regarding events with amounts greater than 50mm, their frequency (1 episode per 1.3 ± 0.2 years) and the duration (3.8 ± 0.1 hours) would remain stable throughout the century under the RCP4.5, but its frequency could decrease 25% under the RCP8.5. Their intensity and concentration show increasing trends under both scenarios, from 0.38±0.01 to 0.40±0.01 in the case of the *n*-index and from 9.5 ± 0.5 mm/5min to 11 ± 1 mm/5min in the case of the reference intensity (Figure 55).

These results highlight that the number of extreme rainfall episodes could reduce in Barcelona under the RCP8.5 and remain constant according to RCP4.5. However, rainfall concentration could increase in any case, which means that episodes involving extreme and potentially dangerous precipitation would be more likely to happen.

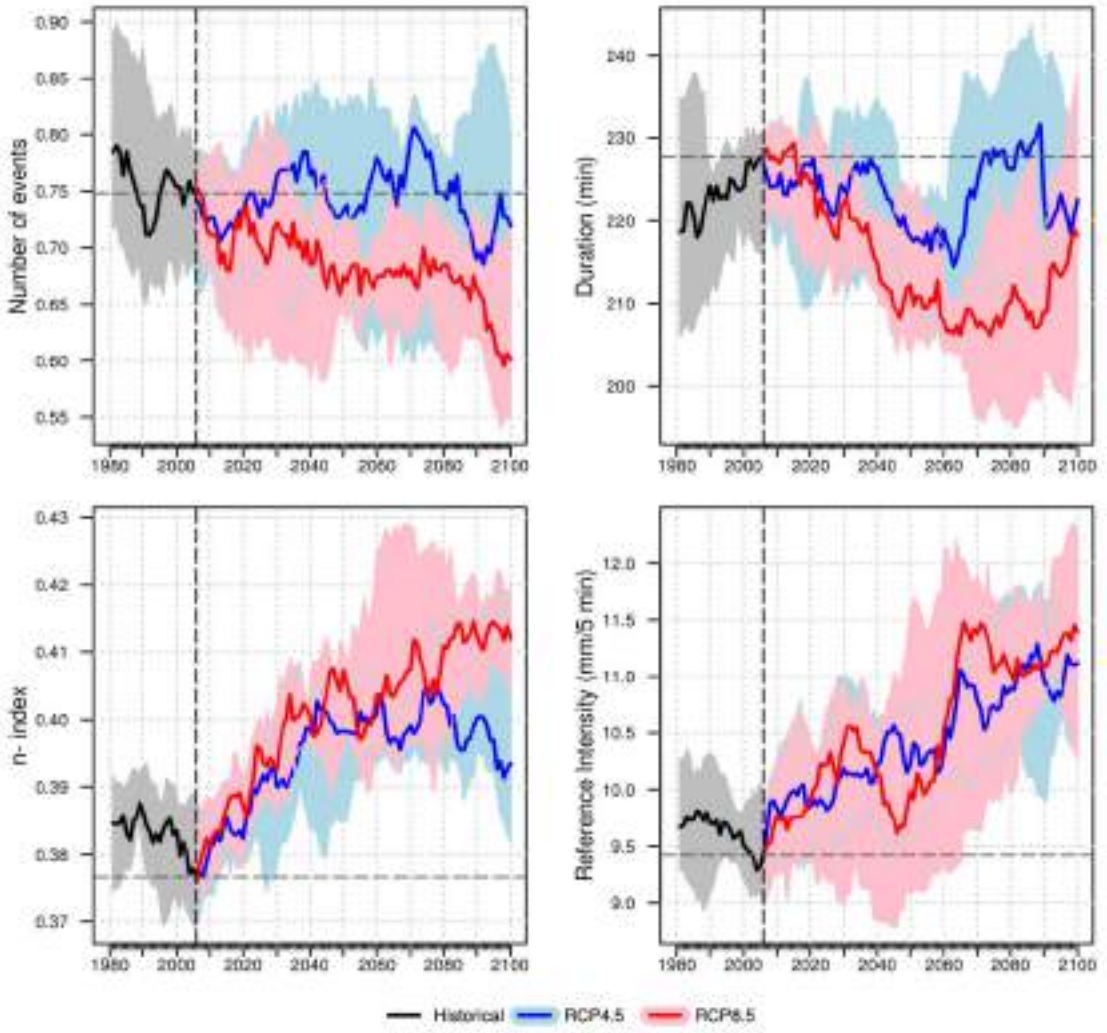

Figure 55. Extreme indices of precipitation according to sub-daily events with precipitation amounts greater than 50 mm in Barcelona: Number of events (top-left), duration (top-right), n-index (bottom-left) and reference intensity (bottom-right).

Intensity-Duration-Frequency (IDF) curves projected along the century shows a probable increase of the rainfall intensity in Barcelona by 2041-2070 for most of return periods. Specifically, change factor trends to 1.1 or 1.2 for all durations with respect to the baseline 1976-2005 period (Figure 56). The uncertainty level is greater for the current thirty-year period (2011-2040), especially for shorter durations.

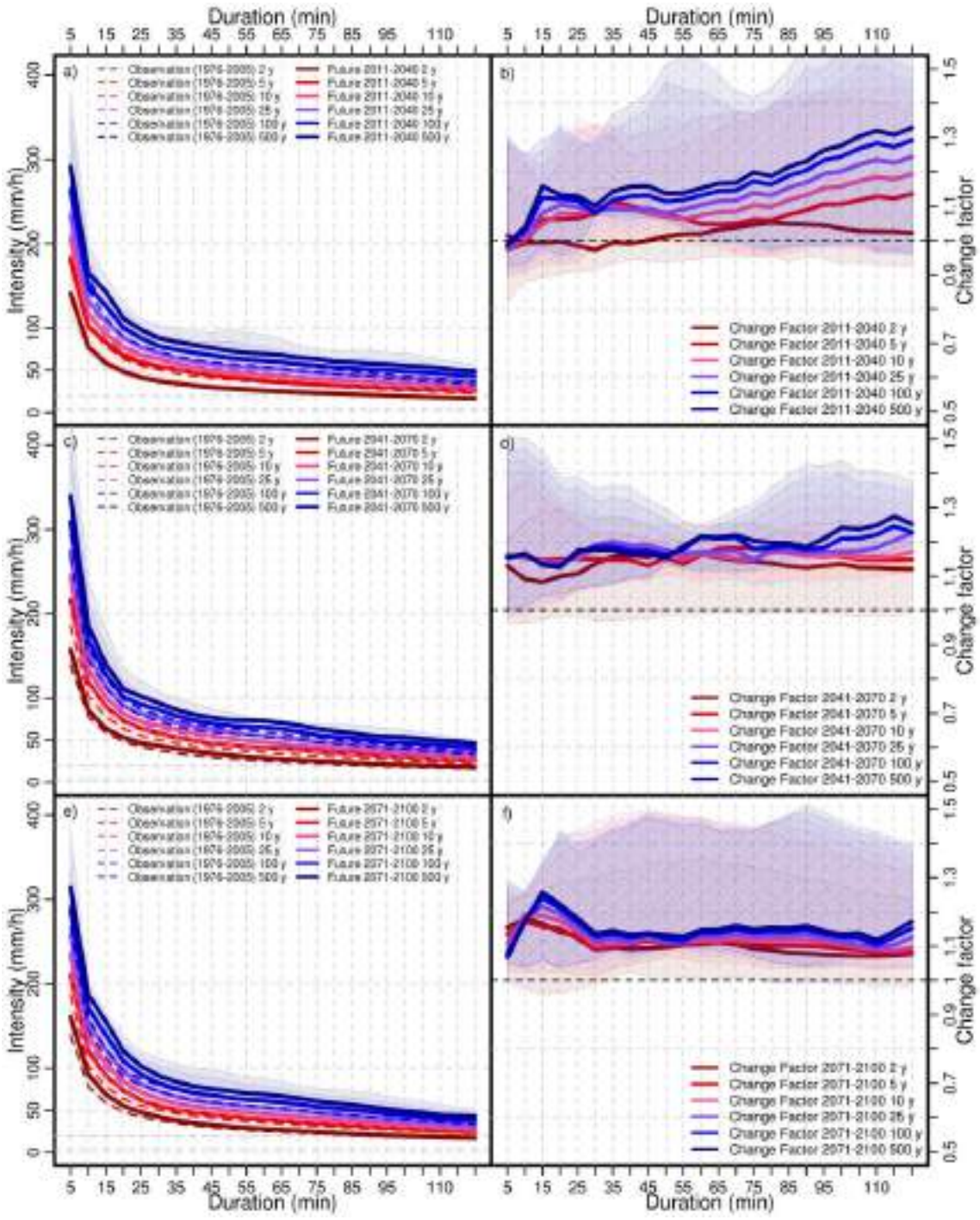

Figure 56. Projected IDF curves for the Barcelona city (Facultat de Física Station) according to absolute values (left panels) and the change factor (right panels) for three future time periods: 2011-2040 (a, b), 2041-2070 (c, d) and 2071-2100 (e, f).

Seasonal forecast

Southern Ter-Llobregat system could experience a positive anomaly in extreme rainfall during the next six months. This anomaly would rise up to even +60 or +80% under the worst-case scenario (Figure 57)

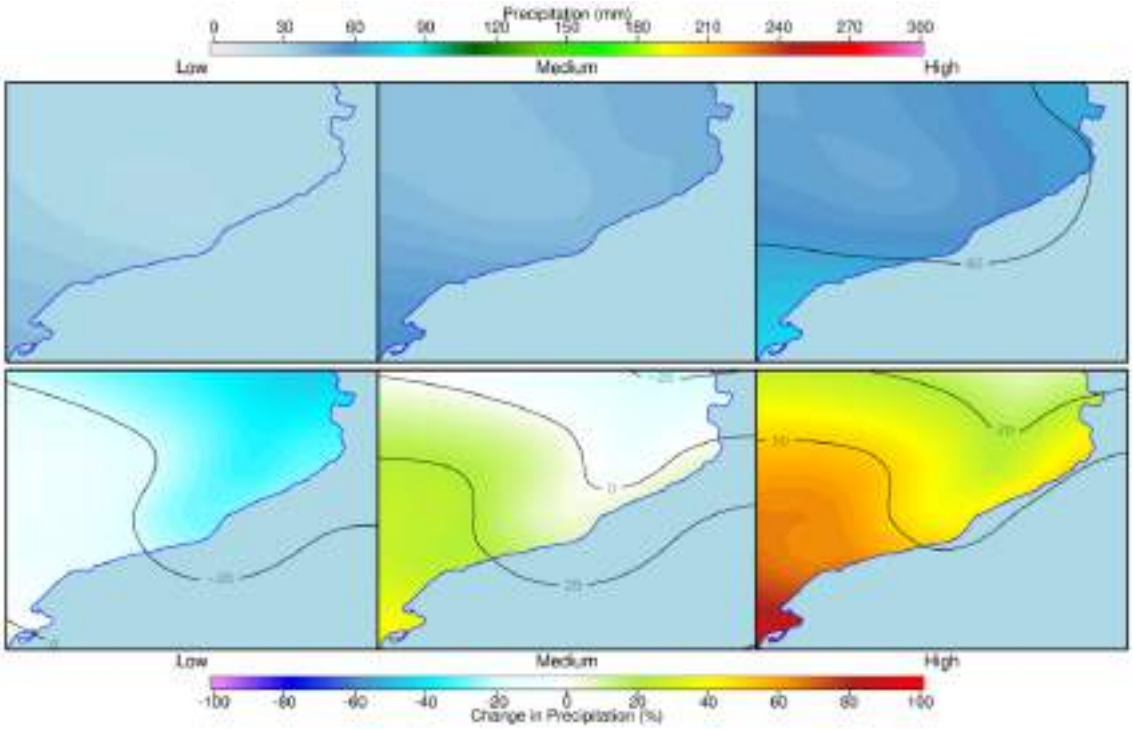

Figure 57. Probable scenarios for extreme daily precipitation expected in the Ter-Llobregat system for the next six months according to the seasonal forecast (bias-corrected dynamical model output from the CFSv4). From the left to the right: low (10%), medium (50%) and high (90%) percentiles of the predicted probability distribution for the expected extreme daily precipitation (top) and the difference with respect to climatology (bottom).

4.1.3. Other variables

4.1.3.1. Extremes in wind

For Barcelona, it is not observed any trend in wind gust throughout the century, but some scenarios suggest that it could rise up to +10% for a return period of 2 years. Not significant changes are expected for a return period of 10 years and a very slight rising trend, about +2%, is expected for a return period of 100 years, being the maximum expected values in one century about 105km/h (Figure 58).

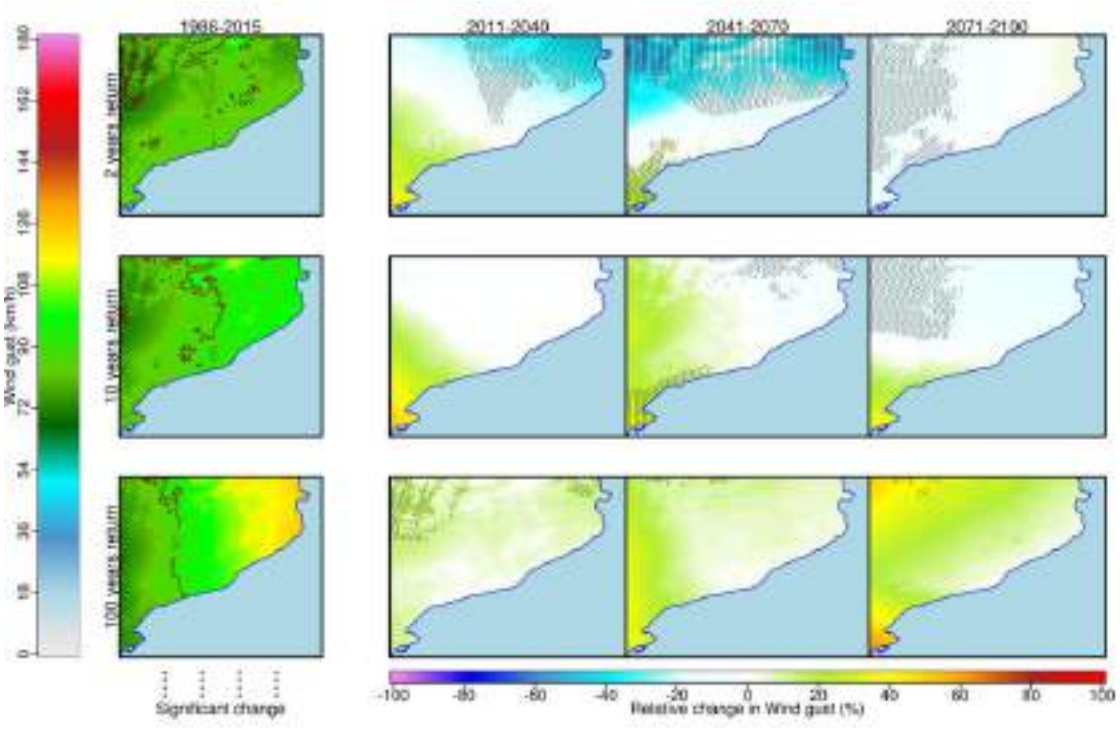

Figure 58. Multi-model median scenario of relative changes in extreme wind gust projected for the Ter-Llobregat system, according to 2, 10 and 100-year return periods (rows) and for three future time periods (2011-2040, 2041-2070 and 2071-2100, second to fourth column) with respect to the reference period 1986-2015 (first column).

The differences between the lowest and highest return period events are due to the nonlinear behaviour of this variable with respect to the global warming. That is, a temperature rising could lead to very opposite wind/calm contributions: 1) Increase of thunderstorms (under summertime barometric swamp), 2) Decrease of windstorms frequency (under a more northern polar jet stream), or 3) Increase of subtropical storms due to a greater effect of moisture plumes from the tropical jet stream.

In the case of the Ter-Llobregat system, it seems that the lesser extreme events (2-year return period) could decrease due to the second contribution, i.e. the upper-level ridge will rise more frequently from North Africa to Spain, displacing the polar Jet Stream to northern latitudes). However, for the most extreme events (100-year return period), the first and third scenarios could influence more due to the more available energy in the atmosphere.

4.1.3.2. *Extremes in snowfall*

Extreme snowfall would dramatically decrease more than 60% for return periods of 2 and 10 years (Figure 59). However, taking into consideration a return period of 100 years, extreme values could increase more than 30%. Thus, the maximum expected value for extreme snowfall in a century could increase from 29cm to 40cm. This could be explained by the expected rise in the average temperature which would difficult snow precipitation to happen. On the opposite, as seen in precipitation, for long return periods a notable increment in heavy rainfall is expected due to augmented moisture, which in the appropriate events would lead to a greater amount of snowfall.

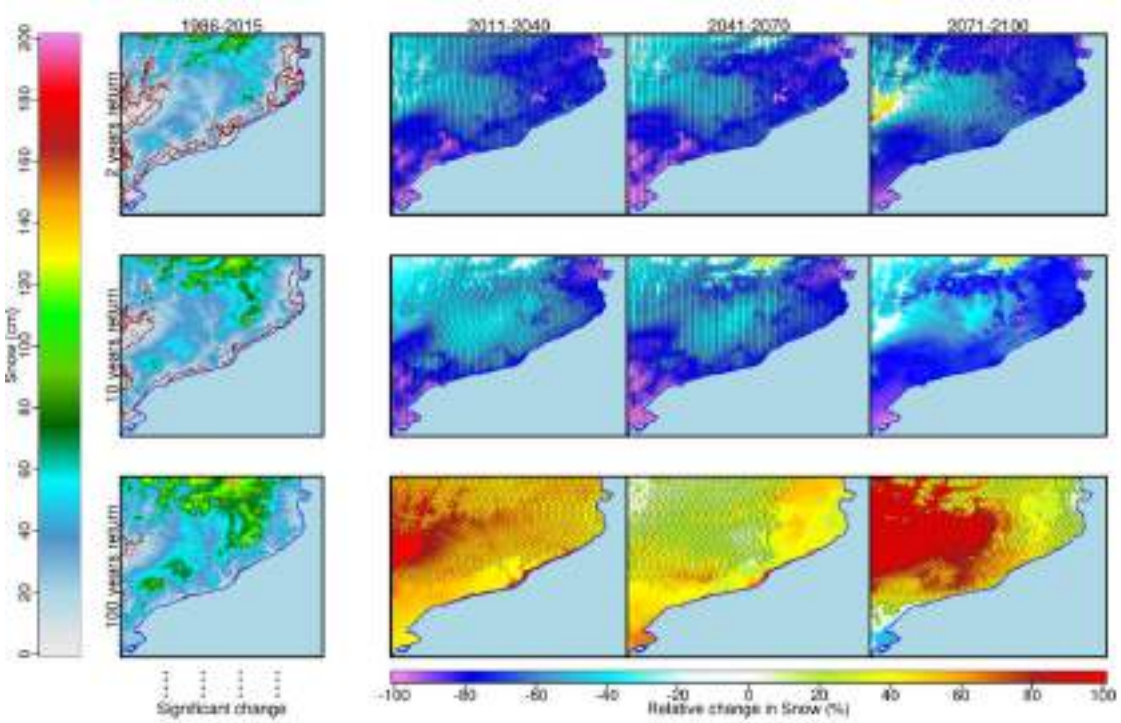

Figure 59. The same as in Figure 58 but for extreme snowfall events.

4.1.3.3. *Extremes in wave height and sea level*

Extreme wave height would decrease slightly, being this decrease a bit more pronounced (greater than 10%) by 2011-2040 in events of 100-year return period. The combination of storm surge and sea level rise present no significant changes for this time period due to a greater frequency of stable atmospheric situations (high pressure systems). Some projections show a reduction for the 100y-return events, decreasing 10% or 30%.

For the rest of analysed periods, the significance level is higher. By the end of the century, most of the downscaled climate models project an increase in 2y-return storm surge (+ sea level rise) between +10% and +75% (median of 45%).

Extreme wave height would tend to decrease around 5% in 2 and 10y-retun. Some downscaled models estimate decreases greater than 10%, while other ones suggest very slight increases lower than +2%. For a return period of 100 years, projected decreases of wave height are a bit greater, around 10%. Any of the model outputs project increases in wave height for this return period.

4.1.4. Summary of changes in extremes for Barcelona

Significant increases in extreme maximum temperature and precipitation are expected over the century for all return periods (Table 6). Wind gusts could increase in the next decade, while snowfall and wave height would decrease during all century.

Table 6. Summary of changes in extremes values for Barcelona according to decadal and climate models.

Variable	Return period (years)	Observed	Decadal forecast	Relative change		
		1986-2015	2016-2035	2011-2040	2041-2070	2071-2100
Maximum Temperature	2	33.7 °C	+0.1 (-0.3/+0.4)	**+1.1 °C** (+0.5/+2.1)	**+2.7 °C** (+1.7/+4.4)	**+3.8 °C** (+2.2/+7.5)
	10	34.7 °C	-0.0 °C (-0.1/+0.4)	**+1.0 °C** (+0.5/+2.1)	**+2.7 °C** (+1.6/+4.2)	**+4.2 °C** (+2.0/+8.2)
	100	37.1 °C	-0.8 °C (-0.9/+1.1)	**+1.2 °C** (0.4 /+2.6)	**+2.8 °C** (1.2 /+5.5)	**+5.1 °C** (+2.3/+8.9)
12h Precipitation	2	80 mm	+0 % (-10/+10)	+7 % (-1/+20)	+19 % (-2/+30)	**+30 %** (+8/+40)
	10	100 mm	+1 % (-10/+10)	+9 % (+1/+20)	**+20 %** (+5/+30)	**+40 %** (+8/+40)
	100	130 mm	-0 % (-10/+10)	**+6 %** (+3/+18)	**+30 %** (+6/+60)	**+45 %** (+30/+50)
Wind Gust	2	85 km/h	**+6 %** (+4/+7)	-4 % (-7/+3)	-3 % (-4/+10)	-3 % (-5/+7)
	10	93 km/h	**+10 %** (+8/+12)	-0.1 % (-2/+8)	-0.3 % (-1/+12)	-0.7 % (-1.6/+9)
	100	103 km/h	**+13 %** (+12/+17)	+2.5 % (-0.1/+3.8)	+1.5 % (-1.7/+3.0	+2.0 % (-1/+4)
12h Snowfall	2	14 mm		**-70 %** (-90/-60)	**-70 %** (-90/-60)	**-70 %** (-80/-50)
	10	20 mm		**-62 %** (-66/-46)	**-67 %** (-76/-43)	**-66 %** (-75/+58)
	100	29 mm		**+40 %** (+5.0/ +50)	+30 % (-10/+110)	+60 % (-3/+300)
Storm surge + sea level rise	2	0.54 m		5% (-30/+10)	30% (-10/+40)	**45%** (+10/+75)
	10	0.74 m		0% (-30/+5)	15% (-15/+20)	**30%** (+0/+50)
	100	1.15 m		-10% (-30/+0)	0% (-20/+10)	10% (-15/+25)
Wave Height	2	6.6 m		-1 % (-7/+3)	-4 % (-7/+1.5)	-4 % (-10/+0.3)
	10	7.7 m		-4 % (-12/+1.4)	-5 % (-11/0.7)	-5 % (-10/+0.4)
	100	9.2 m		**-13 %** (-20/-6)	**-12 %** (-22/-2)	**-11 %** (-20/-1)

Not available

Significant increase	P > 95%
Not significant increase	50% < P < 95%
Not significant changes	P < 50%
Not significant decrease	50% < P < 95%
Significant decrease	P > 95%

Going into detail, 100y-return extreme temperature could rise about +5.1°C, with uncertainty going from +2.3°C up to +8.9°C in the worst-case scenario. Meanwhile, heat wave days will suffer a great increase of 400%, with little uncertainty below median but high above it with the worst-case scenario pointing to an increase of up to 1500%. This increase in both temperature and heat waves will have associated an increase in hydrological drought (from SPEI), with values rising from +50% up to +100% with an expected value of +75% by 2100 (Figure 60).

Extreme rainfall events, which are common in the Mediterranean climate of Barcelona, are presumed to notably increase 30% at subdaily scale and 45% in the maximum daily precipitation with remarkable little uncertainty, ranging from 30 to 50%. These results are also reached by 2071-2100 period regarding 100-year return period events. Most frequent events also present increases in extreme values, although less pronounced. In the case of snowfall only an increase in these events is expected for long return-period events (100 years), being only significant for 2011-2040 period, with a median in the change of 40% ranging values from 5% to 50% in the amount of surface snow measured. For more frequent return periods a decrease in snowfall is expected. Storm surge of 2-year return period would increase by 2100.

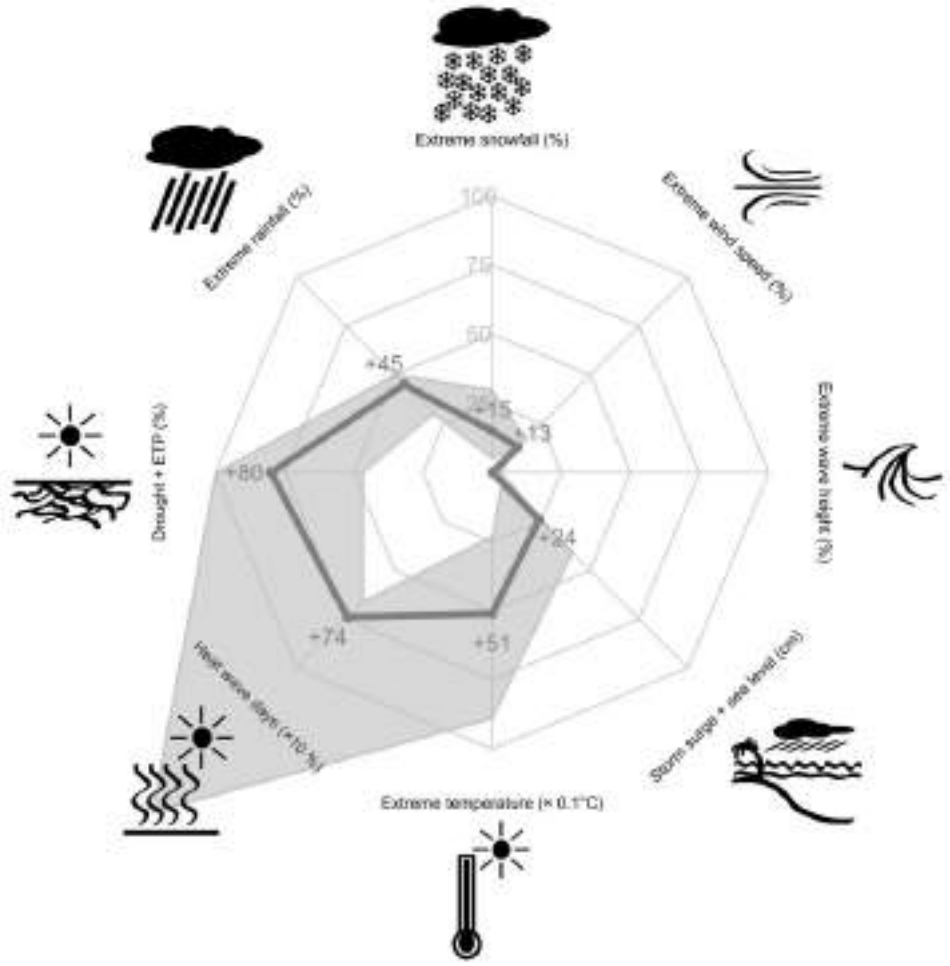

Figure 60. Extremes Compass Rose for Barcelona: Maximum point change in climate extreme events along the century taking into account return periods between 2 and 100 years. The centre represents no changes and the edge corresponds to an increase of 100% for every variable, except for heat wave days (border is +1000%), for storm surge (border is +100 cm) and extreme temperature (border is +10°C). Thick lines represent the median scenario and the shaded area is the uncertainty region (5-95%).

4.2. Lisbon

4.2.1. Extremes in temperature

Near and long-term climate change

Lisbon presents continuous rising trends in maximum temperature throughout the century for the three return periods taken into consideration (Figure 61). These increases would be greater than 1.5°C in 2011-2040, 3°C in 2041-2070 and 5°C in 2071-2100. The maximum expected values for temperature in 2, 10 and 100 years return periods could escalate up to 38.5°C, 41.9°C and 45.6ºC respectively by the end of the century.

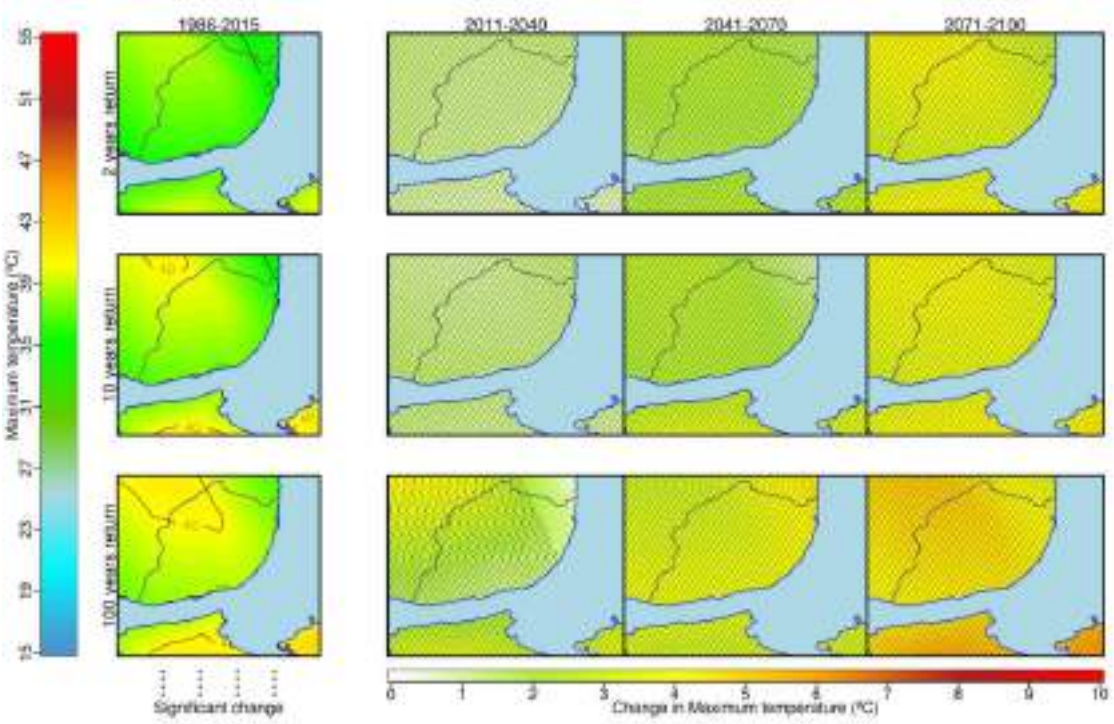

Figure 61. Multi-model median scenario of changes in extreme events of maximum temperature for the Lisbon area, according to 2, 10 and 100-year return periods (rows) and for three future time periods (2011-2040, 2041-2070 and 2071-2100, second to fourth column) with respect to the reference period 1986-2015 (first column).

The decadal forecast based on teleconnections project a similar increase than the climate simulation for the current twenty-year period (2016-2035). The increase is expected to be significant for return periods between 2 and 10 years. Decadal simulation based on drift-corrected dynamical models show no changes for the current time period (Figure 62).

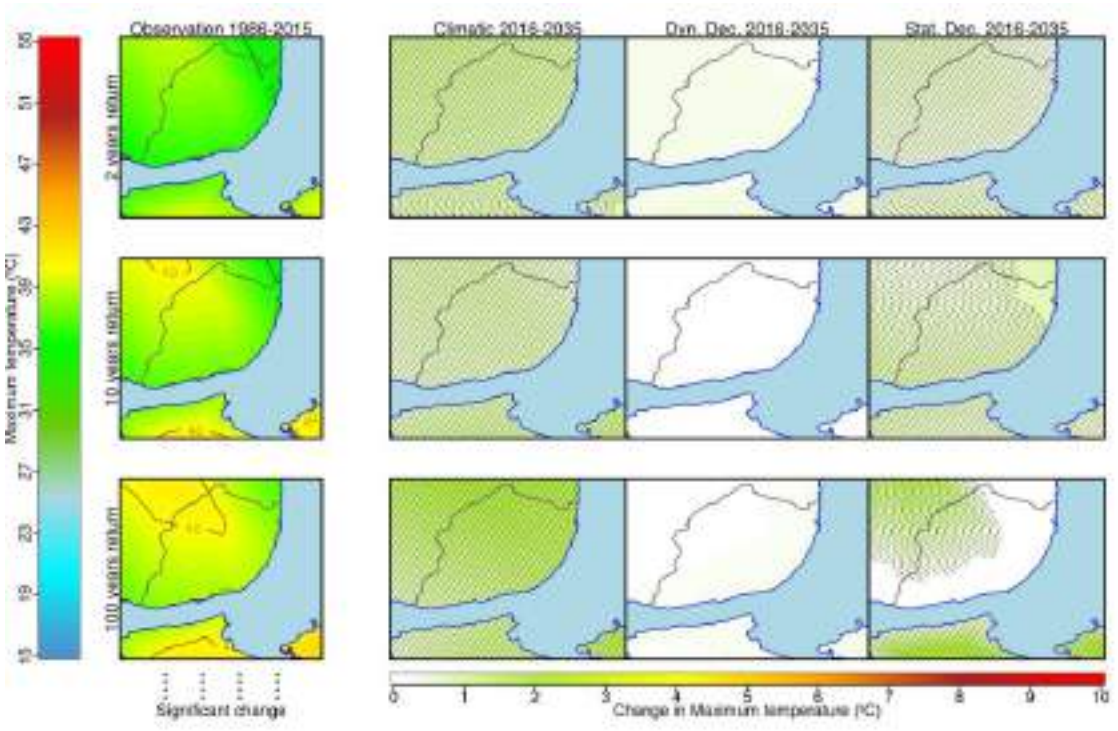

Figure 62. Comparison between three different projections of maximum temperature for the 2016-2035 period for the Lisbon area, according to 2, 10 and 100-year return periods (rows) and for three methods (statistical downscaling of climate CMIP5 models, drift-corrected decadal CMIP5 models and teleconnection-based approach, second to fourth column) with respect to the reference period 1986-2015 (first column).

Results suggest an abrupt decreasing trend for indices related to winter and cold days and an increasing trend for summer indices and warm days in Lisbon. The number of cold days could reduce from 35 to 10, winter duration would decrease from 90 to 30 days and the duration of the coldest period could reduce from 20 days to 10 (Figure 63). The starting days of the winter could delay about one month, from the beginning of December to the beginning of January, and the beginning of the coldest period could delay between one and two weeks. Meanwhile, the beginning of the warmest period would remain stable along the century around the end of July, but the summer is expected to begin one month and a half before. The summer duration could expand from 120 to 200 days and the warmest period from 10 to 50 days. The number of warm days and tropical nights could increase sharply from 40 to 90 and from 10 to 80 respectively. To sum up, in a yearly scale it is expected a clear trend of warming in Lisbon climate characteristics.

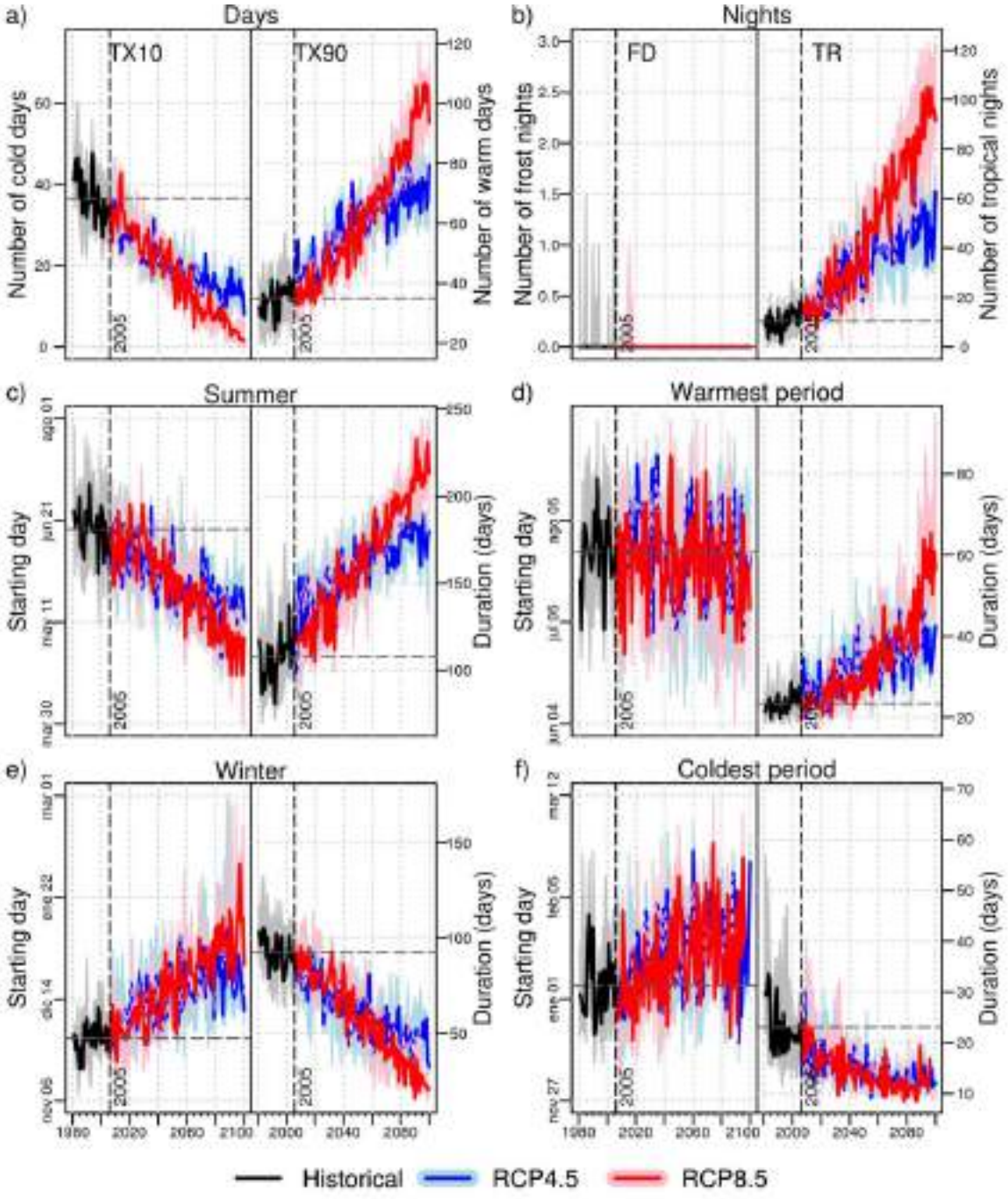

Figure 63. Climate projection of extreme indices (Table 3) based on temperature in Lisbon: a) Cold Days (TX10, left) and Warm Days (TX90, right), b) Frost Nights (FD, left) and Tropical Nights (TR, right), c) Summer starting day (left) and duration (right), d) Warmest period starting day (left) and duration (right), e) Winter starting day (left) and duration (right), f) Coldest period starting day (left) and duration (right).

The expected increase of heat waves in Lisbon is less than in Barcelona. In particular, the average number of events could rise from the average of about 0.8 ± 0.2 waves per year to 3 ± 1 waves per year by the end of the century. In addition, the average duration of a heat wave could be one day longer by 2100. With this, total heat wave days could increase from the initial value of 4 ± 1 to about 20 ± 10 days per year. On

the other hand, the average intensity and the maximum intensity of a heat wave could increase about +1°C by 2100 (Figure 64).

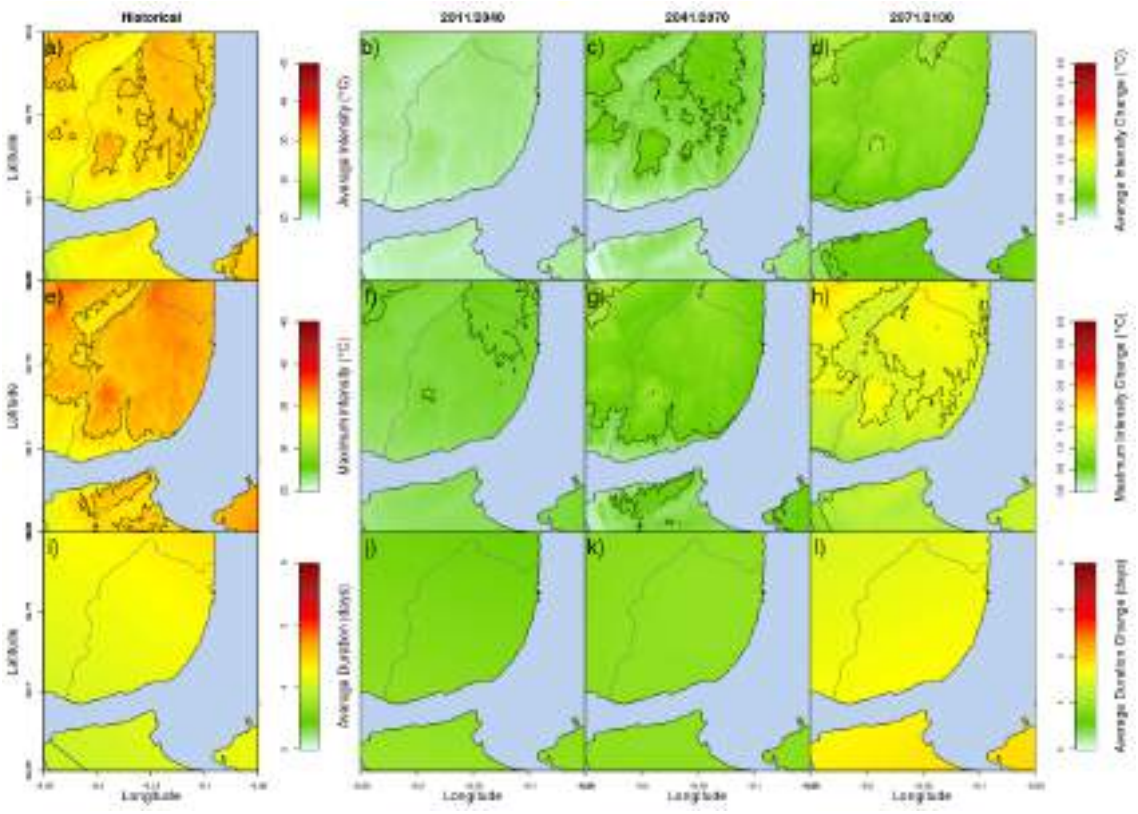

Figure 64. Past values (a, e, i) and projections of absolute change (b, c, d, f, g, h, j, k, l) of heat wave features in Lisbon under the RCP8.5 according to the downscaled multi-model median: Average intensity (a, b, c, d), maximum intensity (e, f, g, h) and average duration (i, j, k, l).

Seasonal forecast

Maximum temperature expected for the next six months in Lisbon is about +2°C greater than the average value obtained from climatology (Figure 65). However, the uncertainty level has a similar magnitude order. This seasonal forecast implies to a probable maximum peak temperature about 39°C in Lisbon city for the summer of 2018.

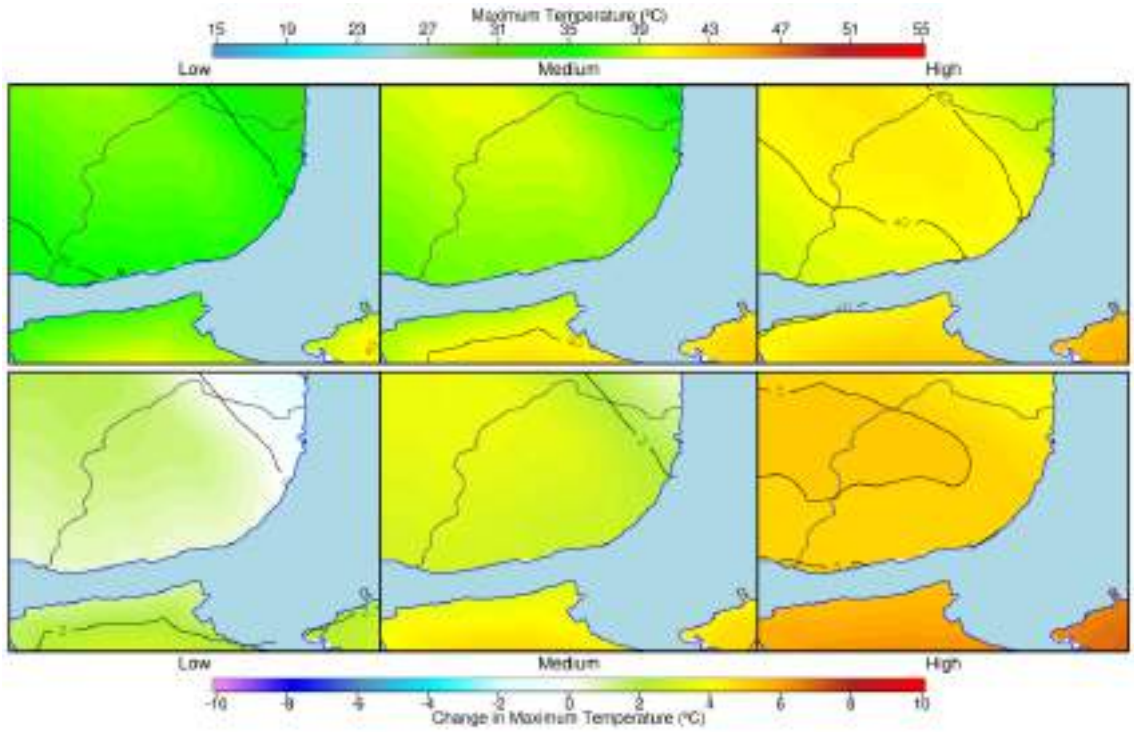

Figure 65. Probable scenarios for extreme maximum temperature expected in Lisbon for the next six months according to the seasonal forecast (bias-corrected dynamical model output from the CFSv4). From the left to the right: low (10%), medium (50%) and high (90%) percentiles of the predicted probability distribution for the expected maximum temperature (top) and the difference respect to climatology (bottom).

4.2.2. Extremes in rainfall

Climate changes in long-duration events

The climate projections for drought in Lisbon are similar to those of Barcelona. It is expected that SPEI decreases down to -1 by the end of the century, although SPI will remain approximately constant (Figure 66). Therefore, an increase of the evapotranspiration will cause a greater water stress and a consequent greater shortage of water.

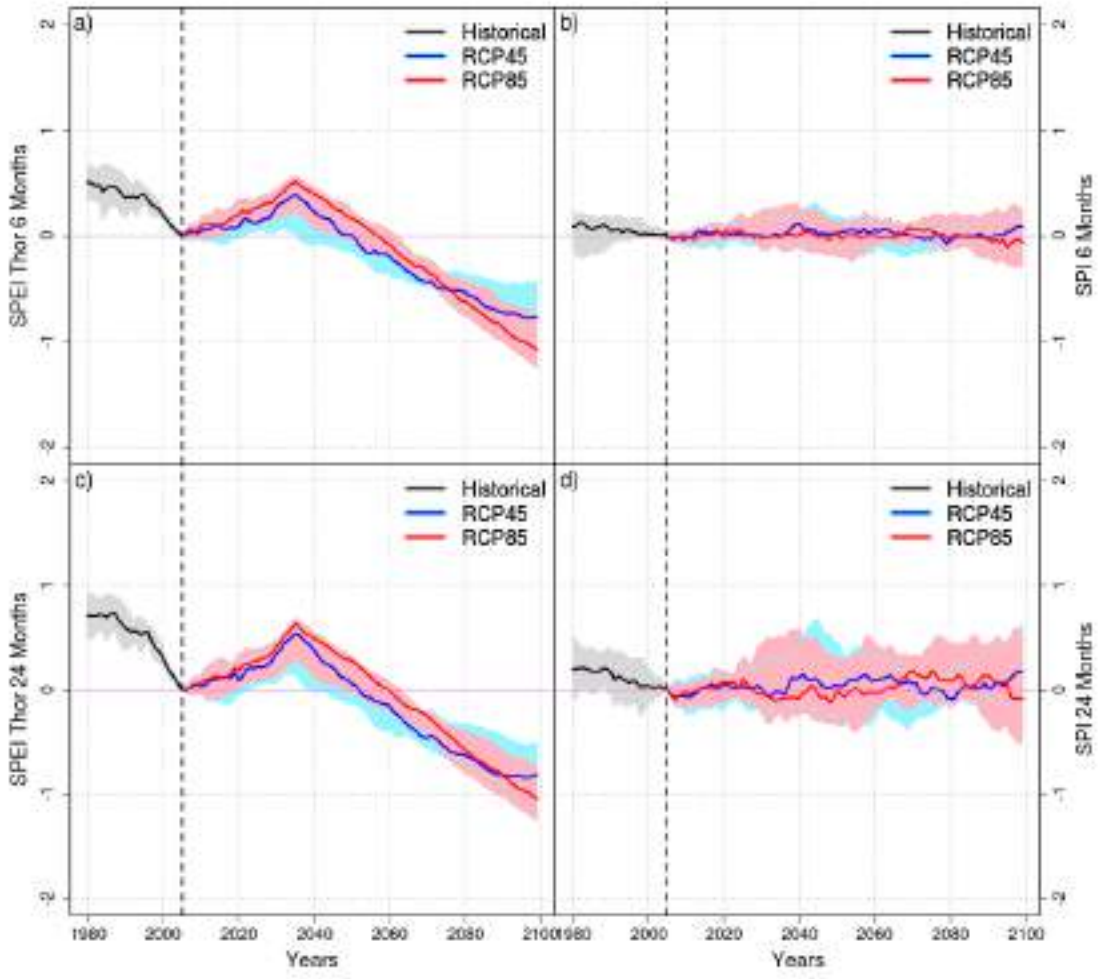

Figure 66. Ensemble of projections for SPEI (left) and SPI (right) for the Lisbon area according to 6 and 24-month moving windows.

Climate changes in short-duration events

Extreme hourly rainfall presents a moderate rising trend in Lisbon from 40mm to 45mm in 2041-2070 period and 47mm in 2071-2100 period for a 100 years return period (Figure 67). That is the increase is about 10% and 20% respectively in the middle and end of the century. Regarding to the daily rainfall, no significant changes are expected in the Lisbon municipality.

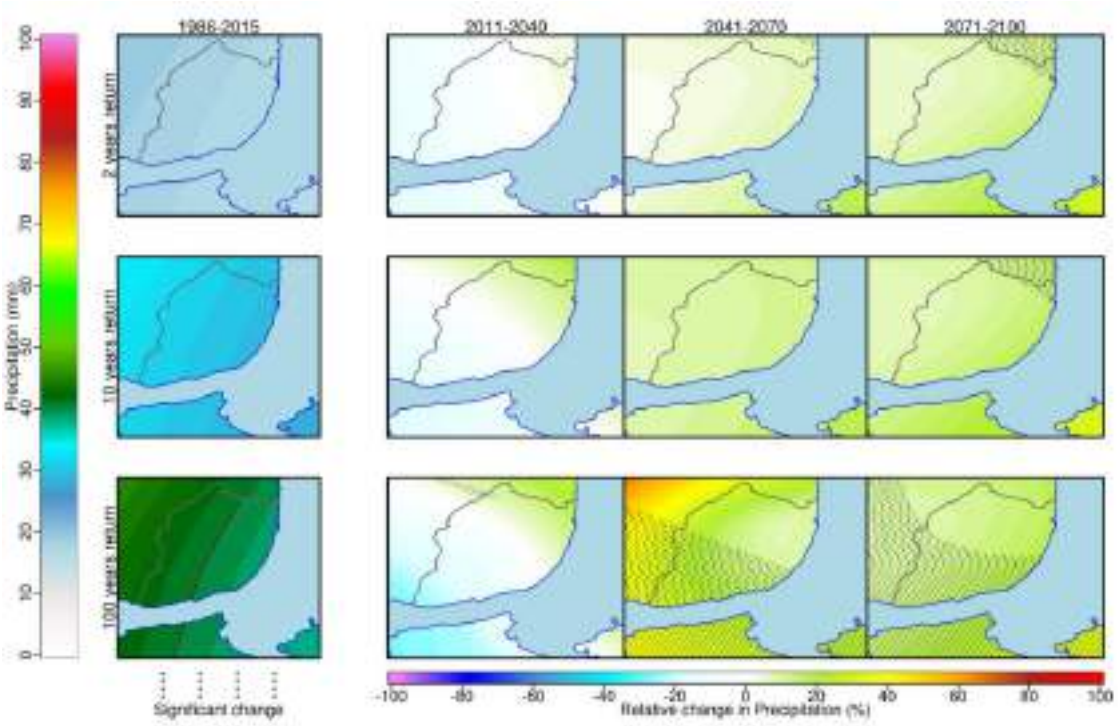

Figure 67. Multi-model median scenario of changes in extreme events of hourly rainfall for the Lisbon area, according to 2, 10 and 100-year return periods (rows) and for three future time periods (2011-2040, 2041-2070 and 2071-2100, second to fourth column) with respect to the reference period 1986-2015 (first column).

Number of subdaily events of heavy rainfall greater than 20mm shows a slight decreasing trend in Lisbon along the century, falling from 0.66±0.02 events per year (expected occurrence period of 18 months) to 0.62 ± 0.04 events per year (19 months).

The duration of the events remains stable in the first half of the century around 260min and it will suffer a decline in the second half of the century to 250min in the case of RCP4.5 and to 230min in the case of RCP8.5 (Figure 68).

The total amount of rainfall per event will increase, so the reference intensity is expected to rise from 2.5 to 2.7mm/5min (+8%) according to RCP4.5 and 3mm/5min (+20%) according to the RCP8.5. The *n*-index would stay stable around 0.410±0.005 along the century under the RCP4.5, or it would reach 0.425±0.005 (+5%) in 2100 according to RCP8.5. This increase in the *n*-index implies that the future rainfall should be more concentrated in Lisbon, which is added to the more intense rainfall.

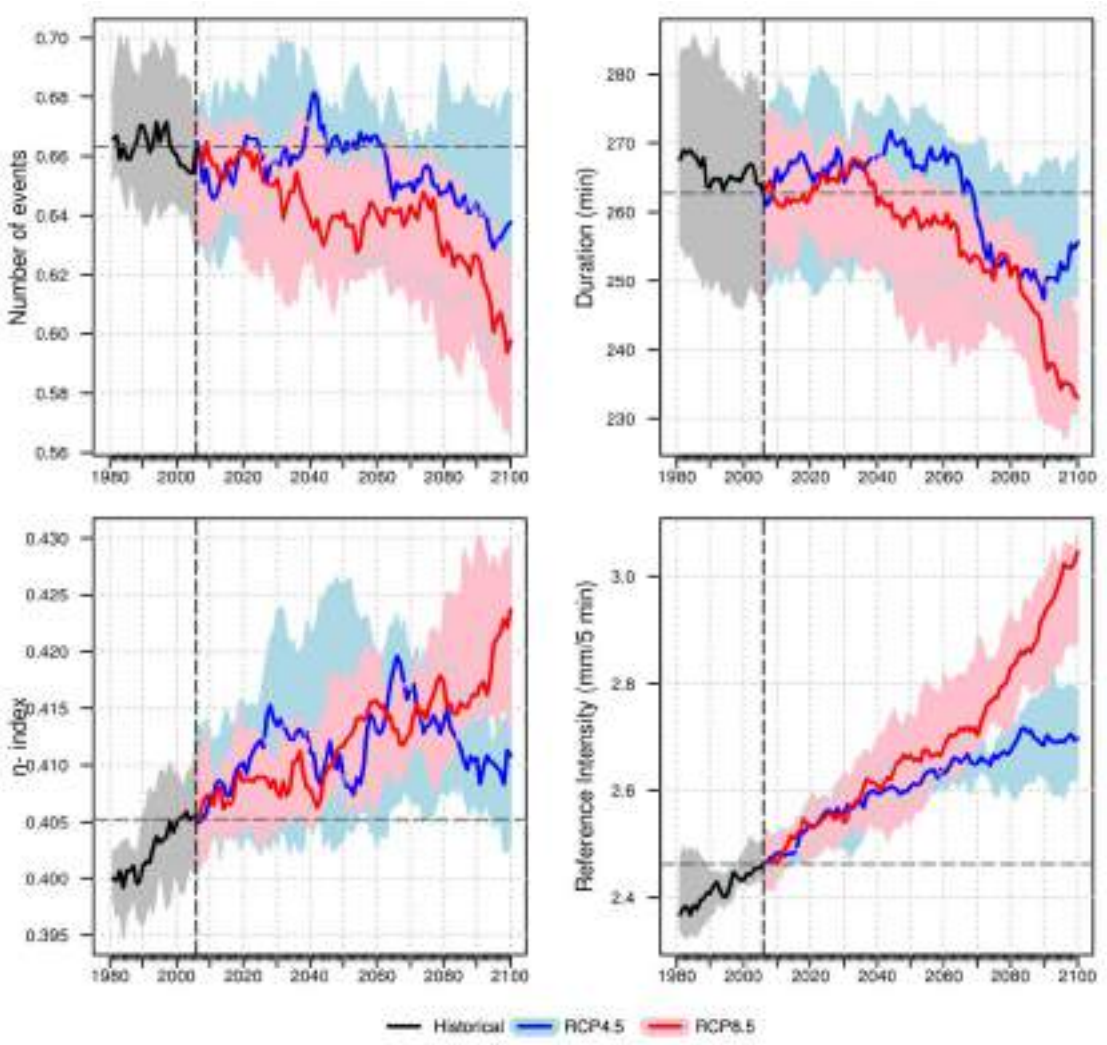

Figure 68. Extreme indices of precipitation according to sub-daily events with precipitation amounts greater than 20 mm in Lisbon: Number of events (top-left), duration (top-right), n-index (bottom-left) and reference intensity (bottom-right).

Regarding to the Intensity-Duration-Frequency (IDF) curves, future climate projections show a probable increase of the rainfall intensity in Lisbon by 2041-2070 for most of return periods. Specifically, change factor ranges between 1.1 and 1.2, especially for shorter durations, with respect to the baseline 1976-2005 period (Figure 69). For the last period (2071-2100), change factor of 1-hour events could rise up to 1.3 but with a high uncertainty level. Finally, non-significant changes are expected for the current thirty-year period (2011-2040).

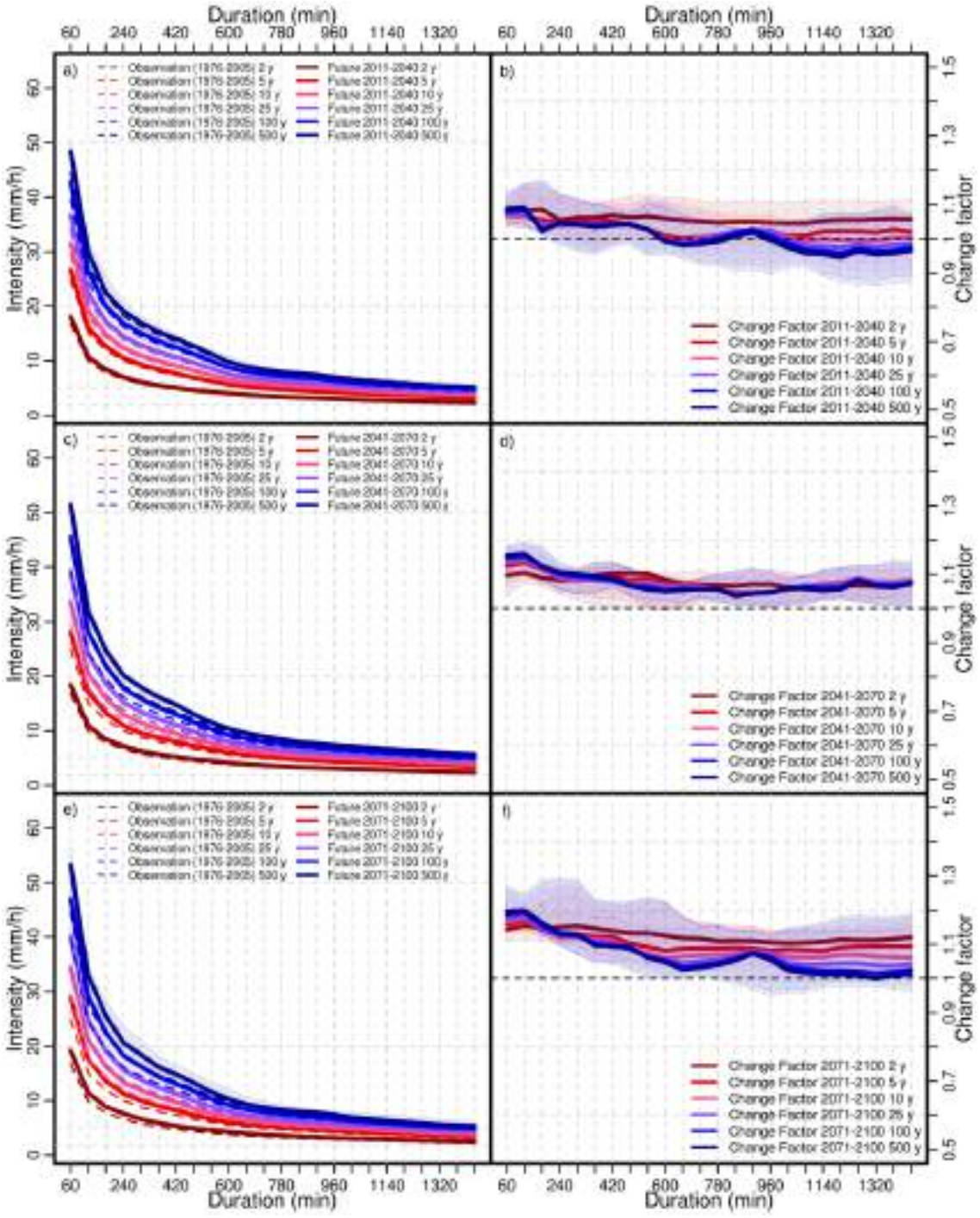

Figure 69. Projected IDF curves for the Lisbon Portela airoport (station No. 085790) according to absolute values (left panels) and the change factor (right panels) for three future time periods: 2011-2040 (a, b), 2041-2070 (c, d) and 2071-2100 (e, f).

Seasonal forecast

Maximum extreme hourly precipitation expected for the next sixth months in Lisbon will probably be close to the average value. Specifically, the predicted anomaly is ±30% with respect to the climatic value (Figure 70)

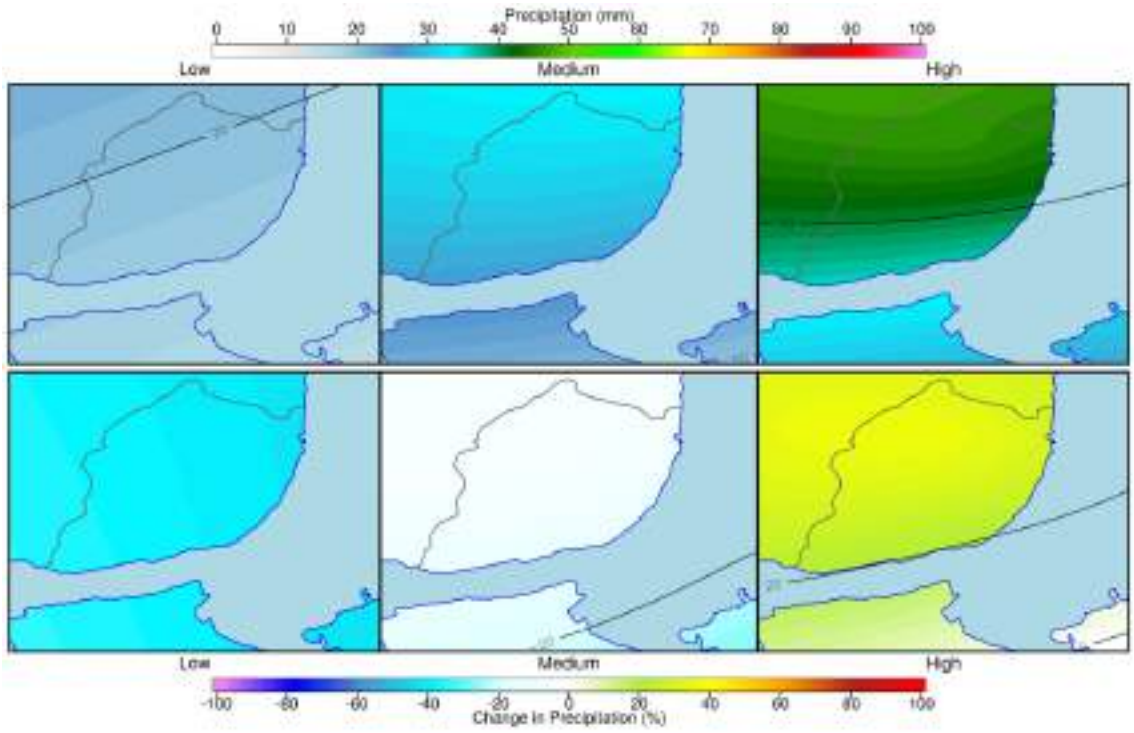

Figure 70. Probable scenarios for extreme hourly precipitation expected in Lisbon for the next six months according to the seasonal forecast (bias-corrected dynamical model output from the CFSv4). From the left to the right: low (10%), medium (50%) and high (90%) percentiles of the predicted probability distribution for the expected extreme daily precipitation (top) and the difference with respect to climatology (bottom).

4.2.3. Other variables

4.2.3.1. Extremes in wind

Climate scenarios for Lisbon did not show significant trends in extreme wind gust for any of the return periods taken into consideration (Figure 71). Only a small zone of the Lisbon municipality presents a significant signal of increment in extreme gust by 2041-2071 period.

This is due to compensation among two opposite wind/calm scenarios caused by the global warming: 1) Increase of thunderstorms (due to more summertime barometric swamp), and 2) decrease of windstorms frequency (because of a more northern jet stream).

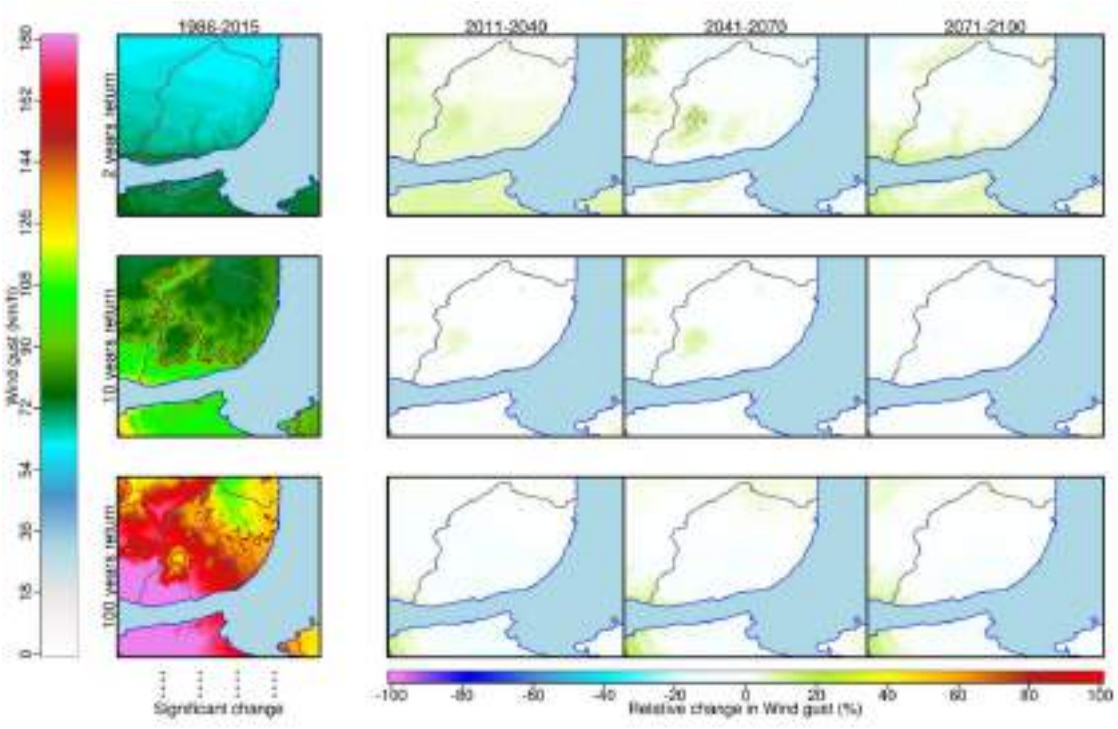

Figure 71. Multi-model median scenario of relative changes in extreme wind gust for the Lisbon area, according to 2, 10 and 100-year return periods (rows) and for three future time periods (2011-2040, 2041-2070 and 2071-2100, second to fourth column) with respect to the reference period 1986-2015 (first column).

4.2.3.2. Extremes in sea level

Results for storm surge (+ sea level rise) suggest a decrease of 20% for the 2011-2040 period according to the three return periods studied. However, for the end of century, an increase of the storm surge is expected between +10% and +60% (median 30%) for the 2-year return period, and about +20% for the 10-year return events. Thus, the maximum expected value in one century for extreme storm surge would reach around 1m.

4.2.4. Summary of changes in extremes for Lisbon

Significant increases in maximum temperature and 1-hour rainfall are expected along the century for all return periods (Table 7). Wind gusts would also increment for high return periods, but only during the next decades. For the end of the century, 2-year return events of storm surge (+ sea level rise) would increase up to +20% by 2100.

Table 7. Summary of changes in extremes values for Lisbon municipality according to the decadal and climate models.

Variable	Return period (years)	*Observed*	*Decadal forecast*	Relative change		
		1986-2015	*2016-2035*	*2011-2040*	*2041-2070*	*2071-2100*
Maximum Temperature	2	34.9 °C	+0.2 °C (-0.3/+0.5)	**+1.2 °C** (+1.3/+2.1)	**+1.9 °C** (+1.7/+3.5)	**+5.0 °C** (+1.9/+7.2)
	10	38.9 °C	-0.2 °C (-0.4/+0.5)	**+1.2 °C** (+0.5/+2.0)	**+2.1 °C** (+2.3/+3.8)	**+4.2 °C** (+4.0/+5.5)
	100	40.7 °C	-0.1 °C (-0.9/+0.4)	**+1.8 °C** (0.75/+3.1)	**+3.3 °C** (+1.0/+3.4)	**+5.1 °C** (+4.7/+5.6)
1h Precipitation	2	17 mm	+5 % (-6/+12)	**+8 %** (+5/+10)	**+10 %** (+7/+13)	**+14 %** (+11/+16)
	10	29 mm	+8 % (-6/+18)	**+7 %** (+3/+12)	**+14 %** (+10/+16)	**+17 %** (+14/+23)
	100	40 mm	+9% (-10/+16)	**+8 %** (+4/+13)	**+15 %** (+11/+18)	**+19 %** (+17/+26)
Wind Gust	2	68.0 km/h		-5.3 % (-5.4/+0.4)	-0.4 % (-6.4/+2.5)	**-2.0 %** (-6.1/-0.8)
	10	95 km/h		**+1.5 %** (+0.5/+1.6)	+1.6 % (-0.3/+2)	+0.7 % (-0.4/+3)
	100	116 km/h		**+4.5 %** (+2.1/+4.6)	**+2.4 %** (+1.2/+5.0)	+4.2 % (-0.9/+4.9)
Storm surge + sea leve rise	2	0.67 m		-10% (-15/+5)	10% (+0/+30)	**30%** (+10/+60)
	10	0.88 m		**-10%** (-25/-0)	0% (-10/+15)	**20%** (+0/+40)
	100	1.26 mm		**-20%** (-30/-10)	-10% (-20/+5)	-5% (-15/+20)

Not available

Significant increase P > 95%
Not significant increase 50% < P < 95%
Not significant changes P < 50%
Not significant decrease 50% < P < 95%
Significant decrease P > 95%

More in detail, extreme temperature peak values are presumed to significantly increase for all time periods of the century and all return periods. Highest increases are expected by the end of the century, with a median increase of +5.1°C and little uncertainty for 100-year events (from +4.7°C to 5.6°C), although the biggest increase is expected for 2-year events, with a median of +5.0°C and a spread ranging from 1.9°C

up to 7.2°C. Heat wave days are also presumed to suffer from a great increase in extreme values, with a median of 250% increase but an uncertainty that makes change non-significant (from 0% up to 1000%) (Figure 72). Hydrological drought values behave the same, with a great median increase of +80% but incertitude ranging from 0% up to +90%. However, pluviometric drought (only-dependent of the rainfall or SPI) is not expected to change. On the other hand, extreme hourly rainfall could rise up to +20% (shown in the Figure 72), but the extreme daily precipitation does not show significant changes.

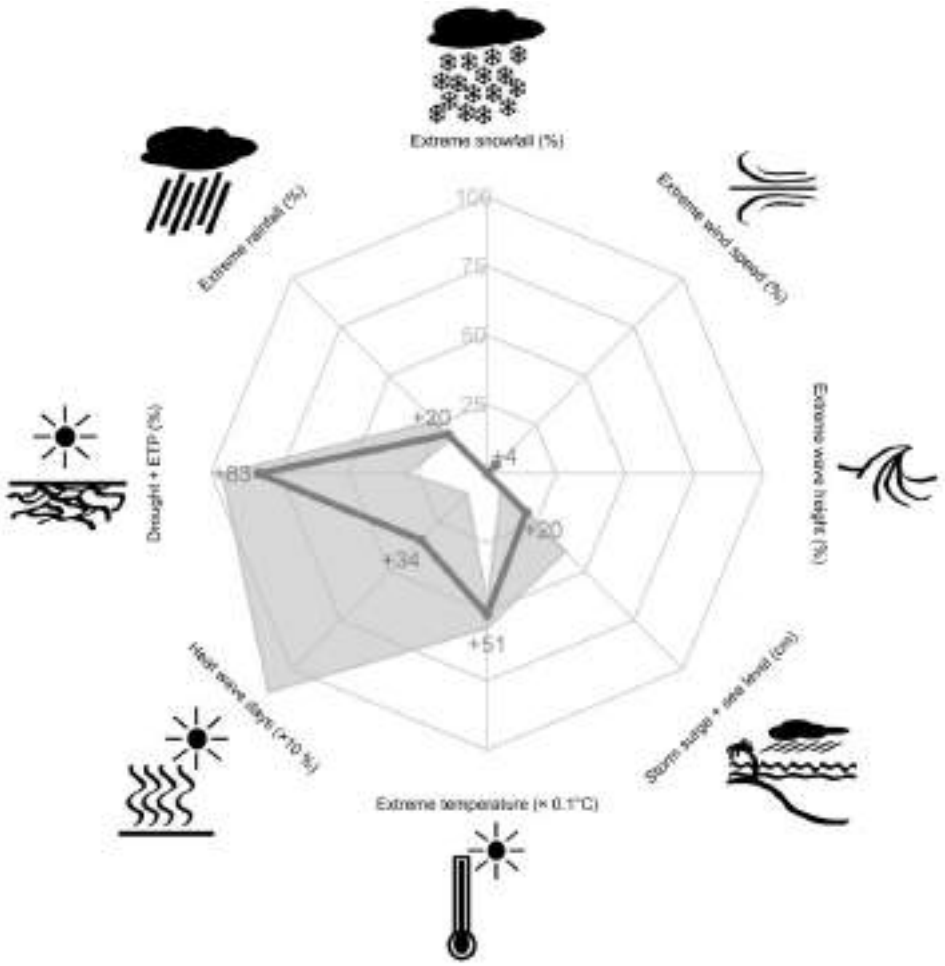

Figure 72. Extremes Compass Rose for Lisbon: Maximum point change in climate extreme events along the century taking into account return periods between 2 and 100 years. The centre represents no changes and the edge corresponds to an increase of 100% for every variable, except for heat wave days (border is +1000%), for storm surge (border is +100 cm) and extreme temperature (border is +10°C). Thick lines represent the median scenario and the shaded area is the uncertainty region (5-95%).

4.3. Bristol

4.3.1. Extremes in temperature

Near and long-term climate change

Bristol case presents continuous rising trends in maximum temperature along the century (Figure 73). Extreme temperature would rise about +1.5ºC until 2040 and between 3ºC and 4ºC in the second half of the century. The maximum expected values could reach 32.7ºC once every two years and 34.7ºC once every 10 years (in average) by the end of the century.

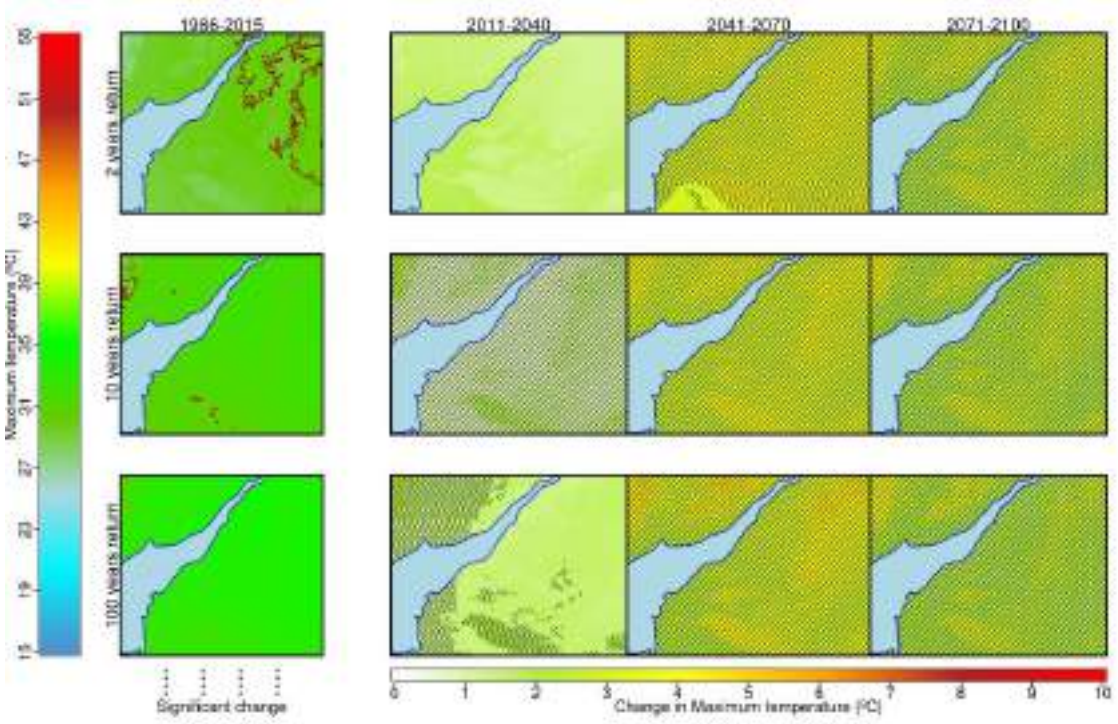

Figure 73. Multi-model median scenario of changes in extreme events of maximum temperature for the Bristol area, according to 2, 10 and 100-year return periods (rows) and for three future time periods (2011-2040, 2041-2070 and 2071-2100, second to fourth column) with respect to the reference period 1986-2015 (first column).

For the current twenty-year period (2016-2035), non-significant differences are found between the simulations obtained from downscaled climate models and the obtained from drift-corrected dynamical decadal models or teleconnection-combined statistical approach (Figure 74).

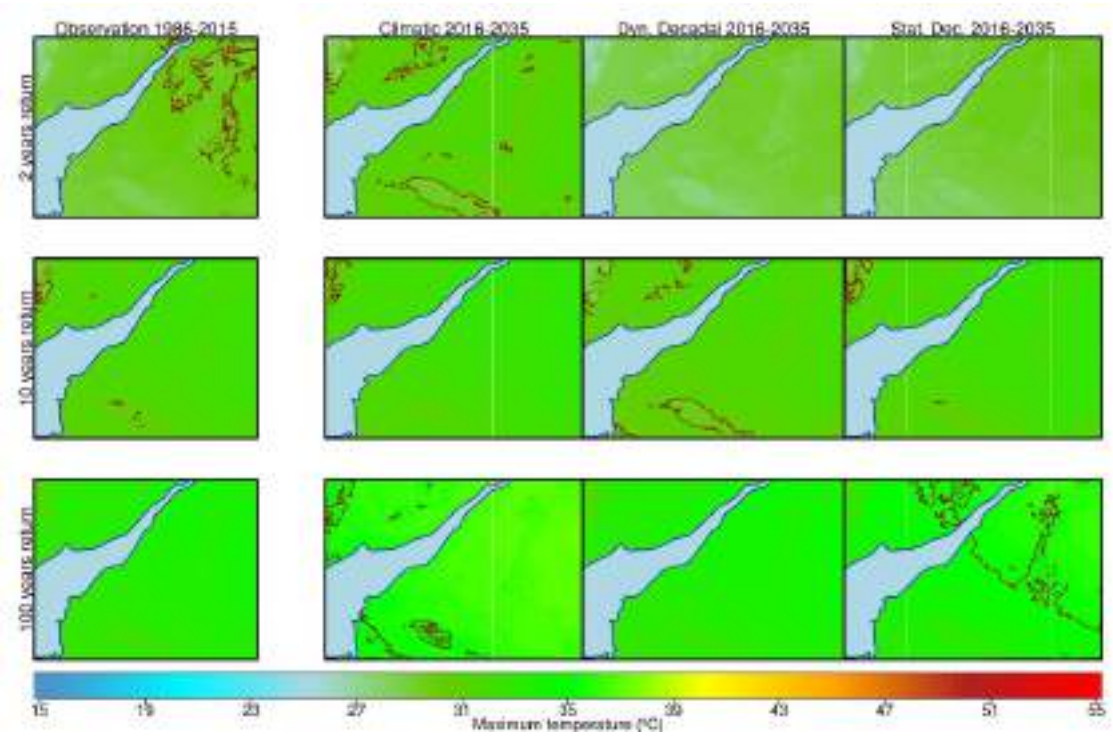

Figure 74. Comparison between three different projections of maximum temperature for the 2016-2035 period for the Bristol area, according to 2, 10 and 100-year return periods (rows) and for three methods (statistical downscaling of climate CMIP5 models, drift-corrected decadal CMIP5 models and teleconnection-based approach, second to fourth column) with respect to the reference period 1986-2015 (first column).

Abrupt decreasing trends are observed for indices related to winter and cold days (Figure 75). Conversely, increasing trends are expected for summer indices and warm days in Bristol. The number of cold days could reduce from 40 to 10, winter duration would decrease from 90 to 30 days and the duration of the coldest period could reduce from 25 days to 10. The number of frost nights would decline from 40 to 10. The starting day of the winter could delay about one month, from the beginning of December to the beginning of January and the beginning of the coldest period would remain unchanged around mid-January. Regarding warm features, the beginning of the warmest period would remain stable along the century around the beginning of July, but the summer is expected to begin one month earlier. The summer duration could expand from 100 to 160 days and the warmest period from 25 to 80 days. The number of warm days and tropical nights could increase sharply from 40 to 90 and from 0 to 10 respectively. To sum up, in a yearly scale it is expected a clear trend of warming in Bristol's climate characteristics.

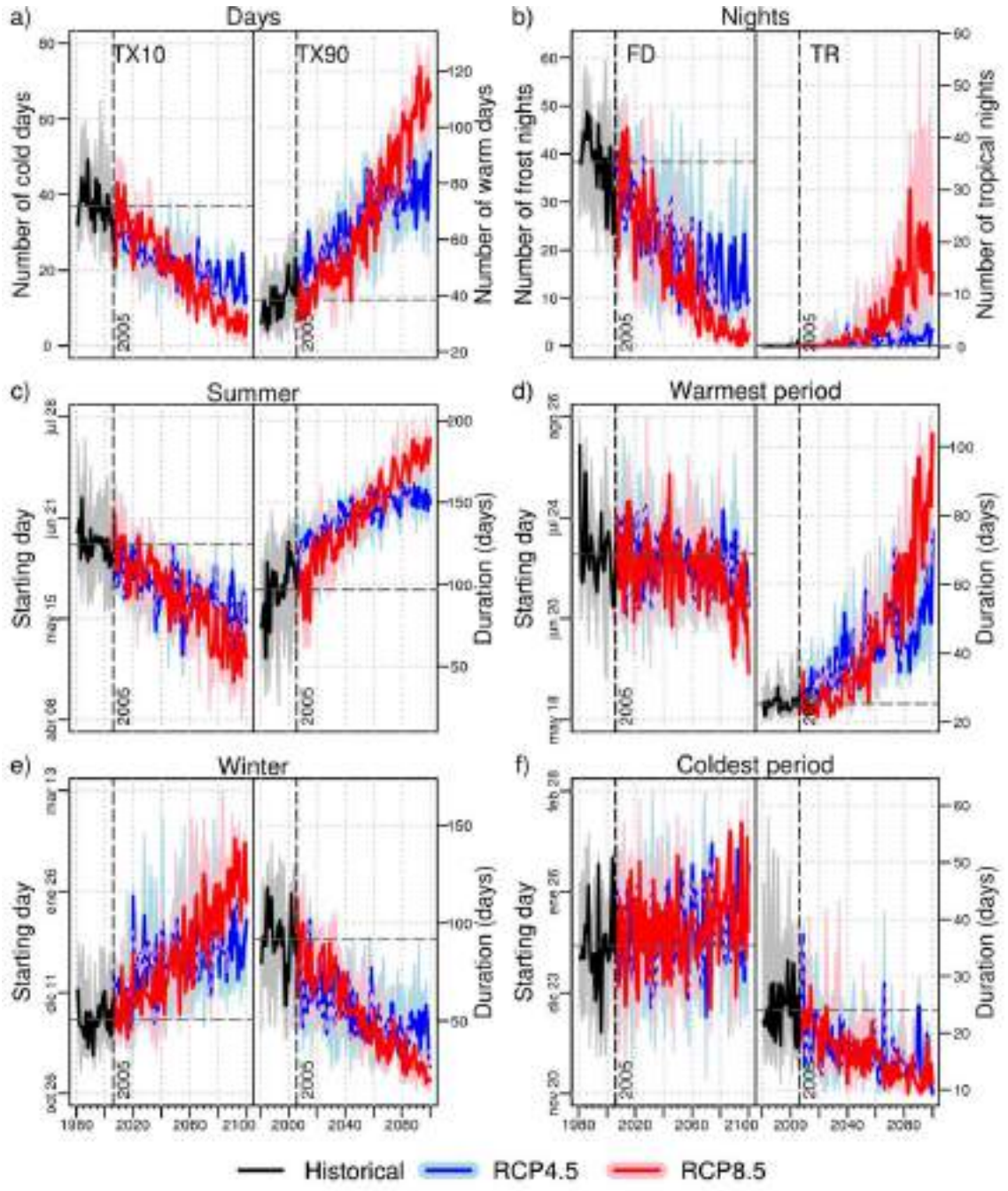

Figure 75. Climate projection of extreme indices (Table 3) based on temperature in Bristol: a) Cold Days (TX10, left) and Warm Days (TX90, right), b) Frost Nights (FD, left) and Tropical Nights (TR, right), c) Summer starting day (left) and duration (right), d) Warmest period starting day (left) and duration (right), e) Winter starting day (left) and duration (right), f) Coldest period starting day (left) and duration (right).

As in Barcelona, a great increase in the number of heat waves is expected for Bristol, rising from the average of about 0.9±0.3 waves per year to 4±2 waves per year by the end of the century. Moreover, the average duration of a heat wave could be doubled by 2100. With this, total heat wave days could increase from the initial value of 5.0 ± 1.0 to 20±10 days per year (Figure 76).

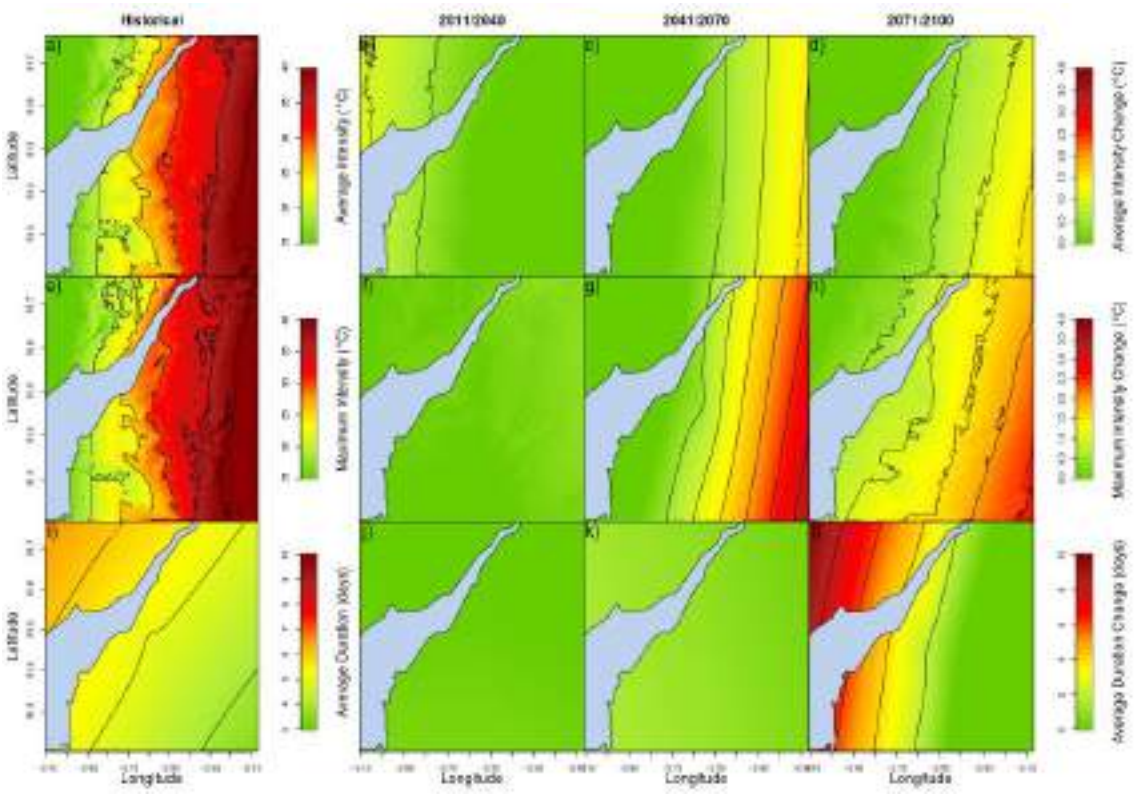

Figure 76. Past values (a, e, i) and projections of absolute change (b, c, d, f, g, h, j, k, l) of heat wave features in Bristol under the RCP8.5 according to the downscaled multi-model median: Average intensity (a, b, c, d), maximum intensity (e, f, g, h) and average duration (i, j, k, l).

Seasonal forecast

The peak value of maximum temperature for this next six-month period, regarding Bristol city, is expected to have no anomaly with respect to the mean extreme climatic value for this period. The signal seems to be unclear, pointing whether to a normal season or to a non-significant prediction, with uncertainty ranging from -3ºC up to +2ºC, with values in the worst-case scenario rising up to 29ºC in Bristol area (Figure 77).

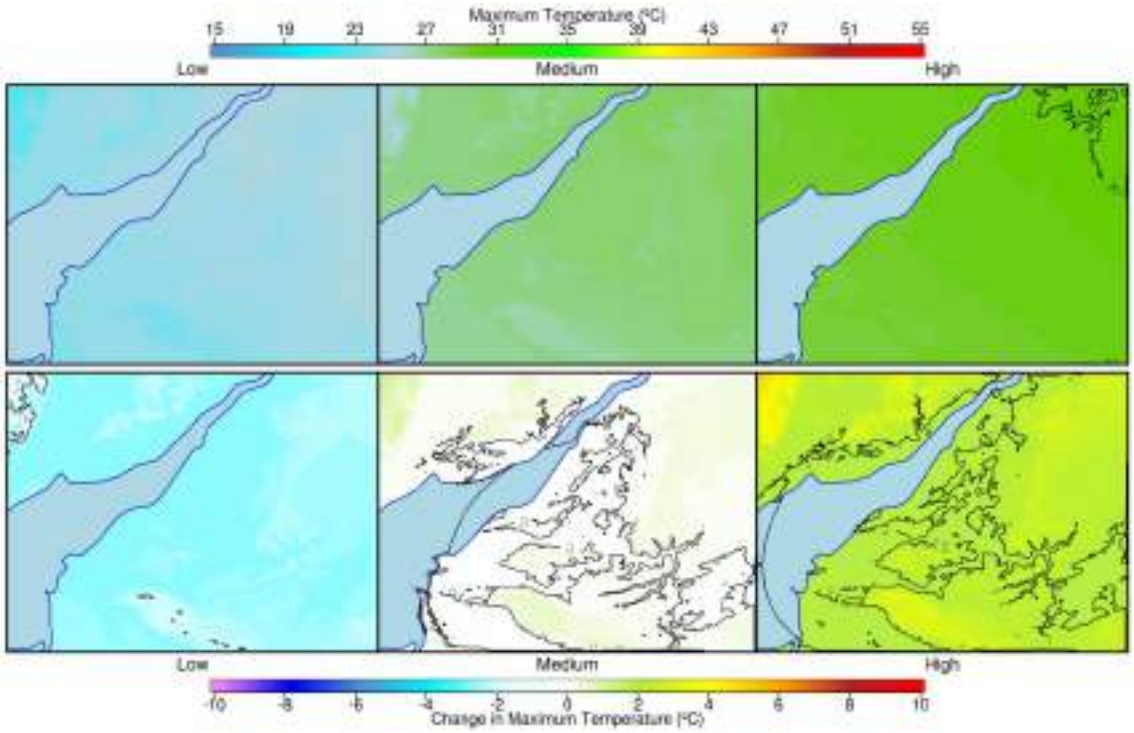

Figure 77. Probable scenarios for extreme maximum temperature expected in Bristol for the next six months according to the seasonal forecast (bias-corrected dynamical model output from the CFSv4). From the left to the right: low (10%), medium (50%) and high (90%) percentiles of the predicted probability distribution for the expected maximum temperature (top) and the difference with respect to climatology (bottom).

4.3.2. Extremes in precipitation

Climate changes in long-duration events

Extreme precipitation in 12h presents very smooth rising trends in 2011-2040 (Figure 78). However, this tendency would be much sharper in the second half of the century, reaching increments of about +30%. Maximum expected values for extreme precipitation in 12h could reach 41mm once in a decade and 46mm once in a century (in average) between 2040 and 2100.

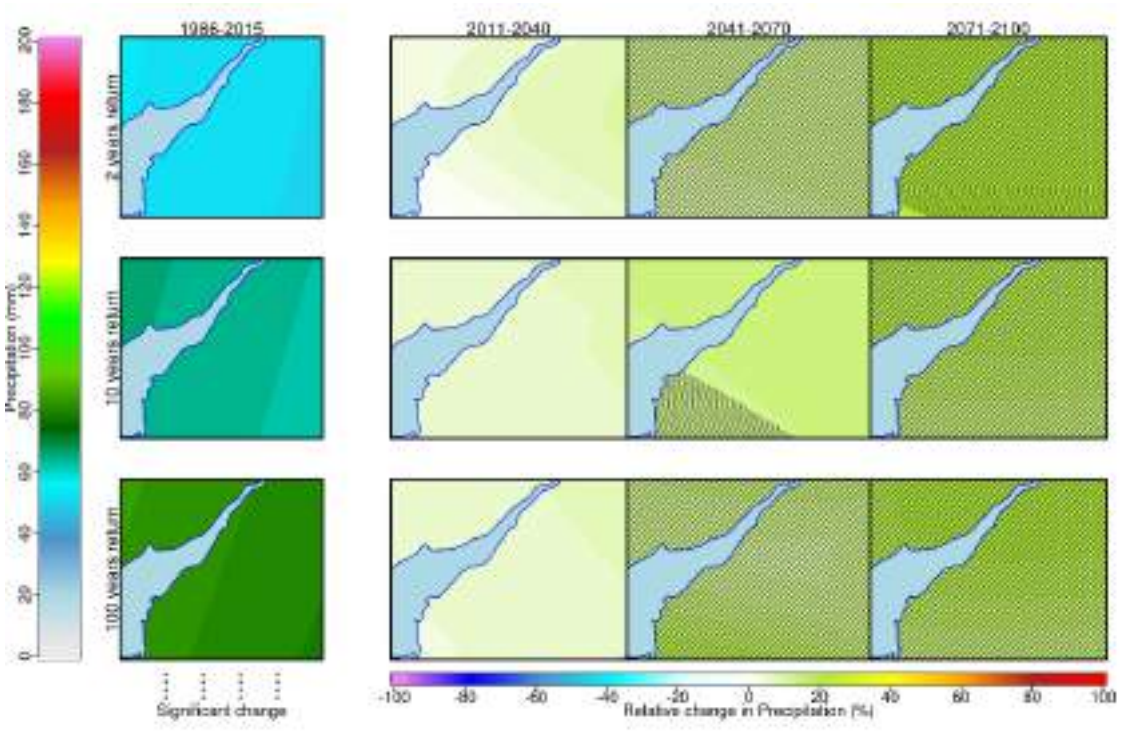

Figure 78. Multi-model median scenario of changes in extreme events of precipitation for the Brsitol area, according to 2, 10 and 100-year return periods (rows) and for three future time periods (2011-2040, 2041-2070 and 2071-2100, second to fourth column) with respect to the reference period 1986-2015 (first column).

Regarding climate projections for drought in Bristol, they are similar to the previous cases. It is expected that SPEI decreases down to -1 by the end of the century, although SPI will rise in concordance with the increase of annual rainfall (Figure 79). Therefore, an increase of the evapotranspiration will cause a greater water stress and a consequent greater shortage of water.

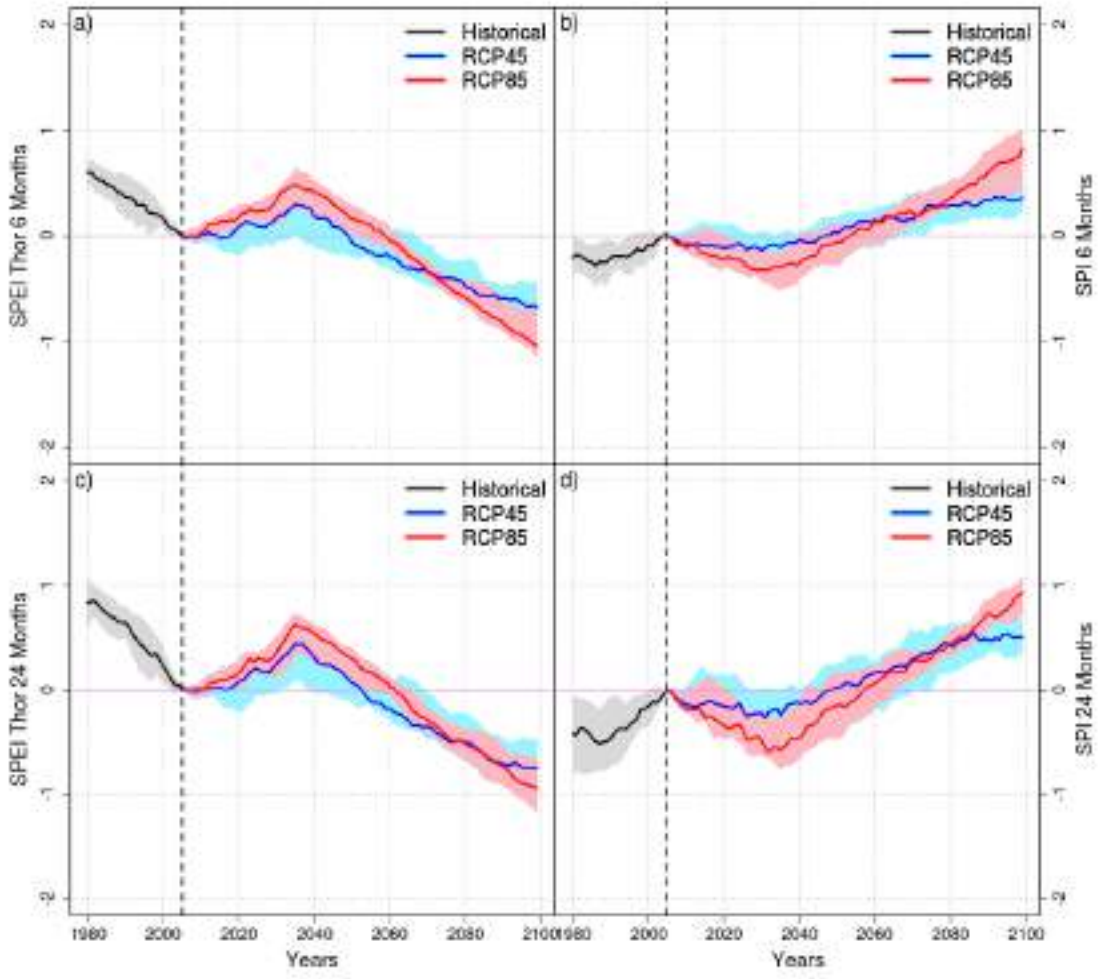

Figure 79. Ensemble of projections for SPEI (left) and SPI (right) for the Bristol area according to 6 and 24-month moving windows.

Climate changes in short-duration events

The number of subdaily events of heavy rainfall greater than 20mm tends to remain stable in the first half of the century (with an expected occurrence period of 18 months). However, it will tend to increase in the second half of the century up to 0.76±0.02 events per year (with an expected occurrence period of 15 months) according to the RCP8.5. The duration of the events would increase slightly in the first third of the century and would remain stable around 170±0.5 min until 2100.

The total amount of rainfall per event will increase, so the reference intensity is expected to rise from 2.4mm/5min to 2.6 or 2.9mm/5min and the *n*-index will also increase throughout the century, from 0.265±0.005 to 0.275±0.005 (Figure 80). All this means that extreme rainfall episodes will tend to increase in Bristol.

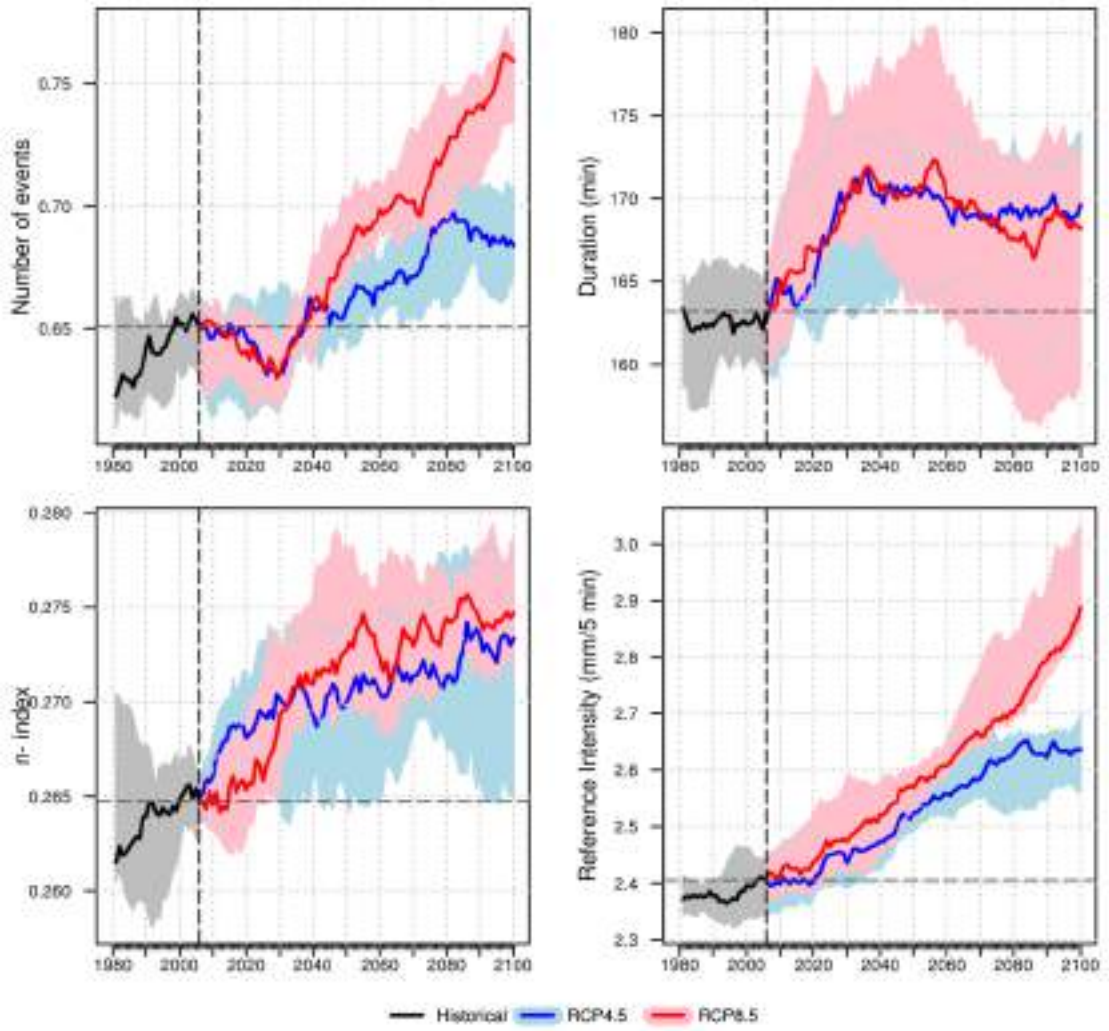

Figure 80. Extreme indices of precipitation according to sub-daily events with precipitation amounts greater than 20 mm in Bristol: Number of events (top-left), duration (top-right), n-index (bottom-left) and reference intensity (bottom-right).

The Intensity-Duration-Frequency (IDF) curves projected for Bristol throughout the century are similar to those from Lisbon and Barcelona: A probable increase of the rainfall intensity is expected by 2041-2070 for most of return periods. Change factor tends to 1.1 or 1.2 for all durations with respect to the baseline 1976-2005 period (Figure 81). The uncertainty level is greater for the current thirty-year period (2011-2040), especially for shorter durations.

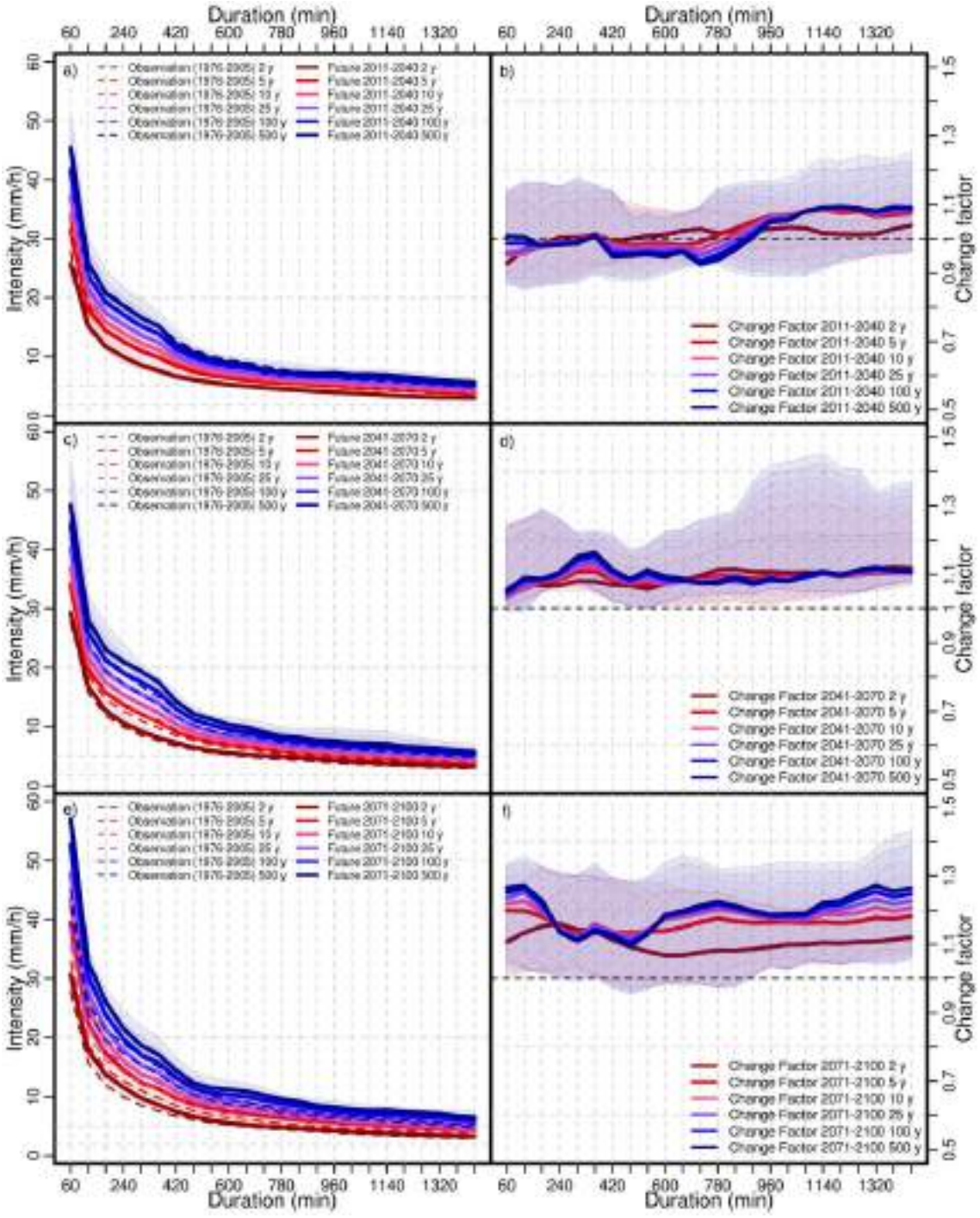

Figure 81. Projected IDF curves for the Bristol area (station No. 24615248) according to absolute values (left panels) and the change factor (right panels) for three future time periods: 2011-2040 (a, b), 2041-2070 (c, d) and 2071-2100 (e, f).

Seasonal forecast

Regarding to the seasonal forecast of extreme daily precipitation in Bristol, a positive anomaly is expected in the maximum amount of rainfall the next six months. In particular, the median value of the predicted anomaly is +15% and the uncertainty value ranges from -10% to +40% (Figure 82).

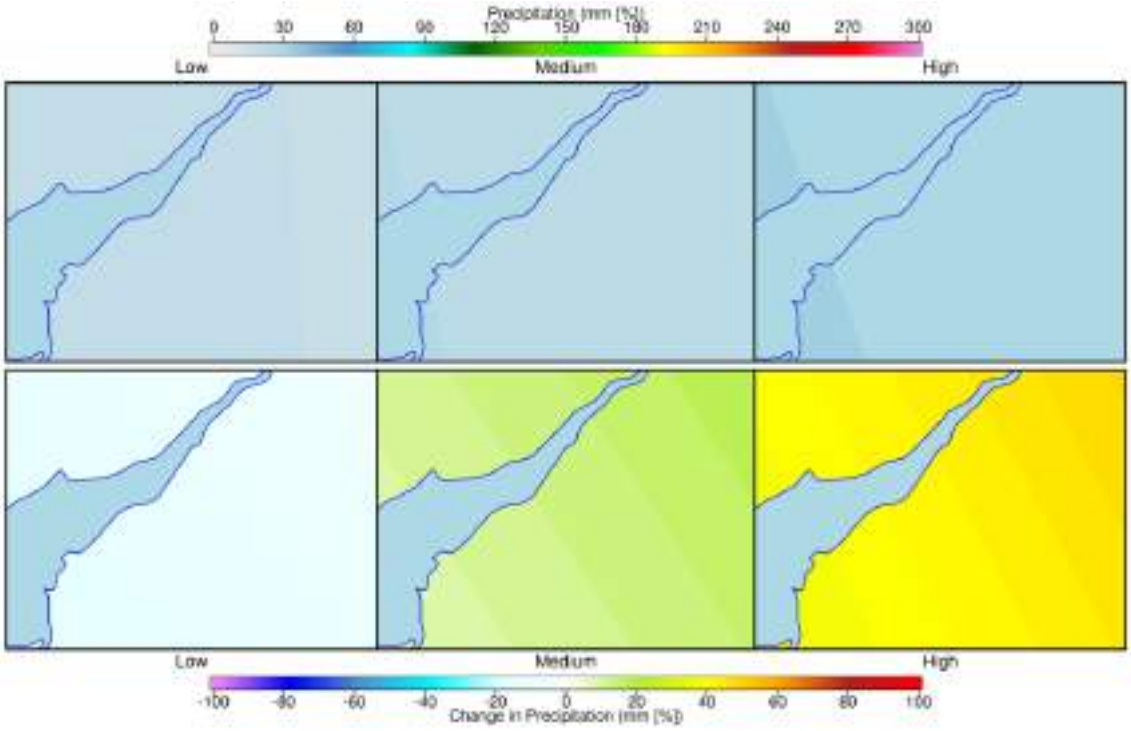

Figure 82. Probable scenarios for extreme daily precipitation expected in Bristol for the next six months according to the seasonal forecast (bias-corrected dynamical model output from the CFSv4). From the left to the right: low (10%), medium (50%) and high (90%) percentiles of the predicted probability distribution for the expected extreme daily precipitation (top) and the difference with respect to climatology (bottom).

4.3.3. Other variables

4.3.3.1. Extremes in wind

Extreme wind gust would remain fairly stable along the century for the three return periods taken into consideration, so maximum expected values could reach 97km/h once in a decade and 119km/h once in a century (in average) (Figure 83).

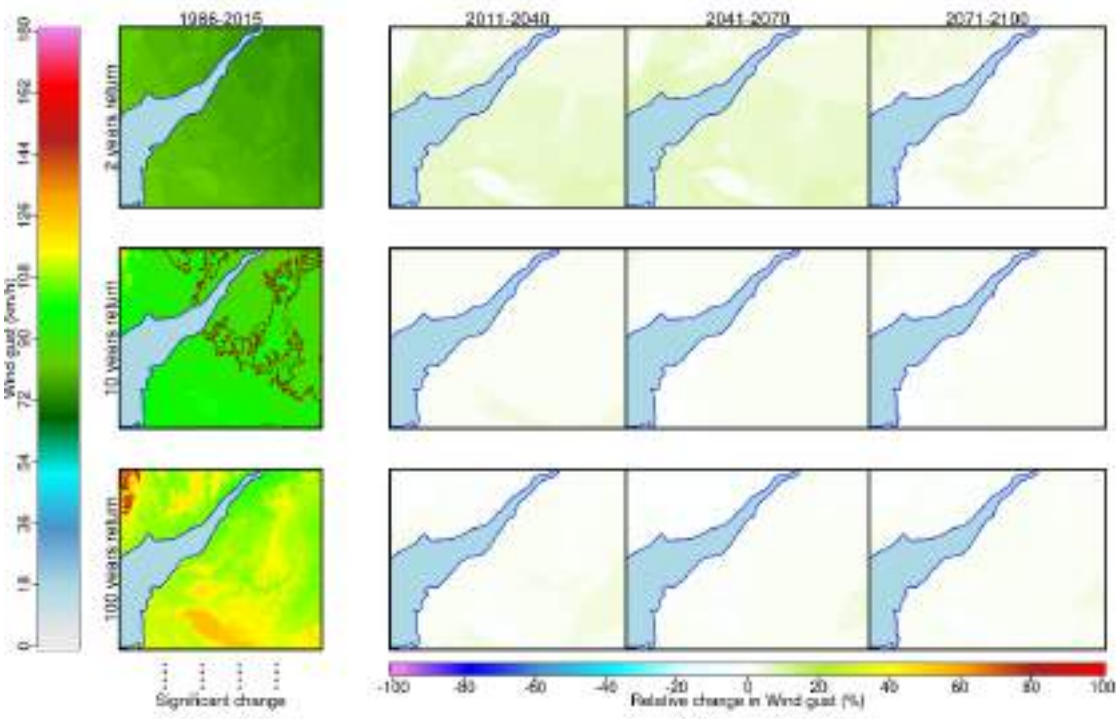

Figure 83. Multi-model median scenario of relative changes in extreme wind gust for the Bristol area, according to 2, 10 and 100-year return periods (rows) and for three future time periods (2011-2040, 2041-2070 and 2071-2100, second to fourth column) with respect to the reference period 1986-2015 (first column).

As in the case of the Lisbon area, the non-significance of the changes in wind speed for Bristol can be explained by the nonlinear behaviour of this variable with respect to the global warming. That is, a temperature rising could lead to two very opposite wind/calm scenarios: 1) Increase of gust fronts caused by thunderstorms (due to more summertime barometric swamp), and 2) Decrease of the windstorms frequency (because of a more northern jet stream). In this case, it seems that both contributions are compensated among themselves.

4.3.3.2. Extremes in snowfall

Extreme snowfall would dramatically decrease more than 60% throughout the century considering return periods of 2 and 10 years. However, no trends are expected for a return period of 100 years even by 2071-2100 (Figure 84). In fact, a non-significant increase up to 20% is projected by some downscaled climate models in low areas due to greater precipitable water, but the warming will cause a general rising of the snow limit height (i.e. the height from which the snow turns to rain).

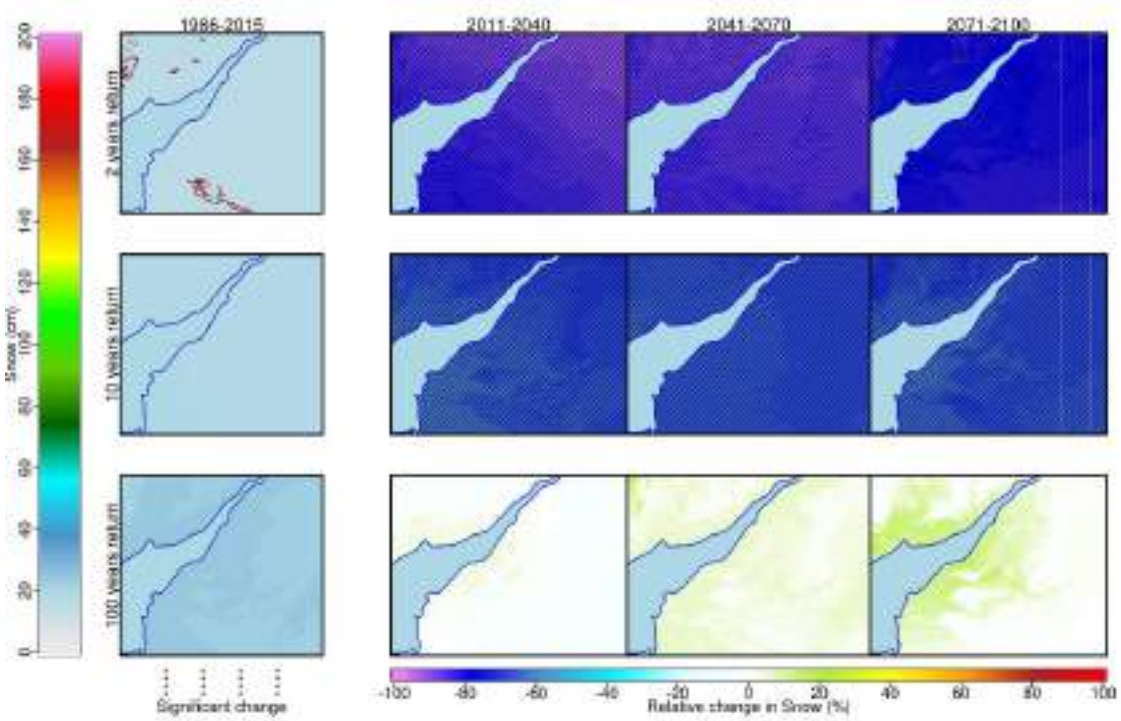

Figure 84. The same in Figure 83 but for relative change in extreme snowfall events.

4.3.3.3. Extremes in wave height and sea level

The combination of extreme storm surge and sea level rise is expected to increase along the century up to +20% or 25%. This increasing trend would be greater in 2070-2100 and statistically significant for return periods between 2 and 10 years. Nevertheless, rest of time periods and return period would remain unchanged.

Extreme wave height is projected to decrease slightly throughout the century for 2 and 10 years- return period, having a high level of uncertainty since climate models show different trends. However, a vast declining trend of about 25%, seen by every model, is expected for a return period of 100 years.

.

4.3.4. Summary of changes in extremes for Bristol

Significant decrease in snowfall and increases in maximum temperature, rainfall, wind gust and storm surge are expected along the century for all return periods (Table 8). Finally, extreme wave height would decrease for the highest return periods.

Table 8. Summary of changes in extremes values for Bristol according to the decadal and climate models.

Variable	Return period (years)	*Observed*	*Decadal forecast*	Relative change		
			2016-2035	*2011-2040*	*2041-2070*	*2071-2100*
Maximum Temperature	2	28.9 °C	+0.3 °C (-2.1/+0.9)	+1.3 °C (-0.4/+2.5)	**+3.8 °C** (+1.0/+4.6)	**+3.3 °C** (+0.6/+9.8)
	10	30.9 °C	-0.5 °C (-2.6/+1.0)	+1.3 °C (-0.3/+2.13)	**+3.8 °C** (+1.8/+5.3)	**+3.2 °C** (+0.9/+9.8)
	100	32.8 °C	-0 °C (-1.8/+0.8)	**+1.4 °C** (+0.18/+4.3)	**+3.9 °C** (+2.3/+6.2)	**+3.1 °C** (+1.8/+10.2)
12h Precipitation	2	27 mm	+ 2 % (-38/+42)	+7 % (-4/+13)	**+19 %** (+10/+34)	**+40 %** (+20/+60)
	10	30 mm	+5 % (-54/+63)	+10 % (-3/+12)	**+25 %** (+12/+38)	**+40 %** (+20/+60)
	100	35 mm	+10 % (-70/+90)	**+13 %** (+4/+14)	**+30 %** (+15/+40)	**+40 %** (+30/+60)
Wind Gust	2	80 km/h	+0 % (-7/+8)	**+3 %** (+0/+4)	+3 % (-1/+4)	**+2 %** (+1/+4)
	10	96 km/h	-2 % (-17/+13)	**+1.4 %** (+0.1/+2.4)	+1.1 % (-1.8/+2.4)	**+1.2 %** (+0.6/+2.5)
	100	119 km/h	+2 % (-5/+10)	-0.4% (-1.7/+0.2)	-0.5 % (-2/+0.2)	-0.4 % (-2/+0.3)
12h Snowfall	2	15 mm		**-85 %** (-94/-73)	**-86 %** (-96/-74)	**-80 %** (-100/-70)
	10	17.5 m		**-69 %** (-76/-58)	**-68 %** (-76/-59)	**-69 %** (-76/-58)
	100	22 mm		-6.0 % (-18/+13)	-0.3 % (-15/+20)	-4 % (-14/+30)
Storm surge + sea level rise	2	2.1 m		5% (-0/+5)	10% (-5/+15)	**20%** (+10/+25)
	10	2.57 m		5% (-5/+10)	5% (+0/+10)	**15%** (+5/+20)
	100	3.34 m		5% (-10/+15)	0% (-10/+10)	10% (+0/+20)
Wave Height	2	6.36 m		-3 % (-8/+2)	-5 % (-11/+4)	**-6 %** (-9/-0.4)
	10	8.5 m		-5 % (-16/+6)	-7 % (-15/+8)	-10 % (-18/+8)
	100	12.08 m		**-17 %** (-19 /-15)	**-25 %** (-36/-15)	**-23 %** (-29/-16)

Not available

Significant increase — P > 95%
Not significant increase — 50% < P < 95%
Not significant changes — P < 50%
Not significant decrease — 50% < P < 95%
Significant decrease — P > 95%

In detail, extreme temperature values are presumed to raise about +3.1°C by 2100, with an uncertainty level between +1.8°C to a remarkable +10.2°C under the worst-case scenario, showing thus a huge spread (Figure 85). These values are practically identical for all return periods considered (2, 10 and 100 years). Great variations are also expected for heat wave days, ranging the increase from +50% to up to +800% having a median of 280%, also by 2071-2100 period. As a result of this, hydrological drought is also expected to rise noticeably with high uncertainty, being the median an increase in 80% with an uncertainty interval from 25% to 90%. Extreme rainfall could increment about 30% at subdaily scale and 40% at daily scale.

No remarkable change in extreme wind speed is expected, although significant, reaching a +3% increase throughout the whole century for 2 and 10-year return period, with a slight decrease (-0.5%) for the 100-year return period. Considering oceanic variables, little change in extreme wave height is observed, being in all case a decrease, with a peak change of -25% in expected maximum height in waves by 2041-2070 period for most extreme events (especially for 100-year return ones). However, storm surge is presumed to increase (also considering sea level rise) with a maximum of a 9% increase by 2071-2100 for most frequent events (2-year).

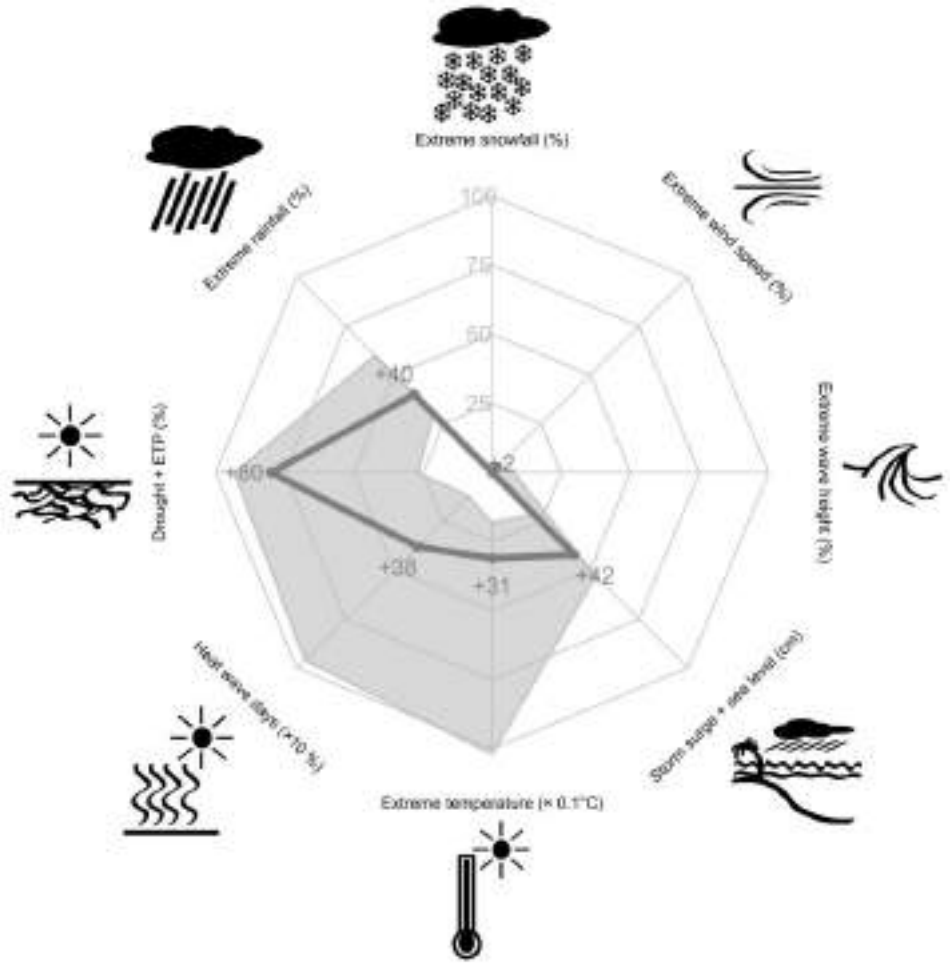

Figure 85. Extremes Compass Rose for Bristol: Maximum point change in climate extreme events along the century taking into account return periods between 2 and 100 years. The centre represents no changes and the edge corresponds to an increase of 100% for every variable, except for heat wave days (border is +1000%), for storm surge (border is +100 cm) and extreme temperature (border is +10°C). Thick lines represent the median scenario and the shaded area is the uncertainty region (5-95%).

5. Accomplishments and conclusions

5.1. Accomplishment summary

All subtasks and the milestone of task 1.4 “Projection/prediction of climate/weather extreme events” have been satisfied between month 12 and 26 of the project.

This deliverable describes the results on the generation of extreme events scenarios for Barcelona, Lisbon and Bristol according to the climate model outputs of the previous deliverable D1.2. For this purpose, several statistical downscaling methods have been combined to project climate extreme events at local scale according to the main identified drivers, specifically: Temperature, rainfall, snowfall, wind, wave height and sea level.

Therefore, non-significant changes have been carried out in this deliverable respect to the Description of the Action (DoA).

5.2. Conclusions

Long-, near- and seasonal-term future projections of climate extreme events have been obtained for Barcelona, Lisbon and Bristol by using several statistical downscaling methods applied to a set of CMIP5 climate models.

The simulation of extreme events was validated according to the performance of the used downscaling models, which were described and analysed in the previous deliverable D1.2. Generally, systematic errors were small for most of the models and therefore they could be corrected, especially in the case of climate timescale. However, some nuances can stand out for the closest time horizons: Seasonal and decadal simulations are adequate for extreme precipitation if the teleconnection-based approach is used, while temperature is best simulated using drift-corrected dynamical outputs. Extreme wind speed cannot be adequately simulated for Lisbon at decadal horizons and, therefore, only the climate timescale is available for this city.

Regarding the results, climate change projections lead to a more extreme heat in the three RESCCUE cities, with a tendency towards more extreme rainfall behaviour (Table 9). Heat wave days will experience an increase equal or greater than +1000%, rising from 5 to 40 days per year in Barcelona, 20 in Bristol and 17 in Lisbon, according to the median of the climate projections by the year 2100.

Extreme precipitation will also increase in the three cities about +30%. Barcelona and Bristol will experience this increment for both daily and subdaily rainfall, while for Lisbon, this change is expected only for 1-hour (or shorter) events. Moreover, extreme snowfall could also increase for 100y-return events in Barcelona, up to 40%. For the lesser extreme events (return periods from 2 to 10 years), snowfall would suffer a great decrease in Bristol and Barcelona due to the temperature rise.

For the evolution of the extreme dryness, it is necessary to distinguish between two types of drought: pluviometric drought (related with the recorded rainfall) and hydrological drought (availability of the ground or surface water). The first type will not change significantly (i.e. SPI will not decrease), but the water shortages (hydrological drought) will increment due to a greater evapotranspiration (decrease in the SPEI).

Regarding windstorms, extreme gusts could increase in Barcelona up to +10±3% the next two decades for all return periods, while storm surge is expected to rise in Bristol for 2y-return period by 2100. However, non-significant changes are projected for the extreme wave heights in the RESCCUE cities.

Table 9. Summary of statistical significance of changes in extreme events projected for each city throughout the century according to RESCCUE climate models.

Variable	Return period (years)	Relative changes in BARCELONA			Relative changes in BRISTOL			Relative changes in LISBON		
		2011-2040	2041-2070	2071-2100	*2011-2040*	*2041-2070*	*2071-2100*	*2011-2040*	*2041-2070*	*2071-2100*
Maximum Temperature	2									
	10									
	100									
Extreme Precipitation	2									
	10									
	100									
Wind Gust	2									
	10									
	100									
12h Snowfall	2									
	10									
	100									
Storm surge + sea level rise	2									
	10									
	100									
Wave Height	2									
	10									
	100									
Heat wave days per year										
Hydrological drought										

Significant increase	P > 95%	Not applicable
Not significant increase	50% < P < 95%	
Not significant changes	P < 50%	
Not significant decrease	50% < P < 95%	
Significant decrease	P > 95%	

References

AMB, Altava-Ortiz V, Barrera-Escoda A, Amaro J, Cunillera J, Prohom M, Sairouni A. 2017. Escenaris climàtics futurs a l'àrea metropolitana de Barcelona. *Direcció de Serveis Ambientals de l'Àrea Metropolitana de Barcelina* (AMB).

Chardon J, Hingray B, Favre AC. 2018. An adaptive two-stage analog/regression model for probabilistic prediction of small-scale precipitation in France. Hydrology and Earth System Sciences, 22: 265–286, doi:10.5194/hess-22-265-2018

Gaetani M, Mohino E. 2013. Decadal Prediction of the Sahelian Precipitation in CMIP5 Simulations. *Journal of Climate* **26**: 7708-2219.

Hargreaves GH. 1994. Defining and using reference evapotranspiration. *Journal of Irrigation and Drainage Engineering* **120**: 1132–1139.

Kim HM, Webster PJ, Curry JA. 2012. Evaluation of short-term climate change prediction in multi-model CMIP5 decadal hindcasts. Geophysical Research Letters 39:L10701, doi:10.1029/2012GL051644.

Martín-Vide J. 2004. Spatial distribution of a daily precipitation concentration index in peninsular Spain. *International Journal of Climatology* **24**: 959–971.

McKee TBN, Doesken J, Kleist J, 1993. The relationship of drought frequency and duration to time scales. In Proceedings of the 8th Conference of Applied Climatology, 17-22 January, Anaheim, CA. American Meterological Society, Boston, MA. 179-184.

Monjo R, Caselles V, Chust G. 2014. Probabilistic correction of RCM precipitation in the Basque Country (Northern Spain). *Theoretical and Applied Climatology* **117**: 317-329. DOI: 10.1007/s00704-013-1008-8.

Monjo R, Gaitán E, Pórtoles J, Ribalaygua J, Torres L. 2016. Changes in extreme precipitation over Spain using statistical downscaling of CMIP5 projections. *International Journal of Climatology* **36**: 757-769, doi: 10.1002/joc.4380.

Monjo, R. 2016. Measure of rainfall time structure using the dimensionless n-index. *Climate Research* **67**: 71-86. DOI: 10.3354/cr01359.

Pepler AS, Díaz LB, Prodhomme C, Doblas-Reyes FJ, Kumar A. 2015. The ability of a multi-model seasonal forecasting ensemble to forecastthe frequency of warm, cold and wet extremes. *Weather and Climate Extremes* **9**: 68–77, doi: 10.1016/j.wace.2015.06.005.

Pezza AB., Rensch P., Cai WJ. 2012. Severe heat waves in Southern Australia: synoptic climatology and large scale connections. *Climate Dynamics* **38**: 209-224.

SMC. 2015. Balanç d'una de les onades de calor més intenses de les últimes decades. Link: http://premsa.gencat.cat/pres_fsvp/AppJava/notapremsavw/286294/ca/balanc-duna-onades-calor-intenses-decades.do

STARDEX. 2004. STARDEX Diagnostic Extremes Indices Software. User Information Version 3.3.1, Link: https://crudata.uea.ac.uk/projects/stardex/deis/Diagnostic_tool.pdf

Redolat, D.; Monjo, R.; Lopez-Bustins, J.A.; Martin-Vide, J. (2019a). Upper-Level Mediterranean Oscillation index and seasonal variability of rainfall and temperature. Theoretical and Applied Climatology, 135: 1059–1077. DOI: 10.1007/s00704-018-2424-6.

Redolat, D.; Monjo, R.; Paradinas, C.; Pórtoles, J.; Gaitán, E.; Prado-López, C.; Ribalaygua, J. (2019b): Local decadal prediction according to statistical/dynamical approaches. International Journal of Climatology, JOC-19-0207.R1.

Ribalaygua J, Torres L, Pórtoles J, Monjo R, Gaitán E, Pino MR. 2013. Description and validation of a two-step analogue/regression downscaling method. *Theoretical and Applied Climatology* **114**: 253-269, doi:10.1007/s00704-013-0836-x.

Thornthwaite CW. 1948. An approach toward a rational classification of climate. *Geographical Review* **38**: 55-94, doi:10.2307/210739

Vicente-Serrano SM, Beguería S, Lorenzo-Lacruz J, Camarero JJ, López-Moreno JI, Azorin-Molina C, Revuelto J, Morán-Tejeda E, Sanchez-Lorenzo A. 2012. Performance of drought indices for ecological agricultural, and hydrological applications. *Earth Interactions* 16: 1-27, doi:10.1175/2012EI000434.1.

WMO. 2001. WCDMP-47: Report on the activities of the working group on climate change detection and related rapporteurs, 1998-2001. WMO/TD-No.1071.

WMO. 2017. Guidelines on the Definition and Monitoring of Extreme Weather and Climate Events, draft version, WMO-No.1204. Link: https://library.wmo.int/opac/doc_num.php?explnum_id=4213. ISBN: 978-92-63-11204-0.

Zhang X, Alexander L, Hegerl GC, Jones P, Tank AK, Peterson T, Trewin B, Zwiers F. 2011. Indices for monitoring changes in extremes based on daily temperature and precipitation data. *WIREs Climate Change*, doi: 10.1002/wcc.147. Link: https://www.geos.ed.ac.uk/homes/ghegerl/WIRES_index.pdf

Appendix I. Generated climate data

This appendix summarises the details of the extreme climate data generated as product of results presented in the D1.3 (Table 10). Long-term climate projections are provided from 10 CMIP5 climate models, while near-term (decadal) predictions correspond to 9 CMIP5 climate models. Main outputs are available in https://www.ficlima.org/intercambio/indexed/RESCCUE/.

Table 10. Summary of all generated data on extreme climate scenarios. Table shows the variables identified as climate drivers in D1.1 (blue cells) for each city and the climate simulations (purple cells) performed for each station. Red parenthesis indicates the number of available combinations *Climate models × Runs*.

Variable	Barcelona[1]	Lisbon[2]	Bristol[3]	Isolines (KML polygons)	Point values (table)	Climate (Historical + RCPs) 1951-2100		Decadal (RCP4.5) 1960-2035		Seasonal Jun-Dec 2018	
						BC-DO (10×3)	BC-AN (10×3)	TC (1×30)	BC-DO (9×4)	TC (1×30)	BC-DO (9×4)
Extreme maximum temperature	X	X	X	X	X		27[a]	27[a]	27[a]	9[b]	9[b]
12h extreme precipitation	X	X	X	X	X		27[a]	27[a]	27[a]	9[b]	9[b]
IDF curves	5min	1h	5min		X		18[c]				
12h snowfall	X		X	X	X		27[a]				
Daily extreme wind gust	X	X	X	X	X		27[a]		27[a]		
Storm surge + sea level	X	X	X		X	SL	3[d]				
Extreme wave height	X		X		X		3[d]				
Drought (SPI and SPEI)	X	X	X		X		2[e]				
Heat waves	X	X	X		X		2[e]				

Legend:

BC-DO	Bias Correction of direct outputs.
AD	Analogous downscaling method.
BC-AD	Bias Correction of Analogous Downscaling.
TC	Teleconnection-based method.
a	3 return periods × 3 probability scenarios × 3 thresholds
b	3 probability scenarios × 3 thresholds
c	6 return periods × 3 probability scenarios
d	3 probability scenarios
e	2 RCP scenarios
SL	The sea level simulation is only available from the BC-DO

[1]Available in https://www.ficlima.org/intercambio/indexed/RESCCUE/Ter-Llobregat/
[2]Available in https://www.ficlima.org/intercambio/indexed/RESCCUE/England-South-Wales/
[3]Available in https://www.ficlima.org/intercambio/indexed/RESCCUE/Lisboa/